Electronic Theses and Dissertations   Theses, Dissertations, and Major Papers

8-29-2018

A 77 GHz BCB BASED HIGH PERFORMANCE ANTENNA ARRAY FOR AUTONOMOUS VEHICLE RADARS

Sreejit Chatterjee
University of Windsor

Follow this and additional works at: https://scholar.uwindsor.ca/etd

A 77 GHz BCB BASED HIGH PERFORMANCE ANTENNA ARRAY FOR

AUTONOMOUS VEHICLE RADARS

by

Sreejit Chatterjee

A Thesis
Submitted to the Faculty of Graduate Studies
through the Department of Electrical and Computer Engineering
in Partial Fulfillment of the Requirements for
the Degree of Master of Applied Science
at the University of Windsor

Windsor, Ontario, Canada

2018

A 77 GHz BCB BASED HIGH-PERFORMANCE ANTENNA ARRAY FOR

AUTONOMOUS VEHICLE RADARS

by

Sreejit Chatterjee

APPROVED BY:

R. Riahi
Department of Mechanical, Automotive and Material Engineering

R. Muscedere
Department of Electrical and Computer Engineering

S. Chowdhury, Advisor
Department of Electrical and Computer Engineering

August 15, 2018

DECLARATION OF ORIGINALITY

I hereby certify that I am the sole author of this thesis and that no part of this thesis has been published or submitted for publication.

I certify that, to the best of my knowledge, my thesis does not infringe upon anyone's copyright nor violate any proprietary rights and that any ideas, techniques, quotations, or any other material from the work of other people included in my thesis, published or otherwise, are fully acknowledged in accordance with the standard referencing practices. Furthermore, to the extent that I have included copyrighted material that surpasses the bounds of fair dealing within the meaning of the Canada Copyright Act, I certify that I have obtained a written permission from the copyright owner(s) to include such material(s) in my thesis and have included copies of such copyright clearances to my appendix.

I declare that this is a true copy of my thesis, including any final revisions, as approved by my thesis committee and the Graduate Studies office and that this thesis has not been submitted for a higher degree to any other University or Institution.

ABSTRACT

A bisbenzocyclobutene (BCB) based 77 GHz aperture coupled microstrip antenna array for frequency modulated continuous wave (FMCW) automotive radars has been developed for use in automotive collision avoidance and cruise control applications.

Each of the microstrip patches of the developed antenna array has been desiged to have a microfbaricated airfilled cavity to realize a synthesized effective dielectric constant of 1.46 in contrast to original BCB dielectric constant of 2.6 to improve the diecrectivity, gain, and bandwidth in a compact footprint suitable for small automotive radars. The developed antenna array has a foot print area of 20 x 21 mm^2 to accommodate 56 micorstrip patches in a 7 x 8 matrix configuration. Each of the gold patches has a length of 1.46 mm and a width of 1.7 mm. The anteena array exhibits an ADS™ (Advanced Dsign Systems) 3D simulated -10 dB bandwidth of 4.2 GHz, 22.5 dBi directivity, and a gain of 19.78 dBi with sidelobe levels lower than 13.78 dB to meet the auto industry roadmap reccommendations. A fabrication process table has been developed and simualated successfully using IntelliSuite™, an industry standard software. The developed process table can be used to fabricate the device.

The developed antenna array will pave the way to manufacture low cost high performance automotive radars to mitigate fatal crashes to save lives and minimize property and infrastructural damage while also forming an integral part of the adaptive cruise control system for autonomous vehicles.

DEDICATION

To my Mom

You are the reason for what I am today. Without your love, support, and guidance I would never have become what I always dreamt of. I thank you for even the minute of things which you did for me and for your ever encouraging words to push forward and chase my dreams until I achieve them.

ACKNOWLEDGEMENTS

TABLE OF CONTENTS

LIST OF FIGURES

LIST OF TABLES

LIST OF APPENDICES

1.   Appendix A: Matlab codes for Antenna Development

2.   Appendix B: Mask files for Fabrication

3.   Appendix C: Process Tables for Fabrication of Top and Bottom Wafers

ABBREVIATIONS

3D – Three Dimensional

ADC – Analog to Digital Converter

ADS – Advanced Design Systems

Au – Gold

BCB – Bisbenzocyclobutene

BW – Bandwidth

Cr – Chromium

DAC – Digital to Analog Converter

DBF – Digital Beam Forming

DSP - Digital Signal Processing

DRIE – Deep Reactive Ion Etching

EM – ElectroMagnetic

FMCW – Linear Frequency Modulated Continuous Wave

FOV – Field of View

HPBW – Half Power Beam Width

IF – Intermediate Frequency

LIDAR – Light Detection and Ranging

LRR – Long Range Radar

MEMS – Microelectromechanical Systems

MRR – Mid Range Radar

NHTSA – National Highway Traffic Safety Administration

Radar – Radio Detection and Ranging

RF – Radio Frequency

RIE – Reactive Ion Etch

RX – Received Signal

Si – Silicon

SRR – Short Range Radar

TEM – Transverse Electro Magnetic

TX – Transmit Signal

VCO – Voltage-Controlled Oscillator

VSWR – Voltage Standing Wave Ratio

NOMENCLATURE

f_h = Upper frequency of the -10dB emission point

f_l = Lower frequency of the -10dB emission point

L_p = Length of patch

W_p = Width of Patch

L_{eff} = Effective length of patch

ε_r = dielectric constant

ε_{eff} = effective dielectric constant

c = speed of light

f_o = frequency of observation

h_p = height of patch dielectric

h_f = height of feed dielectric

ΔL = Patch length increased due to fringing fields

λ = wavelength

$\tan \delta$ = loss tangent

P_d = dielectric loss

Q_c = Quality factor

Δ = skin depth of conductor

P_c = conductor loss

P_r = power radiated from patch

λ_0 = wavelength in free space

$|\Gamma|$ = reflection coefficient

Z_L = Load impedance

Z_0 = Characteristic impedance

G = Gain

η = radiation efficiency

D = Directivity

AF = Array Factor

N = number of elements

AF_{planar} = Array factor for a planar array

k = wave number

β = phase difference

ε_{synth} = synthesized dielectric constant

h_{eq} = equivalent height

$h_{material}$ = material height

h_{air} = air height

V_0^+ = incident voltage

V_0^- = reflected voltage

Q_c = conductor quality factor

Q_T = antenna quality factor

Q_d = dielectric quality factor

W_T = total energy stored in a patch at resonance

In this thesis, a BCB based aperture coupled microstrip antenna array for autonomous vehicle radar is presented. The antenna array can be utilized for short (SRR), mid (MRR) and long range (LRR) radar applications like parking assist, collision avoidance, and cruise control. The antenna array provides a large bandwidth of 4.2 GHz which increases the range resolution capacity of the radar and satisfies the requirements set out by the automotive radar industry.

This chapter provides a background of the project, motivation, the objective and state of the art research work in the field of radar antennas for autonomous driving. It stresses the importance and achievements of the past and ongoing work in this domain. The chapter starts with a brief description of road safety and accident records in the world with a highlight on North America.

The Chapter emphasizes the potential benefits of the antenna array currently being developed at the University of Windsor and how it outperforms most other radar antennas available in the market today.

1.1   Problem Statement

Automotive safety has been a widely sought after topic over the years and ensuring a safer travel lead to progress from using simple seatbelts and airbags to advance telematics systems that provide crash notifications. The automakers have developed advanced technologies which not only mitigate the chances of collisions but also provide significant support and damage control, i.e.

deployment of airbags, locking of seat belts etc. even when a crash occurs. From collision avoidance to cruise control the automakers have developed systems to keep an occupant of the vehicle safe from injuries and damage to property while providing necessary comfort in driving. Existing technologies like LiDAR, cameras, ultrasonic sensors, infrared, and radar often fall short of establishing a safety shell around a vehicle due to adverse climatic conditions, system architectural failure and even lapse of concentration while driving. Automakers find it extremely difficult to manufacture these technologies with a robust design capable of functioning at a varied temperature across the world at a reasonable price. Thereby the situation of road safety falls sharp considering the reasons stated.

About 40,000 people died in the USA in the year 2016 which is a precise 6% rise in the death toll from the year before. The National Highway Traffic Safety Administration (NHTSA) reported that there were 17,775 casualties on the road in the first half of the year with a 10.4% increase from the same period previous year [1] Although the fatality rates per vehicle registered and per vehicle distance travelled has decreased since the advent of significant driver regulations but the increase in the number of fatalities is directly due to the rise in vehicle uses and the population in general. However, a sharp rise in fuel prices and driver behavioral change has reduced the fatality rates to below the 1961 fatality count [2]. Proper law enforcement on the roads has played a key role in maintaining and producing a trustworthy environment for travel.

Table 1.1 is from the World Health Organization on road traffic injury [3]. It gives out a detailed list of the fatalities according to the regional classification of the World Bank, occurred through the years and offers a forecast for the future. Western countries like the United States, Canada and Western and Central Europe have been listed as high-income countries in table 1.1.

Table 1.1 WHO report on road traffic injury [3]

Different Regions	Number of Countries	Yearly fatalities in thousands				Change (%) 2000-2020	Fatality rate (death/100000 people)	
		1990	2000	2010	2020		2000	2020
East Asia and Pacific	15	112	188	278	337	79	10.9	16.8
East Europe and Central Asia	9	30	32	36	38	19	19.0	21.2
Latin America and Caribbean	31	90	122	154	180	48	26.1	31.0
Middle East and North Africa	13	41	56	73	94	68	19.2	22.3
South Asia	7	87	135	212	330	144	10.2	18.9
Sub-Saharan Africa	46	59	80	109	144	80	12.3	14.9
Sub total	121	419	613	862	1124	83	13.3	19.0
High Income countries	35	123	110	95	80	-27	11.8	7.8
Total	156	542	723	957	1204	67	13.0	17.4

The global automotive market is expected to reach US $12.16 billion by 2025, growing at a compound annual growth rate (CAGR) of 20.8% according to a study conducted by The Report, Inc. [4]. The growth of this industry is primarily due to the high demand for active safety features, innovations in the radar technology, decreasing the prices of components and the increasing sale of vehicles around the world. Advanced driver assistance (ADAS) systems like radar, LiDAR, ultrasonic, and cameras help provide effective applications like adaptive cruise control [5], pedestrian detection system [6], blind spot detection [7], automated emergency braking and collision warning [8] and parking [9]. However, some of the devices used in the process lack the ability to work in a varied temperature range and climatic conditions thereby bringing the issue of safety again under considerable doubt. Radar devices are better opted than LiDAR's or cameras as they can work in adverse climatic conditions like heavy snow, fog or rain with little to no effect in their performance of detection. A LiDAR uses pulsed laser light which fails to perform adequately in rain, fog and snow since when used under rain sizable fraction of points from the ground goes missing due to the laser rays being reflected from reflective ground surfaces. Heavy rains cause spurious LiDAR signal returns from plumes of rainwater from cars while in foggy conditions there is significant creation of spurious returns from car exhausts [10]. In heavy snow, the LiDAR fails to perform as the pulsed laser light gets refracted due to the high refractive surfaces of snow [11]. While a radar is much suited to adverse conditions as there is little to no effect in the attenuation or reflection of microwave energy as showed in table 1.2. Table 1.2

shows the amount of attenuation of electromagnetic signal energy between 70-80 GHz which indicates that radar technology is much suited to all weather conditions, unlike their LiDAR counterparts.

Table 1.2 Atmospheric attenuation at 70-80 GHz [12]

Conditions	Precipitation (mm/hr)	Attenuation (dB/km)
Clear, dry air	0.00	0.1
Drizzle	0.25	0.2
Light Rain	1.25	0.5
Medium Rain	12.50	1.5
Heavy rain or Snow	25.00	9.0

"Radar technology is the key to building innovative driver assistance systems to help avoid automobile accidents", says Hans Adlkofer, Vice President and General Manager of Infineon Technologies Sense and Control business unit [13]. Despite the fact that the radar technology first appeared in luxury cars, crash prevention radar systems have made their way down to more reasonably priced vehicles in the present days. This has created a positive competition between automakers and is heading for a huge growth for the market of automotive safety and driver assistance device markets. D. Hoetzer et al. [14] claims that by installing crash prevention system in vehicles the number of accidents can be reduced by 3.8 million in North America alone, with approximately 17000 lives saved in the process every year. This emphasizes the requirement of radar technology to ensure highway safety while minimizing loss of lives and property damage.

1.2   Motivation

Automotive radar is used to detect the proximity of other vehicles and obstacles to initiate actions to prevent and or minimize the loss of lives and damage to property. These radar devices are classified into three different aspects according to the range of coverage. The automotive industry has set various radar standards depending on distance covered by the radar to the angular sector scanned by the radar, pulse type, frequency modulation techniques, etc. [12]. An automotive radar is typically divided into three types mainly on the basis of the range and the application it serves. Figure 1.1 shows a vehicle with different applications provided by driver assistance systems installed in it for safety.
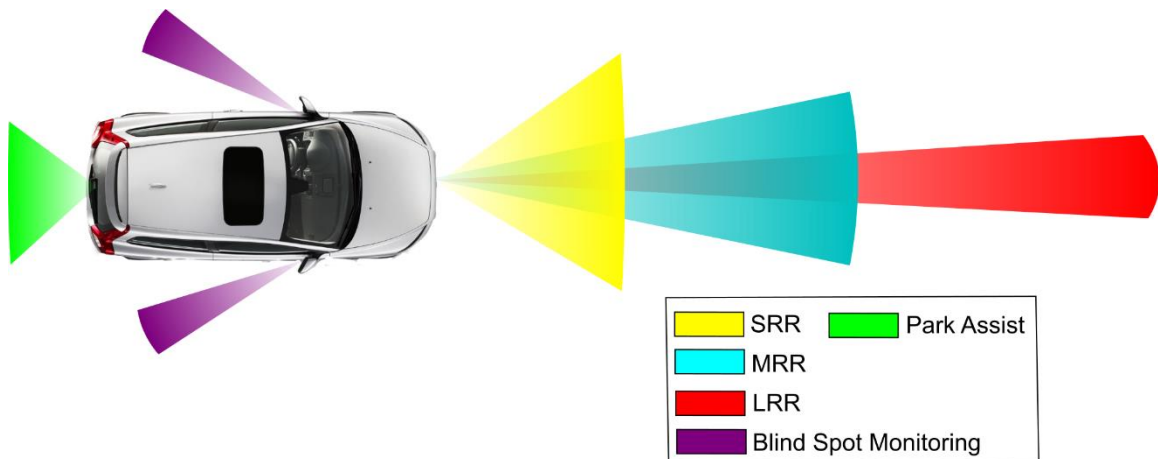
Figure 1.1 Applications provided by Driver Assistive Systems.

The advantages provided by these radars resulted in an increase in their installation in the vehicles worldwide. Various automotive radar systems are available in the market which produces various applications listed below:

- Parking assists with higher precision.

- Blind spot detection.

- Adaptive cruise control systems with a support in a cut in and Stop & Go situations

- Pre-crash detection.

Since its inception in the early 1900's when the first patent on the automotive radar [15] was published a lot of research work has been thoroughly undertaken in this domain to constantly upgrade the level of technology and ease its integrability with the vehicle. The criteria set by the automakers for such devices are small, robust and cheap while providing effective performance across all climatic conditions.

Since the 90s the 77 GHz frequency domain has been opted for the automotive long range radars [16] as it provides excellent performance in range and azimuth angle coverage with producing a narrow beam for long-range applications. In addition to the advantages listed earlier for the 77 GHz frequency allocation, it also helps provide a better resolution since it increases the bandwidth availability in the domain and reduces the chances of signal interference from other devices working in a domain near it. Lower frequency domains like 24 GHz were previously utilized for shorter ranges since it would produce a wider antenna beam; however, the bandwidth allocated for those frequency bands were small which would provide a smaller range resolution while there was a high possibility of signal interference from other devices operating in a frequency near it. The authors in [17] reported that millimeter waves at higher frequencies, i.e. at 77 GHz undergo very less absorption in human tissues due to their lower

penetration through the human skin. An average thickness of human skin lies somewhere between the 0.5 mm (on the eyelids) and 4 mm (on the palms) [18] while the penetration depth of the millimeter waves was under 0.5 mm at 77 GHz compared to twice of it in the 24 GHz frequencies. The authors in [17] also revealed that about 40% of the incident power gets reflected from the skin surface at 60 GHz. Therefore, at higher frequencies the damage to human tissues are less compared to the lower frequency band of 24 GHz previously allocated. Hence the technology drifted towards the 77 GHz where the bandwidth of 1 GHz was allocated between 76 and 77 GHz. Upon further advancement of technology, the European Commission initiated the 79 GHz project for vehicular radars. The new frequency band would work with an even wider bandwidth of 4 GHz between 77 to 81 GHz for shorter ranges and a target resolution level would be brought down to a few millimeters [19]. However, for the long and midranges, the 77 GHz band is still preferred which provides a range resolution of about a meter. Another point is that as the operating frequency increases, the guided wavelength λ_g defined as $\lambda / \sqrt{\varepsilon_r}$ where λ is the free space wavelength and ε_r is the dielectric constant of the antenna substrate decreases. As the antenna patch dimensions are directly related to the guided wavelength, a decrease in the guided wavelength results in a decrease in the patch dimensions to contribute to a decrease in the overall radar size.

1.3   Existing Solutions and their Limitations

Various automotive radar developers like Continental™, BOSCH™, Mitsubishi electric™, etc. have been instrumental in technology development in this industry

and have been constantly providing auto manufacturers with sophisticated radar modules at cost-effective rates. BOSCH™ has upgraded its radar module from the first generation to the fourth generation [20] with a constant improvement of radar performance throughout its journey as a radar developer. Other companies, such as Delphi™ and Denso™ has also produced such modules which are in high demand in the market. However, search for a cheaper product which outperforms other the devices in the market is always desirable and sought after.

Many radars available in the market today offer a smaller range resolution which often leads to the failure of a proper detection of the proximity of the obstacles around the vehicle in shorter ranges as the number of samples generated per second is less when the bandwidth offered by the radar is less [21]. The requirement set forth by the auto industry are not often met at reasonable prices as the expense rendered for manufacturing components increases. Some radar modules offer shorter ranges than the requirements while some even produce false alarms.

Cost effective substrates like Rogers 5880, 3003 [22] have been thoroughly explored over the years for providing a high performing antenna. While these dielectrics helped increase the quality of performance for the products manufactured, the process of integrating the antennas with its signal processing modules became increasingly challenging.

In 2012, [23] Ismail et al designed a radar antenna on a silicon substrate which had an extremely high radiation efficiency. Silicon-based structures are known to

provide high performance but at the cost of an increased price of production in mass scale. In 2013, [24] designed a radar antenna which was a complete package except it was large in size about 5 cm by 2 cm. A lot of advancement has been made in this domain but not a proper solution has been reached which would offer to solve the problem at hand. In 2017, [25] produced a radar antenna at 77 GHz which had a high gain expected to cover 300 m for long-range applications however the bandwidth of the antenna was extremely narrow with a very low reflection coefficient and the size of the antenna array was huge.

Hence, the target of this thesis is to present a smaller sized radar antenna capable at providing a wider bandwidth with higher gain and directivity to cover the range requirement while manufactured at a lower overall cost price.

1.4   Electronically Scanned MEMS Radar

Each radar system is a unique device which is capable of identifying its own signal echoes through the Doppler shift of their radar signatures. A radar is provided with an LFMCW signal which frequency modulates the carrier wave of the device and thereby producing a unique signature for every radar module manufactured. Electronically scanned antenna arrays are extremely beneficial for facilitating radar sensors for various applications like military and broadband communications. The most important feature of an electronically scanned antenna is the phased antenna array system. The phased array system works on the principle of creation of a single beam which is electronically steerable from phasing the individual antenna elements. This single beam is electronically steered by managing the amount of amplitude and phase provided at each

radiating antenna element. A linearly phased array with equal distance between elements is a most desired design form as it is easy to analyze. Figure 1.2 shows a basic electronically beam steerable antenna array module with an inter-element spacing of d between them. By altering the phase and the amplitude of excitation of each element, the direction and the shape of the beam radiated from the antenna array can be easily controlled. The phase excitation Φ_n controls the angle of the directed beam, θ_0 in a phased array. To produce a broadside beam of $\theta_0 = 0$ the phase excitation should be $\Phi_n = 0$.
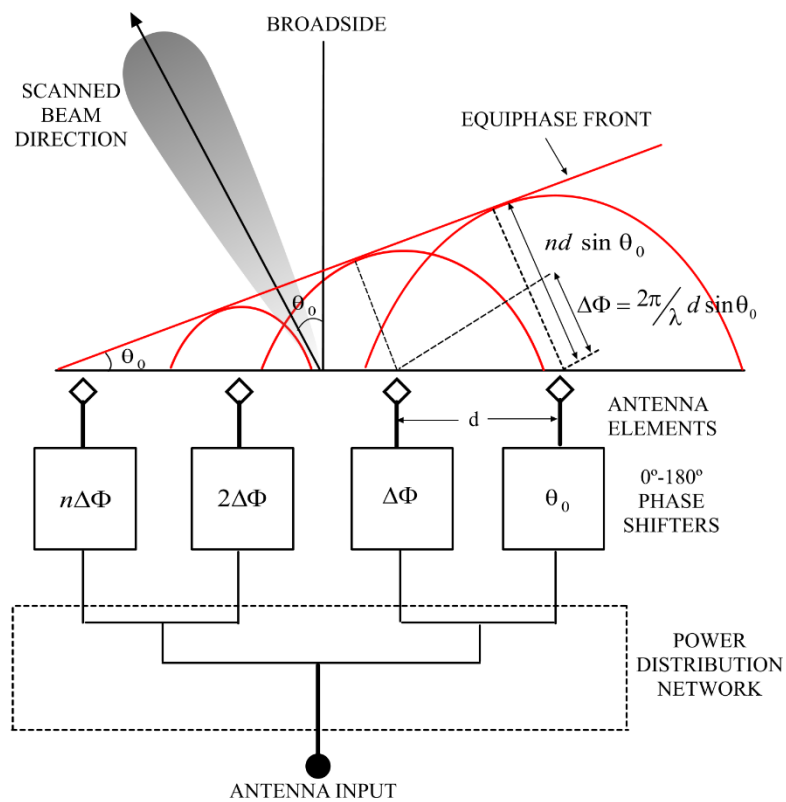
Figure 1.2 Phased antenna array.

Other scan angles require an excitation, $\Phi_n = nkd \sin \theta_0$, for the nth element

where $k = (2\pi/\lambda)$ is the wave number. These electronics actively utilize the

concept of a phase shifter which increases the circuit complexity and the price by

a margin of a thousand dollars or even more [26] [27]. A method to lower the cost

of these radars is to utilize microelectromechanical systems, the approach in

batch fabricating these devices on an inexpensive material and eliminate any

circuit complicacy due to phase shifters. Options like Butler Matrix and Rotman

lens which are beamforming beam steering networks offers cheap and compact

means to extend single beam systems to a fully functional beam steerable

devices. Use of MEMS technology for hardware modules reduces the circuit

manufacturing overhead.
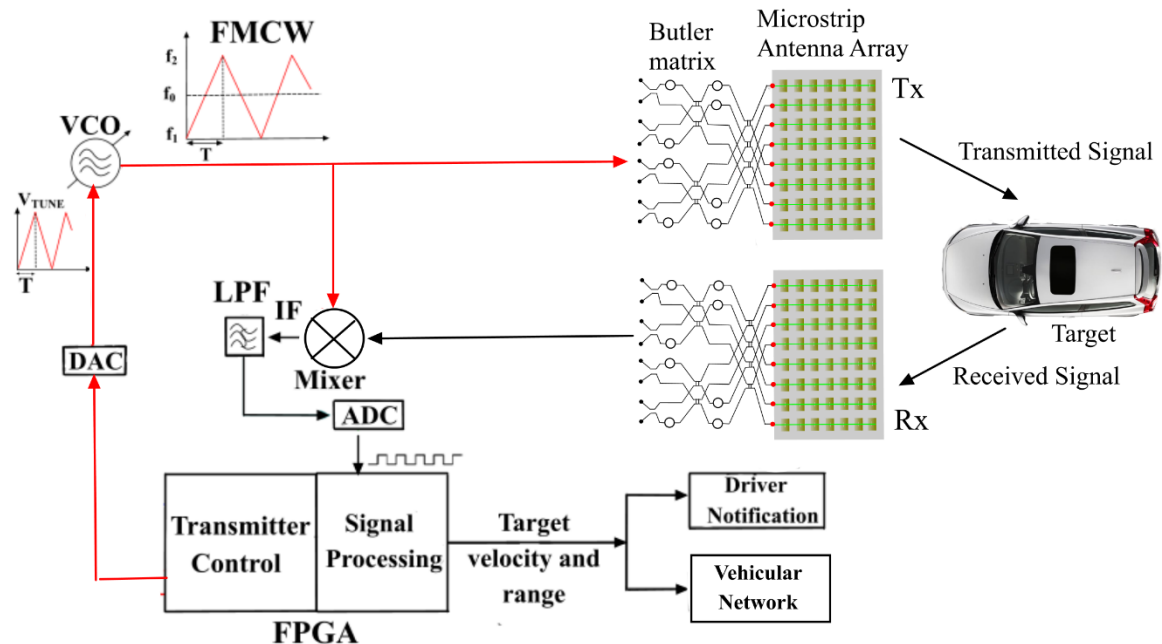
Figure 1.3 Automotive radar system developed comprises of an antenna which utilizes a Butler Matrix.

Not only a beam steering module can be included in the circuitry but also the whole antenna array can be included in a single substrate. This greatly reduces the packaging and interconnect complexity thereby reducing the overall cost. A block diagram for this radar is shown below in figure 1.3. Depending on the range of coverage, the radar antenna's radiation pattern must have a narrow beamwidth of a few degrees, higher bandwidth with lowered sidelobe levels and high radiation efficiency to obtain effective performance while providing low cost for manufacturing. In this context, this thesis presents the design of a highly directive planar antenna on a benzocyclobutene substrate for automotive radar applications. The radar is expected to fulfill the mid and long range requirements set by the automotive radar industry. The advantage of this design is that it allows easy integration to the transceiver modules unlike other dielectrics and also produces a higher bandwidth thereby allowing a better range resolution. Long distance radars require a large high gain antenna and one of the objectives of this research work is to reduce the dimension of the device while providing an optimum amount of gain for the target application. At millimeter wave frequency, the usage of mechanically scanned antennas experiences a slow response and suffers from false alarm due to shock and vibration, while on the other hand antennas with phase shifters are extremely expensive to manufacture and initiate considerable RF losses. By using an innovative technique of utilizing a Rotman lens or a Butler matrix these disadvantages can be minimized to a great extent.

1.5 Benefits of wide bandwidth in Long Range Radars

Automotive radars generally opt for wide to narrow bandwidths depending on the range of their functionality. Traditionally short and mid-range radars with a wider bandwidth are preferred to improve resolution and enhance detection of nearby obstacles. However, a longer range radar functionality can also be enhanced with the improvement of the bandwidth from a narrow band to a wider one [28]. This is due to the fact that a wider bandwidth facilitates detection of smaller sized moving objects effectively. Pedestrians have a comparatively smaller radar cross section and tend to change directions often. Hence a higher resolution radar helps keep track of the sudden direction changes and helps to avoid collisions by facilitating the detection of the pedestrians [28]. On the other hand, a single radar unit with a 4 GHz bandwidth can be used in a multimodal implementation without any significant change of hardware.. A simple experiment was conducted to produce the effective resolution necessary for mid and long range vehicular applications by placing a set of corner reflectors as targets for a radar [28]. Figure 1.4 shows an experimental set up of the designed targets.
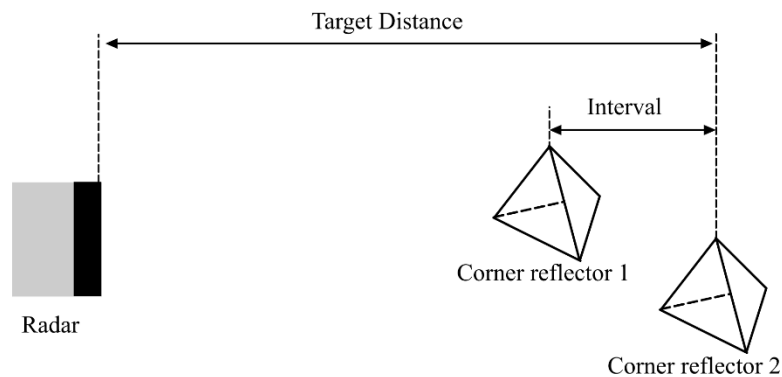
Figure 1.4 Experiment set up with corner reflectors to understand the effectiveness of a large bandwidth

The radars with a 0.5 GHz bandwidth detected only a single corner reflector kept 0.5 m apart while the radar with a 4 GHz bandwidth was able to detect both the target. Figure 1.5 graphically presents the outcome of the experiment done in [28].. Hence, 0.5 m has been set as a standard for mid and long-range radar resolutions. Apart from a higher resolution, the detectable range is an important criterion for radar modules as a wider detectable range reduces the number of automotive radars mounted for fully autonomous driving [28].
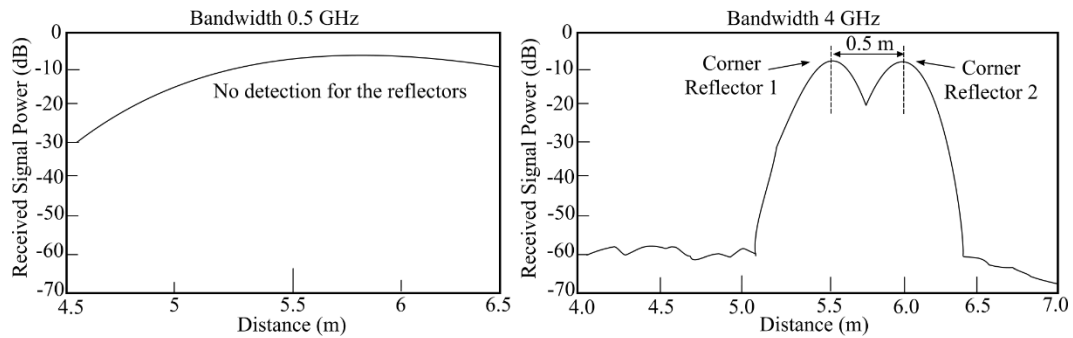
Figure 1.5 Comparison of two radars with (a) 0.5 GHz bandwidth and (b) 4 GHz bandwidth respectively [28].

1.6   Research Objectives

Design an antenna array for the automotive radars functioning at long and mid ranges with the following target specifications to satisfy the auto industry roadmap [16]:

- An antenna array with a higher gain (~20 dBi) and directivity to meet the range requirement of 200-250 m.

- An antenna array with wider bandwidth (~4 GHz) for better range resolution.

- Achieve a smaller form factor by reducing the number of radiating patches when compared to the state of the art antennas available.

- Design an antenna which would be robust and capable of functioning at a varied temperature range (-40 - 85º) [29] as set forth by the auto industry.

- Design the antenna with cheaper materials which can be easily manufactured in mass scale production.

- Utilize materials which would ensure the antenna does not suffer from the problem of integration with its signal processing modules.

1.7   Proposed Solution and Hypothesis

Various antenna studies over the years have revealed that low k dielectric materials are better suited for automotive radars as they provide better insulation and hence a higher gain and bandwidth. Dielectric materials like Rogers 5880, Rogers 3003 [30] [22] have been thoroughly utilized by modern day antenna developers for their obvious benefits of low k values. However, the designs fell short because of considerable complexity in establishing a robust connection between the antenna arrays and other radar components. Hence researchers are always in search of a material which can mitigate this problem at the lowest cost available.

In this thesis, a low-k dielectric derived from B-staged bisbenzocyclobutene (BCB) monomers commercialized by the Dow Chemical Company under the trade name Cyclotene 3000™ has been investigated as the dielectric material to realize an high gain wider bandwidth microstrip antenna array for automotive radar. Investigation by [31] and [32] show that the dry etchable BCB (Cyclotene) with a dielectric constant of 2.65 can be batch fabricated using conventional microfabrication techniques. Utilization of BCB would allow for easy integration

with the radar transceiver module, realizing the necessary gain and bandwidth within a small footprint of an automotive radar is still a big challenge.

Various research works have been reported where several stacked layers of dielectric materials were used to achieve an effective dielectric constant for the antenna which is lower than the dielectric constant of any individual layer [33]. The authors in [33] experimentally have shown that introducing an air filled cavity in a microstrip antenna where high resistivity silicon has been used as the antenna dielectric material can result in an effective dielectric constant of approximately 1 as compared to 11.8 if only a layer of high resistivity silicon was used. This study confirmed that when a material with a higher dielectric constant (e.g. silicon) is placed in parallel to a layer of lower dielectric constant material (e.g. air), the dielectric constant of the combined structure gets reduced. However, other studies have revealed that the volume of each material also plays an important role in determining the new synthesized value. In order to decrease the dielectric constant of the layer of BCB underneath the radiating patch, an innovative air-filled cavity has been introduced in the BCB layer using an deep reactive ion etching (DRIE) method.

This thesis would provide a detailed understanding that how etching a cavity in a layer of dielectric can improve the performance of the antenna modules.

1.8   Principal Results

A DRIE cavity etched microstrip aperture coupled antenna array for use in 77 GHz tri-mode automotive radar application is presented. The developed antenna

array has a foot print area of 20 x 21 mm^2 to accommodate 56 micorstrip patches in a 7 x 8 matrix configuration. Each of the gold patches has a length of 1.46 mm and a width of 1.7 mm. The anteena array exhibits an ADS™ (Advanced Dsign Systems) 3D simulated -10 dB bandwidth of 4.2 GHz, 22.5 dBi directivity, and a gain of 19.78 dBi with sidelobe levels lower than 13.78 dB to meet the auto industry roadmap reccommendations. A fabrication process table has been developed and simualated successfully using IntelliSuite™, an industry standard software. The developed process table can be used to fabricate the device. The vast bandwidth produced by the antenna array results in its direct application in the short-range radar which requires higher range resolution while the highly directional beam with high gain in the broadside direction ensures its usage in the longer ranges in applications like cruise control and collision avoidance. Table 1.3 contains the achieved simulation results of the proposed antenna array.

Table 1.3 Principal Results

Parameters	Results
Gain	19.78 dBi
Azimuth Angle tilt	0º
Elevation Angle tilt	8º
Angle of Opening	±5.5º
Bandwidth	4.2 GHz
Radiation Efficiency	45%
VSWR	1.04

1.9   Thesis Outline

Chapter 1   provides a review of the state-of-the art in automotive radars and their impact in realizing higher level of road safety, driver comfort, and mitigation of

crash damage. This chapter also provides road crash statistics of the World Health Organization and the fatality rate in North American and European countries.

Chapter 2 briefly summarizes the existing literature of automotive radar antenna array technologies. This chapter provides a background about a MEMS-based radar system and its usefulness in the developing automotive radar technology.

Chapter 3 presents a detailed modeling and design strategies of a microstrip antenna. It includes all the essential parameters needed to design a microstrip antenna. This chapter also provides brief details about various antenna design parameters on which an antenna performance is judged. Linear and planar antenna array design methodologies are discussed in this chapter.

Chapter 4 provides details about the importance of a micromachined substrate and how lowering the dielectric constant of the substrate beneath a microstrip patch effects the overall antenna performance. It provides detailed information on design methodology and simulations undertaken to design a single antenna element.

Chapter 5 provides details on the design of the antenna array by using single elements in conjunction to obtain the necessary results for the radar antenna. It provides detailed insight into the antenna array design and simulations undertaken to obtain the targets set before the thesis. It has a comparison with other published results on automotive radar antenna arrays operating in the same frequency range.

Chapter 6 makes the concluding remarks of this research work and provides some remarks on the future directions to extend the performance of the current design further..

This chapter reviews the state-of-the-art in automotive radar systems and associated antenna array modules. The drawbacks of existing technology are highlighted and the reasons for developing a new design are emphasized.

2.1   Review of Literature

Roads around the world are shared by cars, buses, trucks, motorcycles, mopeds, pedestrians, taxis and other categories of vehicles. Travel is made possible by motor vehicles which support economic and social development in many countries. Due to the ever increasing population, road safety has evolved into a serious issue with a sharp rise in vehicle demand all around the world. Statistics published in June 2017 showed that in a developing nation like India there was over 210 million registered vehicles in the year 2015 [34]. While in a developed nation like the US the numbers exceeded 253 million among cars and trucks around with an increase of 1.5% from the year before in 2014 [35]. Due to the increase in on-road vehicles, highway safety, and intercity travel becomes a huge challenge for the people living around the world.

It is reported that each year approximately 1.25 million people are killed on roadways around the world. Each day an estimated 3400 people are killed globally in road traffic crashes involving cars, buses, motorcycles, bicycles, trucks or pedestrian. Half of the number of fatalities involved pedestrians, motorcyclists, and cyclists. These alarming numbers have rendered road traffic

injuries to be the eighth leading cause of death for young aged people between 15-29 years. Current trends predict that by 2030, road traffic injuries will amount to 7% of the deaths worldwide [36].

Even though measures like seatbelts and airbags for crash prevention have been used worldwide the scenario of road traffic comes under heavy scrutiny due to the incompetence of these aforementioned devices to protect and provide adequate safety. Hence auto manufacturers have advocated the use of ADAS to minimize road accidents and ensure driver and passenger safety in all situations. These ADAS systems include devices like radar functioning in different ranges, cameras for rear and front viewing, ultrasonic transducers for blind spot detection [37] and even LiDAR to assist the radar modules in shorter ranges depending on their intended application.

Radar has the unique ability of instantaneously detecting the velocity and range of the target objects via the Doppler shift of their radar signatures and can easily function in adverse climatic conditions like rain, snow, fog, and hail, unlike LiDAR and cameras. These specific benefits have driven the auto manufacturers to adopt radar in increasing numbers. In the US, the NHTSA entered in an agreement with 20 automobile manufacturers, representing more than 99 percent of the automotive market to voluntarily equip all production vehicles with Automatic Emergency Braking (AEB) Systems by 2022 [38]. As the vehicles progress from manually driven ones equipped with ADAS systems to fully autonomous driving the role of radar, LiDAR and cameras becomes increasingly important for sensing the environment around it for the vehicle to make

decisions. Future vehicles might include up to eight radar modules for a 360-degree coverage around a vehicle. [38]

2.2   Radar types

Depending on the requirements, a radar can use different techniques to generate the transmitted signal and identify the received echoes. Previously the radar systems were based on pulsed echo technology that required high power pulses. Even with their advantages of measuring the ranges accurately by calculating the time delay between transmitted and received signals, pulsed echo systems suffered from a drawback of false alarm and were mainly blind in shorter distances of (50-100 m) at the center of the radar. Continuous Wave radars continuously transmit the RF wave at a lower power level (typically less than 50mW) and a selected frequency. The CW radar systems continuously observe the return from a target over a period of time, commonly called the Coherent Processing Interval (CPI). During the CPI, the instantaneous transmit and receive signals are mixed, and the resultant intermediate frequency (IF) signal is assessed over the CPI for valid targets. The CW radar technology is still under constant refinement with new strategies related to both hardware and signal processing algorithms being developed. There are two prime implementations of CW radar: FH- (Frequency Hopping) or FSK-CW (Frequency Shift Keying) radar and FM-CW (Frequency Modulated) radar. In FSK-CW the RF jumps between multiple frequencies over a CPI, whereas FM-CW makes use of a frequency chirp in a sine, saw-tooth or triangular fashion [12].

The German Federal Ministry of Education and Research abbreviated as (BMBF) funded the joint project "Automotive High-Frequency Electronics KOKON" [39] was initiated (September 2004 - August 2007) due to the short range regulation in Europe and a phased array frequency modulated continuous wave (FMCW) systems with beamforming and beam steering capability became the technology of choice for the forward ranging application. The FMCW technique is advantageous as the received signal is a time-delayed copy of the transmitted signal where the delay, Δt is related to the range. The received signal always sweeps through a frequency band at any moment during the sweep, the frequency difference, f_b (beat frequency) is a constant between the transmitted and the received signal. Since the sweep is linear one can derive the time delay from the beat frequency and translate the delay into the range. Key advantages provided by FMCW based phased array radar are:

- Low power

- Beam steering capability without mechanical rotation of the mounted base

- Reduced clutter and phase noise

- High precision in measurement of target range and velocity

- More immune to interference from devices working in a similar frequency

- No theoretical blind spot

2.3   Microelectronic beamforming

The beamformer is a device when used in conjunction with a sensor array helps to provide a versatile form of spatial filtering. In other words, the module is

designed to direct the transmitted or received signal from an antenna array to a chosen angular direction to realize spatial selectivity. When in transmitting mode a beamformer directs the amount of phase and amplitude at each transmitter to create a pattern of constructive and destructive interference in the wavefront, while at receiving the information from different receiving sensors the information is combined in a way where the expected pattern of radiation is preferentially observed.

High directivity is often desired in communication systems, especially in automotive radars, in order to establish a low noise high fidelity link to collect ranging and velocity information in the direction of the signal source. In radar systems, the beamforming allows a process of electronic steering of the highly directive beam to detect targets with higher angular resolution. The beamforming network controls the phase and amplitude of the signal at each transmitting element in order to form a pattern of constructive and destructive interference in the wavefront.

2.4 Types of Microelectronic Beamforming

Microelectronic beamforming is a process of both generation and steering of a directional pattern of the main lobe in the azimuth and elevation planes and can be categorized in two different modes:

- **Analog beamforming**:

Analog beamforming refers to the combination of the received signals from each element at a carrier frequency level. Beamforming controls both the amplitude and the phase directed to each element of the antenna array. A combination of

phase and amplitude control can facilitate better adjustment of side lobe levels and steer nulls to minimize false alarm and no detection.

In a beamforming network, the signals fed at each individual element are combined methodically through electronic means to form a single desired beamformed output. Before the incoming signals are formed, they are brought down to baseband or intermediate frequencies. Receivers connected at the output of individual element perform the necessary frequency down conversion. Hence it becomes imperative for the digitization of the down-converted signal before they are processed. Analog to Digital Converters (ADC) are connected to the outputs for this purpose. For accurate performance, they are required to provide an accurate translation of the RF signal from analog to digital domain.

Auto manufacturers like BOSCH™, Delphi™, TRW™, Fujitsu Ten™, and Denso™ have all used the analog beamforming technology in their 77 GHz Long Range Radars. Other manufacturers like Mitsubishi electric™ and Celsius Tech™ used mechanical mechanisms in conjunction with ADCs to steer the beam in azimuth. [16]
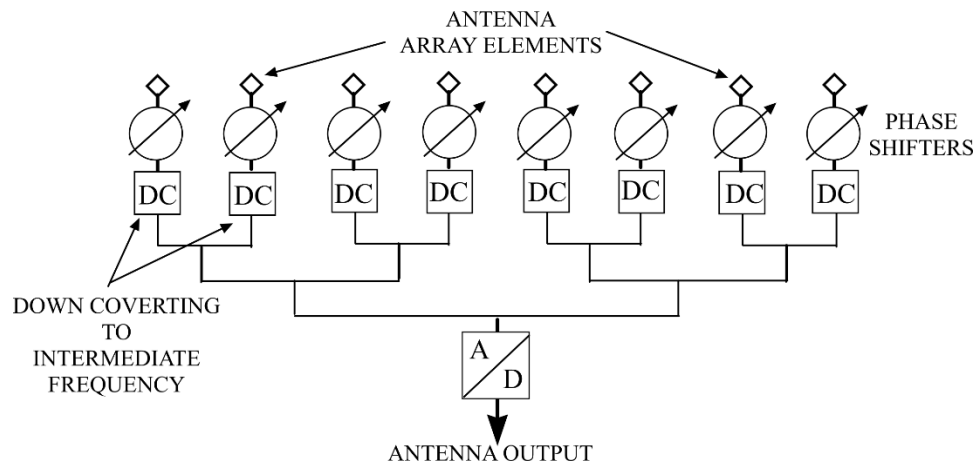
Figure 2.1 Analog Beamforming.

- **Digital beamforming**:

In Digital beamforming, the operations of phase shifting, amplitude scaling and summation for receiving of individual antenna element are done digitally. Multiple independent beams can be transmitted in all directions which can be steered are formed in the digital beamforming processor. The benefits of digital beamforming are:

o Multiple beams can be controlled

o Improved dynamic range

o Improved and faster control of phase and amplitude

Although the digital beamformer requires memory blocks, adders and multipliers as system building blocks to function yet it is considered to be more efficient than an analog beamformer [40]. Digital beamforming utilizes many digital receivers that can be utilized. Converting to an intermediate frequency by digitizing the signal is realized at each antenna element. Figure 2.2 shows a digital beamforming network. In 2003 radar sensors with digital beamforming was introduced in the market by Japanese companies. Denso built a bistatic LRR with planar patch antennas with a range capability up to 150 m and a field of view of approx. ±10 degrees. [41]
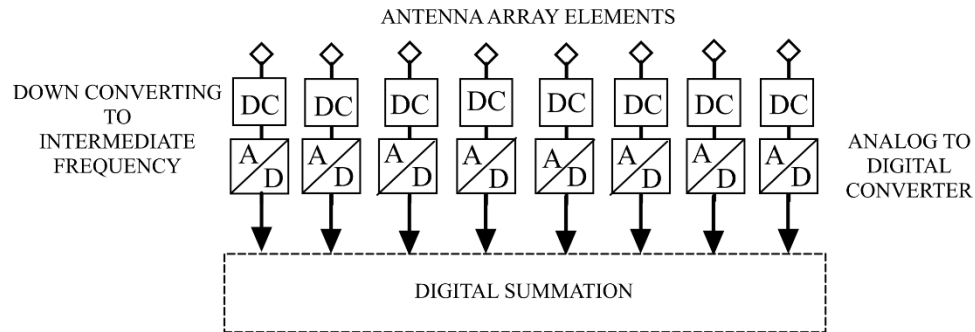
Figure 2.2 Digital beamforming network.

- **Butler Matrix and Rotman lens beamforming:**

The Butler Matrix is a microwave network, normally employed in beamforming and scanning networks for linear and circular antenna arrays [42]. This feed network typically is in the form of Figure.2.3, which is an N input and N connection. A Butler matrix can also have N inputs with N outputs. It comprises of different hybrid junctions and phase shifters that can be implemented with discrete microwave techniques such as waveguides and also as a microstrip technique.

Main features of Butler Matrix are:

o   The Butler matrix has 2^n inputs and 2^n outputs

o   It has (N/2) $\log_2$ N hybrid junctions, where N=2^n

o   The outputs are Fourier transform of the inputs

o   The schematic of the Butler Matrix is identical with the programming structure for the Fast Fourier Transform
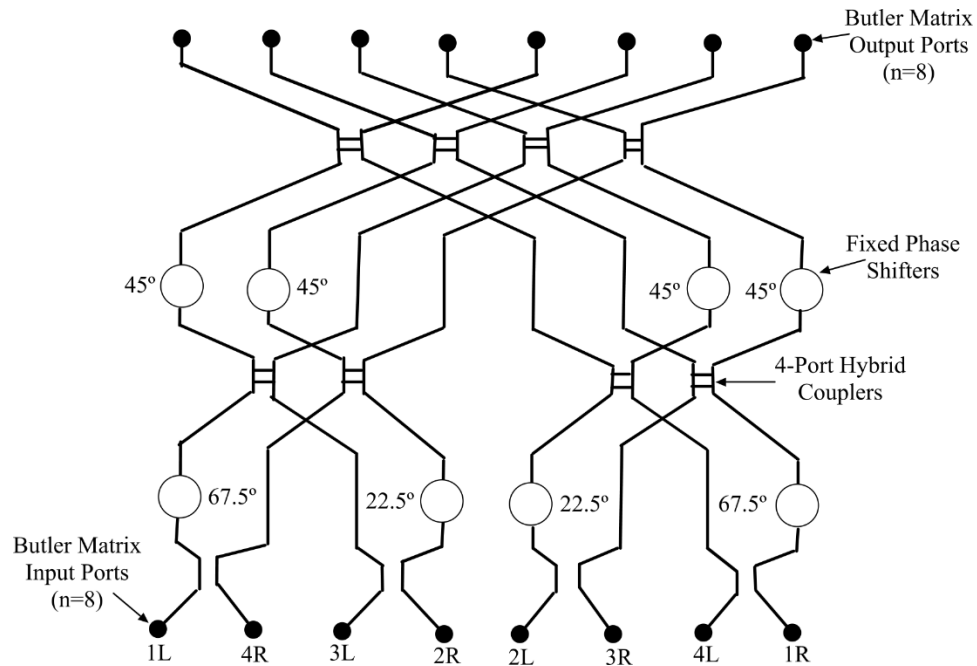
Figure 2.3 Eight input and eight output port Butler Matrix.

If a Butler matrix is connected to an antenna array, the matrix will act so that the array will have a uniform amplitude distribution and a constant phase difference between neighboring elements:

$$\exp(-jknd_x u_i) \tag{2.1}$$

For $u_i = \left(\frac{\lambda}{Nd_x}\right)i$. where $i = \pm\left(\frac{1}{2}, \frac{3}{2}, \frac{5}{2}, ...\right)$ for N even and $i = \pm(0,1,2,3,...)$ for N odd.

This results in radiation at one of N unique discrete directions covering a 180⁰ angular sector of space figure 2.3. The actual direction of the beams is dependent on which one of the input the signal is introduced. The phase difference between radiating elements for a Butler Matrix with N elements and the pth beam location is given by [42]

$$\psi_n = \frac{2\pi d}{\lambda}\cos\alpha = \pm\frac{2p-1}{N}\times 180^\circ \tag{2.2}$$

Where the phase difference, ψ_n is plus or minus depending upon whether the beam is to the right or left of the broadside respectively. Equation (2.2) depends on λ, therefore the beam angles u vary with frequency. The Butler matrix thus forms phase steered beams which squint with frequency. The beam cluster is narrow for higher frequencies and broad for lower frequencies.

Rotman Lens: Much like the previously discussed Butler matrix, a Rotman lens also offers an inexpensive and compact solution to extend the single beam systems to fully beamsteering modules. The microstrip line flexibility and the fast simulation packages allow the Rotman lens to be designed at millimeter wavelengths. A Rotman lens offers beam steering and beamforming advantages without any requirement of a microelectronic signal processing network unlike the analog and digital beamforming networks. Figure 2.4 shows a Rotman lens design geometry designed at the University of Windsor [43].
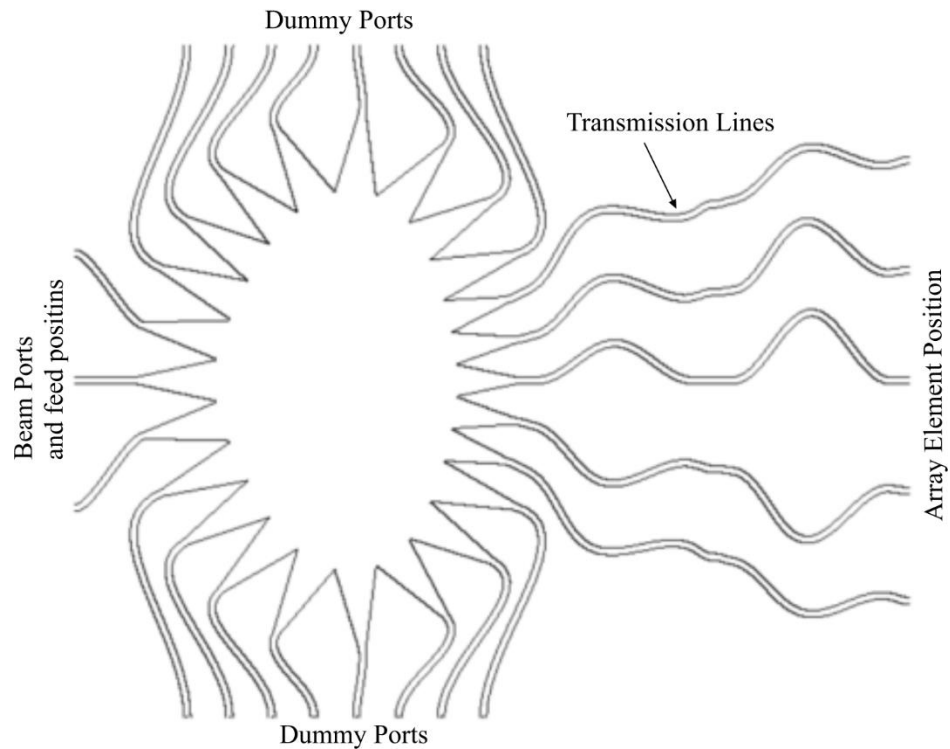
Figure 2.4 Rotman Lens.

2.5 Antenna Arrays

Antenna arrays play a crucial role as it acts as a radiating and receiving unit of the radar systems. Planar antenna arrays can satisfy the automotive radar market demands of low-profile, low weight and fast beam steering ability at a lower cost. The antenna array parameters like gain, bandwidth, and radiation efficiency mark the performance of the antenna array. Microstrip antennas are traditionally preferred as radar antennas as they are light in weight, easily manufacturable and also inexpensive. However, even with their benefits of simpler low cost fabrication, the microstrip antennas are historically have been recognized to provide lower gain. A gain of 8 dBi per patch is considered to be standard in terms of performance provided by the antenna [44]. However, research work conducted in [45] reports a microstrip antenna gain of 12 to 12.60

dBi. It is extremely difficult to design an antenna with high gain, necessary beam directivity and HPBW at the same time maintaining all specifications set by the automotive industry. Hence, the auto manufacturers rely on antenna arrays which is a group of similar radiating structures made to work in unison.

Modern effective techniques of utilizing a beam steering beamforming device like Butler Matrix or Rotman lens can aid in steering the beam to the desired angle to get an effective angular coverage as necessary for a specific safety requirement. The Butler Matrix can help in directing the beams in different directions as desired. In addition, the idea of utilizing a Butler matrix provides a uniform amplitude distribution and the constant phase difference between the neighboring elements while ensuring a low cost manufacturing. Thus the combination of a Butler matrix and a microstrip antenna array can provide a high performance low cost solution for multi range automotive radars. Figure 2.5, presents the proposed Butler Matrix and the microstrip antenna array combination as an integral part of an automotive radar
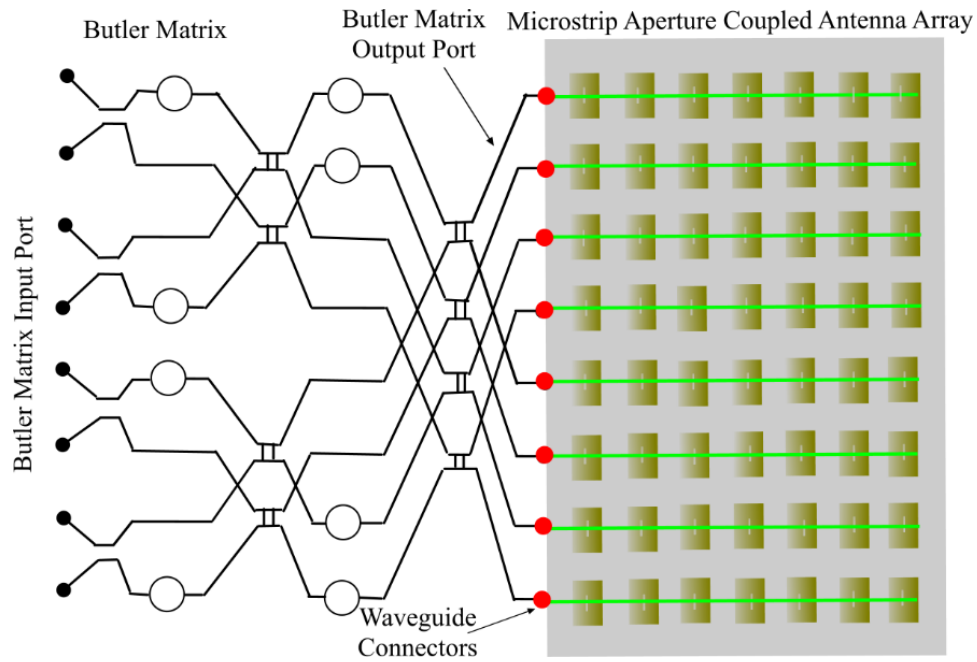
Figure 2.5 Butler Matrix with Microstrip Aperture Coupled Antenna Array.

2.6 State of the art Automotive Radar

Since its first successful test in 50's, the automotive radar manufacturers have continued massive development and slowly have ventured into the microwave frequencies. From 17 GHz to 24 GHz, systems slowly shifted their operating frequencies and have ventured into 77 GHz with a prediction of systems working at 79 GHz in the future years. The main reason for choosing a high frequency for automotive radar application is due to the available bandwidth at higher frequencies and the formation of the highly directive beam with lower HPBW at higher frequencies necessary for long range applications like collision avoidance and cruise control without any health hazard.

Even the short range radar industry has slowly drifted towards the 79 GHz operating frequency with a bandwidth of 4 GHz from 77 to 81 GHz centered at 79

GHz [19]. The reason for the shift is mainly due to the lack of bandwidth available for the previously chosen 24 GHz band and also a high frequency determines a high directive beam which can be easily steerable without a false alarm. Higher bandwidth is necessary for shorter and mid ranges as they create enough number of samples to obtain a very high resolution which results in improved detection of the nearby proximity of obstacles.

Quite a few specifications have been set by the automotive radar industry for the radar designers on the basis of the mode of applications of these devices. Long and mid range radars have typically lower bandwidth compared to a short-range radar since the target resolution output is not required to be high. Table 2.1 shows the specifications set by the automotive radar industry for short, mid and long-range radars. A modest 0.5-0.72 m for midranges while 0.5-1 m for long-range radars are desired by the auto industry [46] [20]. A 4 GHz dedicated bandwidth is expected to provide for a high resolution as much as ~0.1 m which is ideally required for short range applications [29]. Most long range radars are currently functioning at 76-77 GHz frequency band with 1 GHz of bandwidth allocated for the application. The reason for the lowered bandwidth allocation is due to lesser resolution requirement for the long range mode. [47].

Table 2.1 Radar Classifications [47]

Radar	Frequency	Bandwidth	Angle of coverage	Range	Resolution
SRR	77-81	4 GHz	±20-50º	0.15-30 m	~0.1 m
MRR	77-81	4 GHz	±6-10º	1-100 m	~0.5 m
LRR	76-77	1 GHz	±5-7.5º	10-250 m	~0.5 m

The idea of automotive radar was driven ahead due to the necessity to build a system detecting and preventing a collision, the idea has provided enormous motivation for many engineers over the past decade to provide the world with a smart autonomous vehicle capable of preventing collision and maintain on-road safety [23]. Applications like parking assist collision avoidance and cruise control were among the first ones to be tested with fully functional automotive radar sensors. In the 90's, Greyhound was among the first group of bus companies who installed more than 1600 radar systems functioning at 24 GHz in their bus lines. The idea of radar installation was a massive success as it brought the reduction of accidents by 21 percent in 1993 from the previous year. In 1999, Mercedes introduced the 77 GHz "Distronic" into the S class. Other auto manufacturers like BMW™ in their 7 series, Jaguar™ (XKR. XK6) Cadillac™ (STS, XLR), Audi™ A8 also started installing ACC systems. Automakers like Honda™ CRV (2015) to the more recent version of Honda™ Odyssey (2018), Alfa Romeo™ Giulia (2016), Audi™ Q5 (2013), Chrysler™ Pacifica (2017), Ford™ Fusion (2017), Lincoln™ Continental and MKZ (2017), Mazda™ CX-5 (2016) etc. have all installed fully functional radar-based adaptive cruise control to help facilitate stop and go and assist in lane change [48]. Various car manufacturers and suppliers are developing optimized sensor configurations according to the requirements set by the auto industry. The table provides with a few details about various sensors available in the market manufactured by some of the biggest automotive radar manufacturing companies.

Table 2.2 Automotive Radars Available

Company	Frequency	Radar Type	Range of Coverage	Relative velocity	Field of view
TRW (AC20)[49]	77 GHz	LRR	1-200 m	±60	±8
Delphi (ESR)[50]	76.5 GHz	LRR	1-175 m	±20	±20
Denso[51]	77 GHz	LRR	2-205 m	±50	±10
Fujitsu-Ten[52]	76~77 GHz	LRR	2-170 m	-25 to 70	±8
BOSCH (LRR4)[20]	77 GHz	LRR	0.3-250 m	-75 to +60	±30
Mitsubishi electric[53]	76~77 GHz	LRR	0-120 m	-25 to +55	±8

From all the manufacturers listed in table 2.2 BOSCH™ claims to have the world smallest Radar sensor package the LRR4 version (launched in 2017) with dimensions 74 mm x 77 mm x 58 mm [20].

2.7 State of the art antenna array

This section provides an overview of the state-of-the-art in antennas for automotive radars. In this section, the long range radar antennas would be discussed and the ongoing research work being undertaken in this domain has been highlighted.

The design process of an antenna array can be challenging as it requires combining the state-of-the-art antenna technology to the automotive radar requirements while ensuring the performance improvement of the overall radar system performance. Antenna array comes in a large variety of different geometries i.e. microstrip inset fed structures, coaxial cable fed, aperture coupled

antennas working at a prescribed frequency for providing adequate bandwidth and desired radiation patterns.

Table 2.3 State-of-the-art antenna arrays for automotive radars

YEAR	CENTER FREQUENCY	RADAR	ANTENNA	ANGLE	GAIN	BW
2010 [54]	77 GHz	LRR	Rectangular Microstrip (8x8)	±9°	20 dBi	1 GHz
2012 [23]	77 GHz	LRR	Rectangular Microstrip (5x14)	10⁰	20.5 dBi	1.5 GHz
2013 [55]	77 GHz	LRR	Varying Patch dimensions (8x18)	±40°	20.8 dBi	1 GHz
2014 [56]	80 GHz	LRR	Varying Patch dimensions (16x16)	±50°	25.6 dBi	1.5 GHz
2015 [57]	76.5 GHz	LRR	Varying Patch dimensions (2x1)	±15°	18.5 dBi	2.4 GHz
2016 [58]	77 GHz	LRR	Microstrip combline fed (32x32)	10⁰	24.7 dBi	700 MHz

2.8   Summary

The state of the art of the automotive radar system and antenna arrays provide the objective for this thesis and set the goals for efficiency and performance of the antenna array required for the current automotive radar systems available.

This chapter presents the basic theory behind the microstrip patch antenna, an analysis of them and their feeding methods that are essential for the antenna presented in this thesis. A review of planar antenna theory is also presented as the target microstrip antenna array will have a planar configuration for its better performance in conjunction with a Butler matrix. Finally, this chapter presents a design methodology of microstrip antenna arrays for use in mid and long range radars for automotive applications.

3.1 Microstrip Patch Antenna

Microstrip antennas are most renowned for its simple design, small size, planar configuration, low cost in manufacturing and easy integrability with transceiver modules. Therefore it is chosen by various antenna designers around the world when comes to design integrated antennas. Due to their excellent features, it has been a popular choice not only in the automotive sector but also in various other industries. Government, military and even medical facilities are leading research initiatives for the development and deployment of microstrip antennas in wearable communication systems [59] for improving system portability and ease of constant monitoring of a target system. The advantages of these antennas have eased their usage in wireless communication, satellites, GPS systems, Radio Frequency Identification (RFID), Worldwide Interoperability for Microwave Access (WiMax) and Rectenna Applications [60].

A microstrip antenna operates in a similar method as a resonant cavity where the metal patch forms the top of the cavity while the ground plane is the bottom of the cavity. The edges of the patch form the sides of the cavity. The edges of the metal patch electrically behave like an open circuit boundary condition. Thereby, resulting the patch acting almost like a cavity with perfect electric conductors on the top and bottom surfaces and a perfect magnetic conductors on the sides. For an effective antenna performance, a thick dielectric substrate with a low dielectric constant is desirable as it provides a better efficiency, larger bandwidth and higher gain [61]. However, such an antenna configuration leads to increased antenna dimensions. Figure 3.1 shows a basic top and cross-sectional view of a microstrip patch antenna.
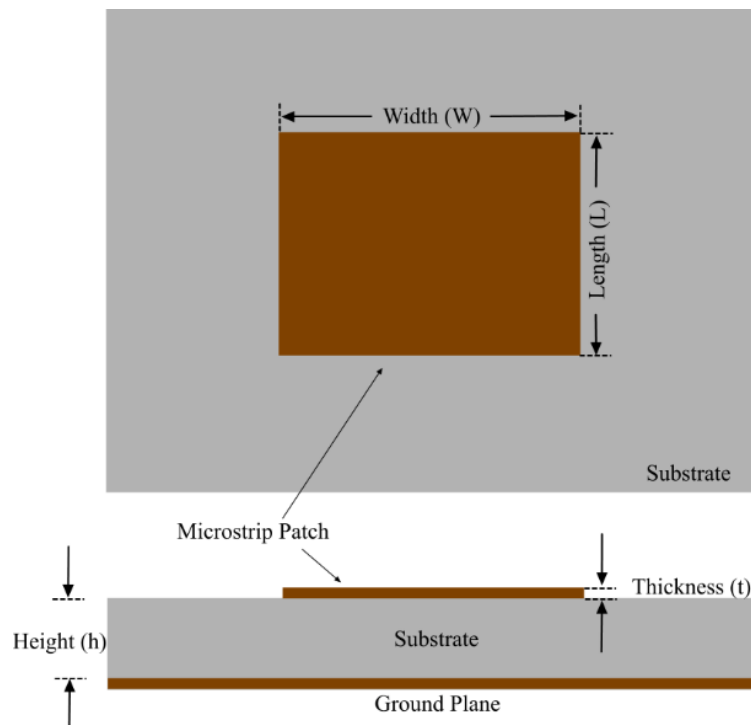
Figure 3.1 Microstrip Antenna top and cross-sectional view.

Various geometries have been chosen over the years as shapes of the metallic radiating patch. Square, rectangular, and circular geometry patches made of highly conductive materials such as gold and copper have been extensively researched over the years [23] [62] and have been widely used due to their simple geometry that facilitated low cost fabrication.

Square

Rectangular

Circle

Triangular

Circular Ring

Ellipse
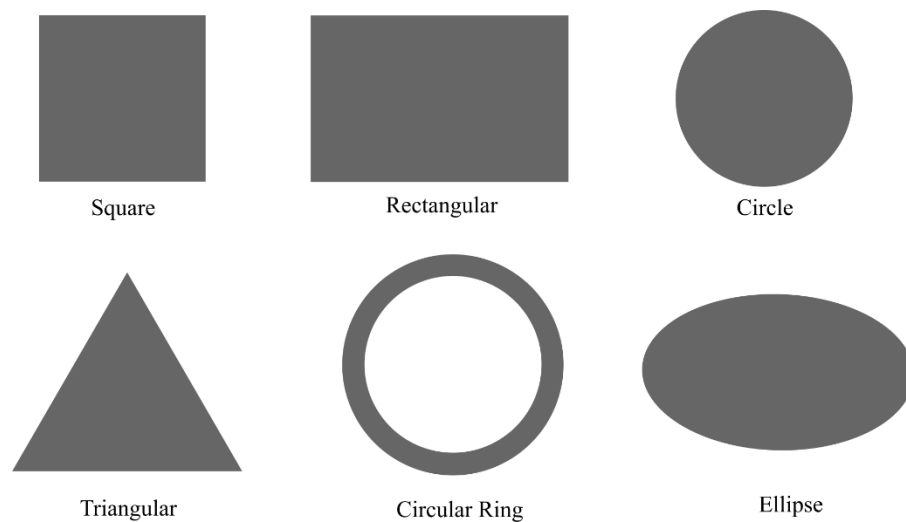
Figure 3.2 Microstrip antenna patch geometry

While Rectangular, square and circular geometries are widely chosen for their simplicity and effective performance there are other geometries which have also been used as antenna radiating patch geometries over the years. Figure 3.2 shows different geometries which have been used as radar and communication antennas. For the target application, a rectangular geometry patch has been chosen as the radiating element as it provides the largest impedance bandwidth compared to the other available geometries.

3.2 Basic Principle of Operation

The basic cause of radiation produced by the microstrip antennas is due to the fringing fields between the patch edge and the ground plane. There are many ways of analyzing a microstrip patch antenna and the most popular ones are the transmission line model, the cavity model, and the full-wave model. The transmission line model is the simplest among the three and it gives proper physical insight but is less accurate compared to the other methods [63]. The cavity model is more accurate compared to the transmission line model but is more complex. The full wave model is extremely accurate, versatile and can evaluate single element, finite and infinite arrays, stacked elements, arbitrary elements and element coupling. This model is perfect when compared to the previously mentioned ones but is far more computationally intensive [63] often needing 3D finite element method (FEM) based solvers. In this thesis the transmission line model has been utilized to determine initial specifications of the proposed structure which is then optimized using full wave analysis in a software (Advanced Design Systems (ADS™) based on the method of moments (MoM).

3.2.1 Transmission Line Model

The transmission line model represents the microstrip antenna by two slots of width (W) and height (h), separated by a transmission line of length (L). The microstrip antenna is a non-homogenous line of two dielectrics the substrate underneath the patch and the air. Hence, from the figure, it can be expressed that most of the electric field lines are confined in the substrate and some parts of the lines are in the air. Due to this fact, the transmission line cannot support pure

transverse electromagnetic (TEM) mode of transmission since the phase velocities would be different in the air and the substrate. Hence, the dominant mode of transmission becomes the quasi TEM mode. An effective dielectric constant (ε_{eff}) has to be obtained to account for fringing effect and the wave propagation in the line. The value of ε_{eff} is slightly less than the dielectric constant ε_r because of the fringing fields around the periphery of the patch is not confined to the dielectric substrate but also spread in air as shown in Figure 3.3. Following [63], the effective dielectric constant ε_{eff} can be expressed as:

$$\varepsilon_{\text{eff}} = \frac{\varepsilon_r + 1}{2} + \frac{\varepsilon_r - 1}{2} \left[1 + 12 \frac{h}{W} \right]^{-\frac{1}{2}} \tag{3.1}$$

where ε_{eff} is the effective dielectric constant, ε_r is the dielectric constant of the substrate, h is the height of the dielectric substrate, and W is the width of the patch.
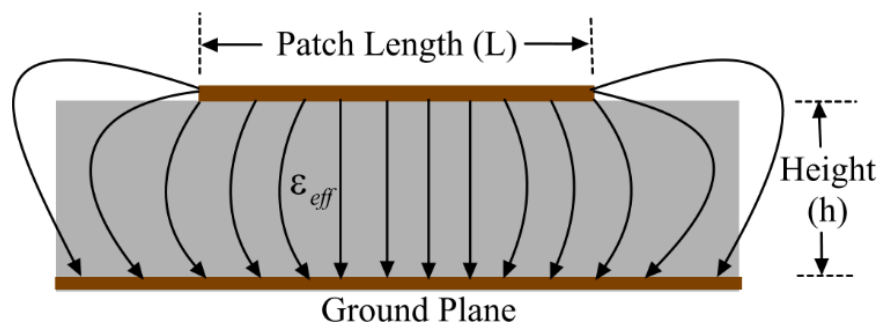
Figure 3.3 Effective dielectric constant and fringing effect [63]

Figure 3.4 shows a basic microstrip aperture coupled antenna with the length (L), width (W), and feedlines marked in the figure. A substrate height of h is chosen to house the microstrip antenna and a dielectric cavity is etched

underneath the radiating patch. The coordinate axis is selected such that the length is along the y-axis, the width is along the x-axis while the height of the structure is along the z-direction.
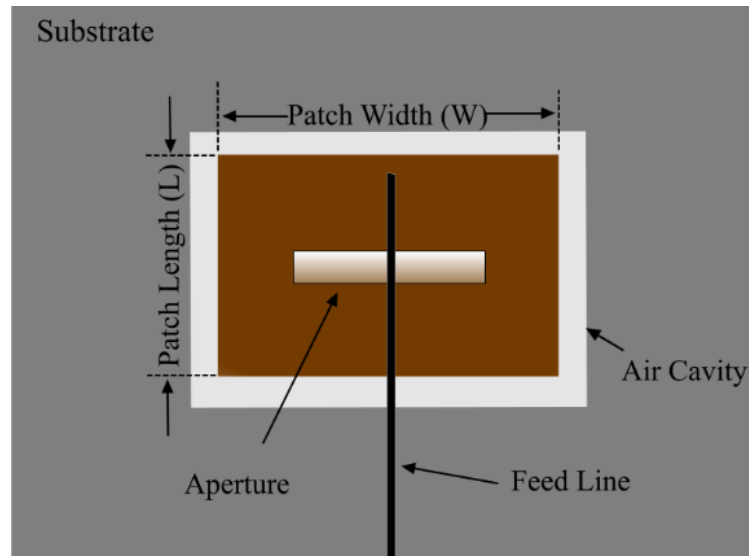
Figure 3.4 Aperture Coupled Microstrip Antenna Geometry.

In order to make the antenna function in the TM10 mode, the length of the patch must be less than $\lambda_g/2$ where λ_g is the guided wavelength or the wavelength in the dielectric medium and can be expressed as $\lambda_o/\sqrt{\varepsilon_{eff}}$ where λ_o is the wavelength in free space. The TM10 mode refers to that the field varies one $\lambda_g/2$ cycle along the length of the patch with no variation in its width. The figure 3.5 shows the microstrip patch antenna is represented by two slots separated by a transmission line of length L and open circuited at both ends. The voltage is maximized while the current is minimized along the width of the patch due to open ends. The fields along the edges can be resolved in tangential and normal components with respect to the ground plane.
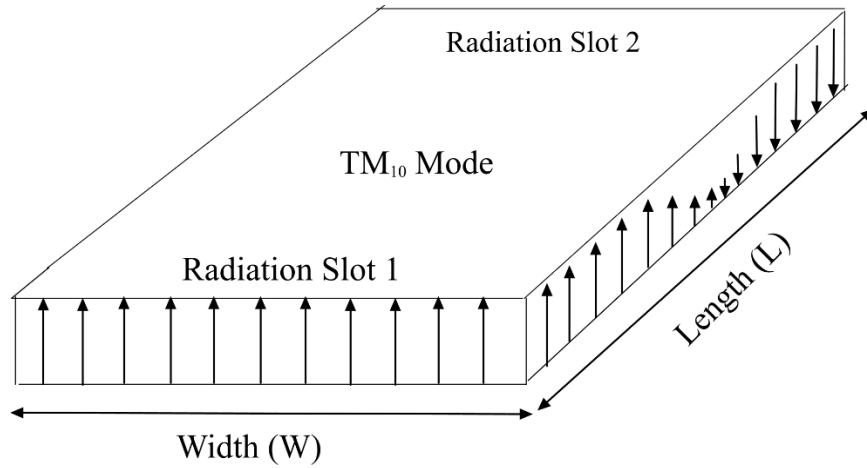
Figure 3.5 Transmission Line model with two rectangular slots [23].

3.2.2 Cavity Model

The cavity model was first introduced by Lo in 1970 [64]. This model is more complex than the transmission line model and more accurate. This model identifies the region inside patch as a cavity bounded by electric walls on both sides while the magnetic wall is considered through the periphery.
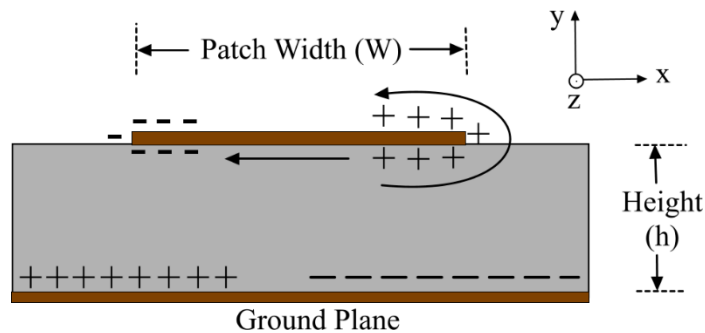
Figure 3.6 Cavity Model Charge distribution [63].

The charge distribution can be seen from the Figure 3.6 with the upper and lower surfaces of the patch and the bottom ground is due to the power supplied to the microstrip patch. As mentioned by Lo in his research that this phenomenon is due to two mechanisms- the attractive and repulsive mechanisms. The attractive

mechanism is due to the attraction of the opposite charges underneath the patch and on the top of the ground plane. This phenomenon maintains the charge concentration underneath the patch. While the repulsive mechanism is between the similar charges underneath the patch which causes some of the charges to push to the top of the patch. As a result of this movement, current flows at the top and bottom surface of the patch [58]. The assumption is based on the following observations for thin substrates ($h \ll \lambda$):

- Due to the substrate being thin the fields in the interior do not vary normally to the patch.
- The electric field is directed as normal to the patch while the magnetic field is divided into the transverse components of H_x and H_y in the region bounded by the patch and the ground plane.

Since the cavity material and its walls are considered as lossless, the cavity is unlikely to radiate as its input impedance would be purely reactive. Therefore to account for radiation and loss mechanism, a radiation resistance R_r has to be introduced along with a loss resistance R_l. Correspondingly the cavity starts acting like an antenna and the effective loss tangent δ_{eff} is given as:

$$\delta_{eff} = \frac{1}{Q_t} \qquad\qquad (3.2)$$

Where Q_t is the antenna quality factor and can be expressed as in [64]

$$\frac{1}{Q_t} = \frac{1}{Q_d} + \frac{1}{Q_c} + \frac{1}{Q_r}$$ (3.3)

Where Q_d is the dielectric quality factor:

$$Q_d = \frac{\omega_r W_T}{P_d} = \tan^{-1}\delta$$ (3.4)

Where, ω_r is the angular resonant frequency, W_T is the total energy stored in the patch at resonance, P_d is dielectric loss and $\tan\delta$ loss tangent of the dielectric substrate.

The Q_c represents the conductor quality factor and can be expressed as:

$$Q_c = \frac{\omega_r W_T}{P_c} = \frac{h}{\Delta}$$ (3.5)

Where h is the substrate height, Δ is the skin depth of the conductor, P_c is the conductor loss.

Q_r, the radiation quality factor can be expressed as:

$$Q_r = \frac{\omega_r W_T}{P_r}$$ (3.6)

Where P_r is the power radiated from the patch.

After substituting eq (3.5)-(3.6) in eq (3.7) the effective loss tangent can be expressed as:

$$\delta_{eff} = \frac{1}{Q_T} = \tan\delta + \frac{\Delta}{h} + \frac{P_r}{\omega_r W_T} \qquad (3.7)$$

3.2.3 Full-wave Model

The Full wave model is a complex model compared to the cavity and the transmission line model. This model is essentially based on the idea of Method of Moments. In this method, the surface currents are used to model the patch and the volume polarization currents are used to model the fields in the dielectric slab. Newman and Tulyathan [65] published a theory on forming integral equations from these currents using the method of moments. These integral equations are converted into matrix equations which can be solved to provide the result.

3.3   Radiation Conductance

The rectangular microstrip antenna can be expressed in an equivalent transmission line model. The equivalent circuit represents the whole antenna in the form of two radiating slots modeled using parallel R-C circuits and the patch connecting these RC circuits is in the form of a transmission line whose characteristics are computed in a similar manner as a normal microstrip transmission line. Figure 3.7 shows a simple equivalent circuit transmission line model of a microstrip patch antenna.
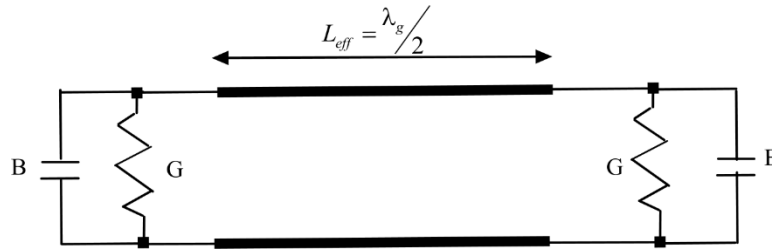
Figure 3.7 Equivalent circuit transmission line model of a simple microstrip patch [23].

In figure 3.7, G is the radiation loss and B is the equivalent susceptance, which represents the capacitance of the slot. Since both edges are identical the value of edge conductance can be written as:

$$G = \begin{cases} \dfrac{1}{90}\left(\dfrac{W}{\lambda_0}\right)^2 & W \ll \lambda_0 \\[2em] \dfrac{1}{120}\left(\dfrac{W}{\lambda_0}\right)^2 & W \gg \lambda_0 \end{cases} \tag{3.8}$$

Where, λ_0 is the free space wavelength.

3.4   Input Impedance

The total admittance produced at one radiating slot is determined by transforming the admittance at the other radiating slot using transformation equations of the transmission line. Figure 3.8, shows the circuit model after $\lambda_g/2$ transformation
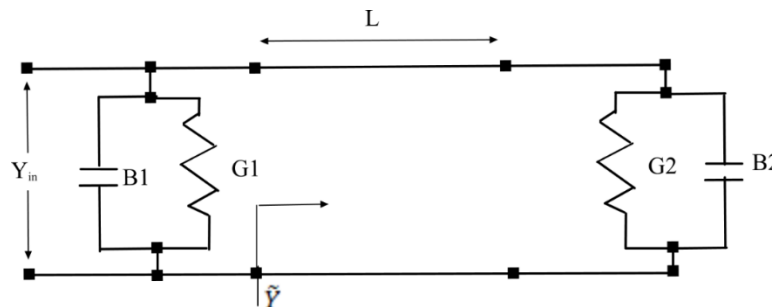
Figure 3.8 Transmission Line model [23].

The admittance at each slot is identical

$$Y_1 = G_1 + jB_1 \tag{3.9}$$

The total real resonant input admittance is given by [63]:

$$Y_{in}\left(L_{eff} \approx \lambda/2\right) = B_1 + G_1 - B_1 + G_1 = 2G_1 \tag{3.10}$$

Where the total input impedance at resonance is expressed as

$$Z_{in} = \frac{1}{Y_{in}} = R_{in} = \frac{1}{2G_1}$$

Taking into consideration the mutual conductance

$$R_{in} = \frac{1}{2(G_1 + G_2)} \tag{3.11}$$

Where,

$$G_{12} = \frac{1}{120\pi^2} \int_0^\pi \frac{\sin^2\left(k_0 W \cos\theta/2\right) \mathrm{J}_0\left(k_0 L \sin\theta\right) \sin^3\theta}{\cos^2\theta} d\theta \tag{3.12}$$

3.5   Fringing Effect

The fringing field around the edges of the microstrip patch is the extended parts of the electric field which does not abruptly end at the edge of the microstrip patch. The fringing fields result in the microstrip patch in obtaining an increased length due to the fields extending over the original length of the microstrip patch.
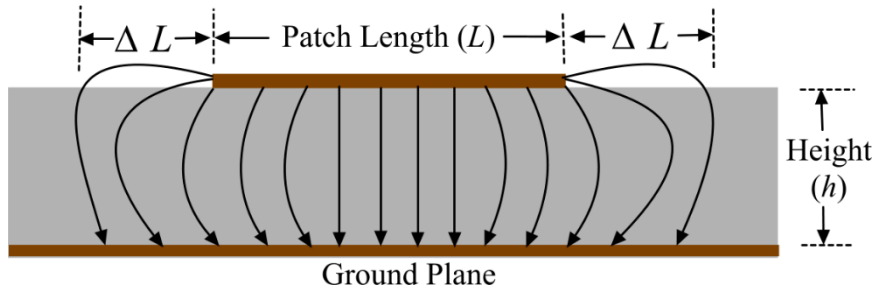
Figure 3.9 Length of the patch increased due to the fringing effect.

Figure 3.9 shows the increase of the patch length due to the fringing effect. The microstrip patch produces the normal components of the electric field along the edges of the width which are in opposite direction and thus out of phase and therefore they cancel each other in the broadside direction. However, the tangential components are in phase which results in their adding up to produce a maximum radiated field normal to the surface of the microstrip patch. Hence the edges along the width can be represented as radiating slots which are $\lambda_g/2$ apart, excited in phase and radiating in half space above the ground plane. The fringing effects make the microstrip antenna look greater than its physical dimensions. This is demonstrated as where the dimensions of the patch along its length have been extended on each end by a length ΔL. The increased length of the patch due to fringing can be expressed as [63]:

$$\Delta L = 0.412h \frac{\left(\varepsilon_{\text{eff}} + 0.3\right)\left(\dfrac{W}{h} + 0.264\right)}{\left(\varepsilon_{\text{eff}} - 0.258\right)\left(\dfrac{W}{h} + 0.8\right)} \tag{3.13}$$

Hence utilizing (3.14) we can come to the effective length of the patch which is

$$L_{\text{eff}} = L + 2\Delta L \tag{3.14}$$

3.6   Antenna Parameters

This section discusses the overview of the antenna patch design parameters which identifies the performance of the patch antenna. For designing a desirable performing antenna these parameters play a key role along with dimensions of the structure.

3.6.1 Return Loss and VSWR

In communication, return loss is defined as the loss of signal power due to the reflection at a discontinuity in a transmission line. The discontinuity can arise from a mismatch between the feedline and the port or with a device inserted in the line. The return loss is related to both voltages standing wave ratio (VSWR) and the reflection coefficient (Γ) or S11. The increase of return loss corresponds to the increase of VSWR which is undesirable in a higher magnitude.

VSWR is a measure of the efficiency of RF power transmission through a transmission line. An ideal transmission line should have a VSWR of 1 with the entire amount of power getting transferred without any reflection. In practical cases, any value of VSWR to a magnitude of 2 is also considered to be satisfactory.

The reflection coefficient (Γ), it is the ratio of the amplitude of the reflected wave (V_0^-) to the amplitude of the incident wave (V_0^+). Return Loss is a measurement of how well the devices or lines are matched and a match is good if the return loss is high.. The return loss is expressed in dB as [63]:

$$RL(dB) = -20\log|\Gamma| \tag{3.15}$$

Where the reflection coefficient Γ can be expressed as:

$$|\Gamma| = \frac{V_0^-}{V_0^+} = \frac{Z_L - Z_0}{Z_L + Z_0} \qquad (3.16)$$

Where, V_0^+ is the incident wave, V_0^- is the reflected wave and Z_L, Z_0 are the load and characteristic impedances. For practical applications, a VSWR of 2 which corresponds to a return loss of -9.54 is desirable [63].

3.6.2 Radiation pattern

The radiation pattern is a mathematical function or graphical representation of the antenna radiation properties as a function of space coordinates. Radiation properties include power flux density, radiation intensity, field strength, directivity, phase, or polarization. It is determined in the far field region and is represented as a function of the directional coordinates. The current flowing through the patch antenna is utilized for obtaining the far field radiation pattern. If the substrate underneath the patch is not considered for calculation of the far-field radiation pattern, the pattern can be found from image theory.
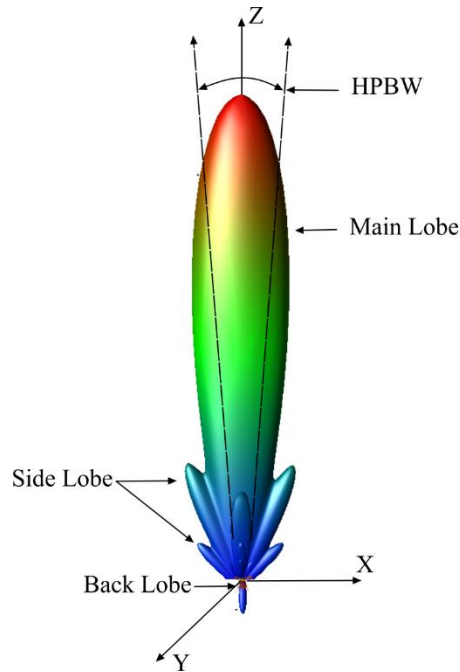
Figure 3.10 Radiation pattern of a directional antenna.

When the substrate is taken into consideration and is assumed to be infinite, the reciprocity method can be used to determine the far field radiation pattern [27].

Radiation pattern can be defined as the power radiated or received by an antenna in a function of the angular position and radial distance from the antenna. It describes how an antenna directs the energy it radiates. The figure 3.10 shows a common radiation pattern produced by an antenna which consists of the main lobe, side lobes, and a back lobe. Side and back lobes are energy radiated in unwanted directions as the antenna is expected to be utilized in the direction of its main lobe.

- **Main lobe**: It represents the part of the radiation pattern which comprises the maximum amount of energy radiated by the antenna.

- **Side Lobe**: The lobes apart from the main lobe are the energy wasted by the antenna in radiating in different directions. These structures are minor compared to the main lobe of the antenna due to the lesser power radiated in these directions. A significant lobe is observed in the opposite direction of the main radiation of the antenna and this is known as the back lobe. This lobe has the least amount of energy in its radiation.

- **HPBW**: HPBW or Half Power Beam Width is the width of the main beam of the antenna. It can be defined as the angle subtended by the half power beamwidth points of the radiation pattern. Generally, HPBW of an antenna is expressed as 3 dB beamwidth.

3.6.3 Gain

The Gain of the antenna is a measure of the capability of an antenna to radiate power in a constricted angular region of space. It is a very necessary quantity to determine the antenna performance as it denotes the capability of the antenna to concentrate energy through a specified direction. The quantity of gain is expressed in dBi where it is basically a ratio of the gain in dB to the gain of an isotropic antenna which radiates equally in all directions. The gain of a rectangular patch antenna can be expressed as:

$$G = \eta \times D \tag{3.17}$$

Where η is the radiation efficiency and D is the directivity of the patch antenna.

The directivity of an antenna is defined as the ratio between the radiation intensity in a given direction to the radiation intensity averaged over all directions

i.e. for an isotropic antenna. From the figure 3.10, the shape of the beam depends on the directivity of the antenna while the amount of power packed in the beam is due to the gain of the antenna.

3.6.4 Bandwidth

The bandwidth of an antenna specifies the range of frequencies over which its performance does not suffer due to a poor impedance match. Primarily, the term bandwidth refers to the frequency span from a low to a high frequency allocated for the device to operate in. At the higher frequencies, the bandwidth is broader for a given design similarly at lower frequencies the bandwidth is insufficient for antennas to function [66]. The bandwidth can be expressed as:

$$BW = \frac{f_H}{f_L} \tag{3.18}$$

$$BW(\%) = \left[\frac{f_H - f_L}{f_C} \right] \times 100 \tag{3.19}$$

A practical method of obtaining the bandwidth among antenna designers is to use the -10 dB frequencies in the plot of return loss.

3.6.5 Input Impedance

Input impedance plays an important role in determining the amount of power delivered to the feed line. A perfect impedance matching is necessary to transfer the maximum amount of power from the port to the feed line which it is connected to. A standard idea is to use a 50Ω feed line impedance to match a 50Ω port in connection. The main dimension which determines the feed line

impedance is the width of it. The feed line length and width of a microstrip aperture coupled antenna is shown in the figure 3.11 below.
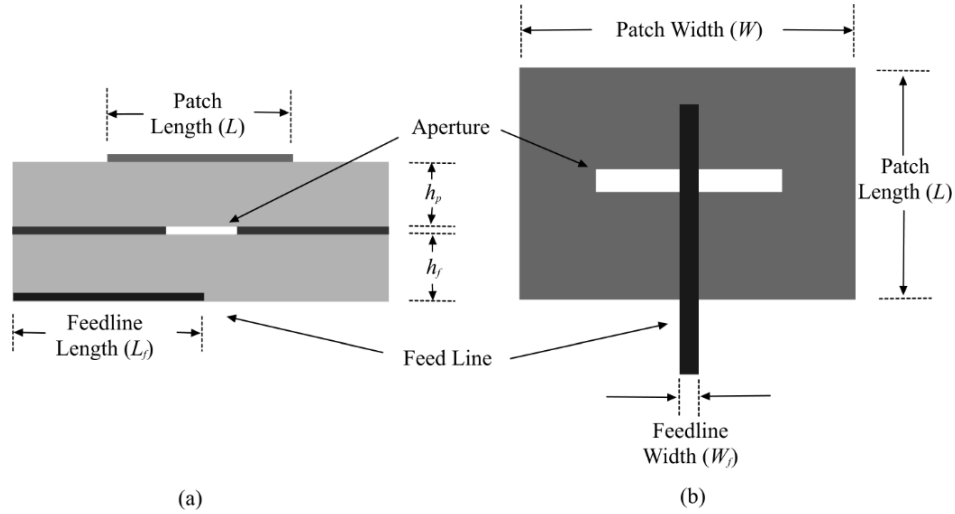
Figure 3.11 Microstrip Aperture coupled Antenna showing (a) cross-sectional and (b) top view of the feed lines.

Ref. [67] reports new techniques to find out feed line dimensions to ease the process of designing perfect impedance matched feed lines for various dielectric substrates used. The author in [68] reports a mathematical model to find the width of the feed line for an aperture coupled design of patch antennas. The feed line width can be iteratively solved from the expression of characteristic impedance and it is expressed as:

$$Z_c = \frac{1}{2\pi} \sqrt{\frac{\mu_0}{\varepsilon_0 \varepsilon_{\text{eff}}}} \ln\left(F \times \frac{h_f}{W_f} + \sqrt{1 + \left(\frac{2h_f}{W_f}\right)^2} \right) \qquad (3.20)$$

Where, $F = 6 + (2\pi - 6)\exp\left[-\left(30.666 \frac{h_f}{W_f} \right)^{0.7528} \right]$ \qquad (3.21)

3.6.6 Polarization

Polarization is defined as the property of an electromagnetic wave describing the time-varying direction and relative magnitude of the electric field vector [69]. The type of polarization is mainly dependent on the axial ratio of the radiated electromagnetic energy from the antenna. If the axial ratio is found to be between 0 to 1 in ideal cases it is believed to be purely polarized or have circular polarization. However, for practical cases, the magnitude of the ratio is considered till 3 for circular polarization [70]. If the axial ratio is found to be infinite then the wave is linearly polarized [23]. The linear polarization is also another pure form of polarization. Any value of axial ratio above the value of 3 is considered as elliptically polarized. It is practically very hard to realize a purely polarized wave. The types of polarization schemes are listed as:

- **Linear Polarization**: A linearly polarized antenna radiates entirely in a single plane containing the direction of propagation. Figure 3.12 shows a linearly polarized wave, the electric field vector remains constant in length but rotates around in a circular patch. Linear polarization can also be further classified into vertical and horizontal linear polarization as shown in the Figure 3.12.
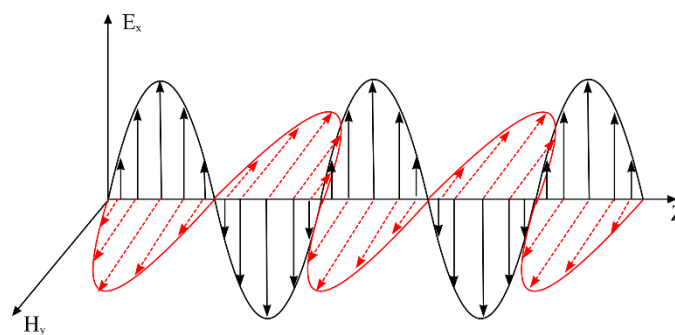
Figure 3.12 Linear Polarization.

- **Circular Polarization**: A circularly polarized wave has the electric field vector remains constant in length but rotates around in a circular path. Figure 3.13 shows a circularly polarized wave. The LHCP (Left Hand Circular Polarization) and RHCP (Right Hand Circular Polarization). The LHCP has the wave turning counter-clockwise while the RHCP is the opposite.
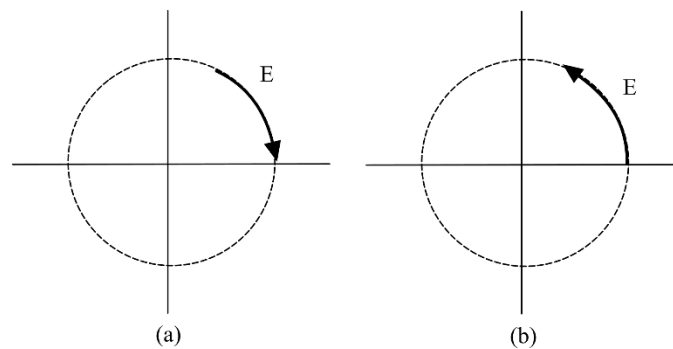
Figure 3.13 Circular Polarization (a) RHCP and (b) LHCP.

3.7 Antenna Array

A single microstrip patch antenna does not have enough ability to produce a highly directional beam with sufficient amount of gain. Hence the idea is to utilize multiple such antenna elements working in unison to provide for the requirements set by the antenna manufacturers. The antenna array provides multiple advantages as:

- Improves amount of gain produced by the antenna

- Improves directivity of the antenna

- Reduces number and level of sidelobes produced by the antenna

- Reduces the HPBW of the main lobe by focussing the beam in an intended direction.

The antenna array is of mainly two different types:

1.   Linear Antenna Array:

Antenna arrays geometrically structured in lines are known as linear antenna arrays. The elements are uniformly placed on a single axis connected by a single feeding mechanism thereby making them function in series to each other. Figure 3.14 shows a linear antenna array. The radiation pattern of the linear antenna array is the magnitude of the product factor and the element field [63].

$$AF = 1 + e^{j\psi} + e^{j2\psi} + e^{j3\psi} + ... + e^{j(N-1)\psi} \tag{3.22}$$

$$E_a(q) = \sum_{n=0}^{N-1} a_n \exp\left[j\left(\psi_n + nkd \sin\theta\right)\right] \tag{3.23}$$

Where, $\psi = -nkd \sin\theta_0$

Advantages of this array pattern:

- Simple and easy to design.

Disadvantages of this technique:

- This type of an antenna array can only scan the main beam in one polar plane (φ or θ)
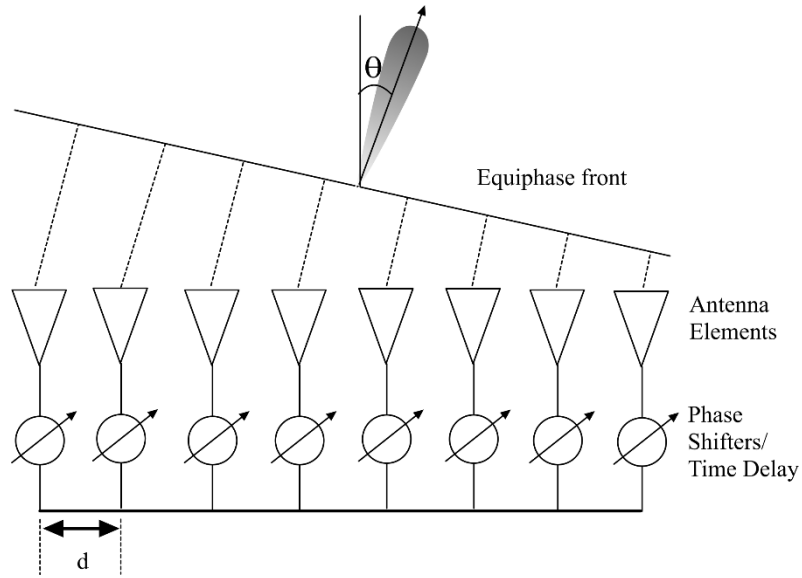
Figure 3.14 Linear Antenna Array.

2.   Planar Antenna array:

Planar antenna arrays are designed in a fashion so that all the radiating elements are in one plane. Since the elements are placed in two dimensions the array factor of a planar array can be expressed as the multiplication of the array factors produced by the arrays on x and y axis [63]. Figure 3.15 shows a planar array. The combined array factor can be expressed as:

$$AF_{planar} = (AF_x)(AF_y)$$
(3.24)

$$AF_n(\theta,\varphi) = \left\{ \frac{1}{M} \frac{\sin\left(\frac{M}{2}\psi_x\right)}{\sin\left(\frac{\psi_x}{2}\right)} \right\} \left\{ \frac{1}{N} \frac{\sin\left(\frac{N}{2}\psi_y\right)}{\sin\left(\frac{\psi_y}{2}\right)} \right\}$$
(3.25)

Where, $\left. \begin{array}{l} \psi_x = kd_x \sin\theta\cos\varphi + \beta_x \\ \psi_y = kd_y \sin\theta\cos\varphi + \beta_y \end{array} \right\}$
(3.26)

k is the wave number while β is the phase difference

Advantages of this array method:

- The array can scan the main beam along two planes of θ and φ

- This array offers more gain and directivity compared to linear arrays

- It can be used in conjunction with a reflecting screen behind the active plane

Disadvantages of this array method:

- Designing is complicated.

- Antennas require more electronically controlled phase shifters
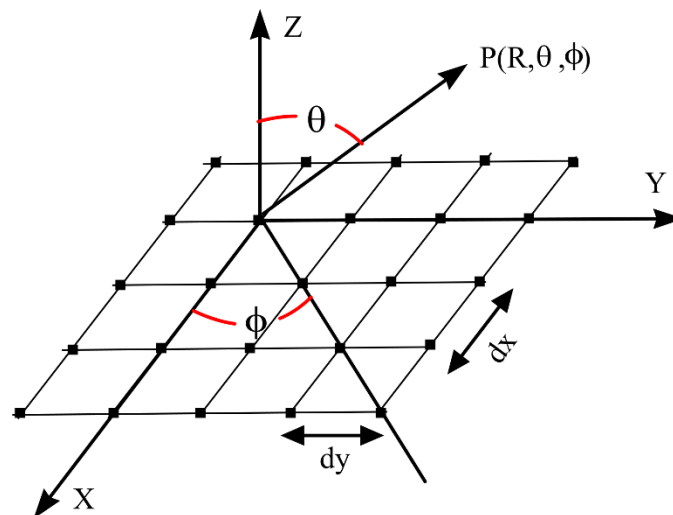
Figure 3.15 Planar Antenna Array.

3.8   Microstrip Antenna Feeding Techniques

A microstrip patch has been devised to be fed in various ways over the years. Most popular designs among these methods are the strip line feed, coaxial feed, inset feed (all three involves contact of the feed to the radiating patch), the proximity feed and the aperture coupled feed (both non-contacting schemes).

In the contacting scheme, the RF power is fed directly to the radiating patch using a connecting element such a microstrip line or a coaxial probe.
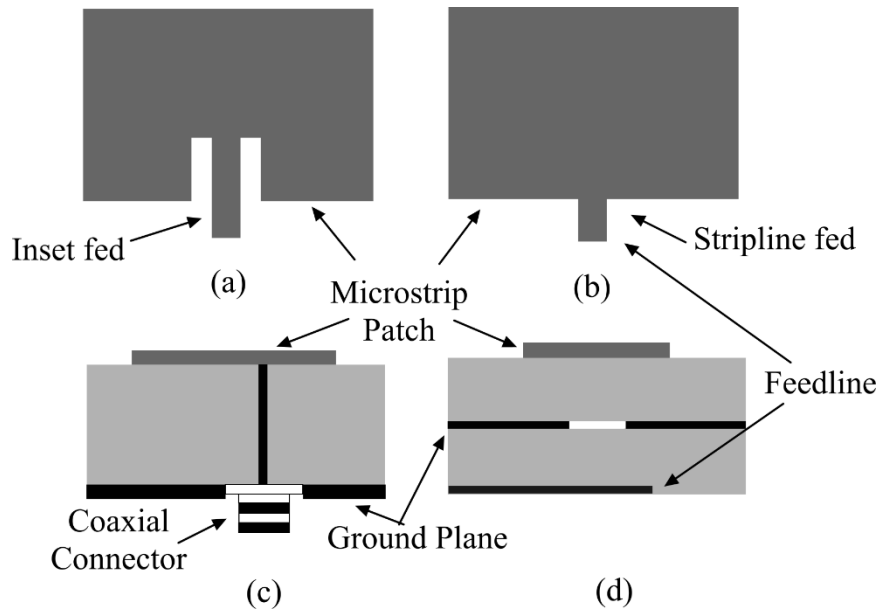
Figure 3.16 Different feed techniques (a) inset feed (b) stripline feed (c) coaxial feed and (d) aperture coupled feed.

Table 3.1 Comparison of Various Feeding Techniques [23]

Characteristics	Stripline Feed	Coaxial feed	Aperture Coupled feed	Proximity coupled feed
Spurious Radiation	High	High	Minimum	Minimum
Reliability	High	Poor due to soldering issues	Good	Moderate
Fabrication	Easy	Soldering and drilling required in the substrate and patch	Alignment required with aperture	No alignment required
Impedance matching	Easy	Easy	Easy	Difficult
Bandwidth	Low	Low	High	Moderate

While in the non-contacting method of feed the electromagnetic field coupling is done to transfer power between the microstrip line and the radiating patch.

Figure 3.16 shows various feeding techniques for a patch antenna. The contact and non-contact schemes have various advantages and disadvantages according to the design layout. Due to the observable performance benefits of the aperture coupled feed, the design of aperture coupled microstrip antenna has been chosen for this thesis as a high bandwidth was targeted for short mid and long-range radars which would generate a higher number of samples per second to improve the resolution of the radar as required by the auto industry.

3.9   Summary

A summary of the basic antenna design theory has been provided in this chapter. A microstrip antenna essentially comprises a metallic patch realized on a dielectric substrate which is an insulator used to insulate the region between the metallic patch and its reference plane or ground plane. Different design considerations related to a microstrip antenna are reviewed. Due to the significant performance benefits of an aperture coupled planar microstrip antenna array, in this thesis an aperture coupled microstrip antenna array has been selected for the target short, mid, and long-range automotive radar to generate a higher number of samples per second to improve the radar resolution as necessary by the auto industry.

This chapter presents the roadmap followed for designing a microstrip patch antenna. Details about the choice of dielectric and how the permittivity of it has been synthesized to improve antenna performance have been presented in this chapter. Finally, a single antenna element has been modeled based on the design roadmap established in the earlier section of the chapter.

4.1   Dielectric material Selection

The selection of the antenna dielectric material is an important step of the design of microstrip patch antennas as a number of performance parameters such as antenna directivity, gain, bandwidth depend on the properties of the dielectric material.. A general conception of transmission lines is to utilize a thin layer of dielectric material with a high dielectric constant in order to generate guided waves [71]. However, the antennas work in the principle of generating space waves hence the dielectric has to be thick and have a low dielectric constant. Figure 4.1 shows a relation between the dielectric constant and the directivity achieved by an antenna. It can be concluded from the figure that a material with a low dielectric constant is best suited for antenna designs to obtain a high directivity and gain. The low dielectric constant is also experimentally proven to provide a higher bandwidth and better isolation [72] as necessary for an automotive radar. Following Figure 4.1, air with a dielectric constant of 1 is the best possible dielectric material for high gain/high directivity antenna. However,

due to fabrication difficulties, various other low k dielectric materials, such as Rogers 5880, 3003, RF-35 FR4 etc. have also been thoroughly experimented on over the years [22] [30]. but due to difficulties in connecting the transceiver modules to these antenna substrate using them to meet specific performance standards have found to be highly challenging. Consequently, the search for a robust low k dielectric material has always been a demand.
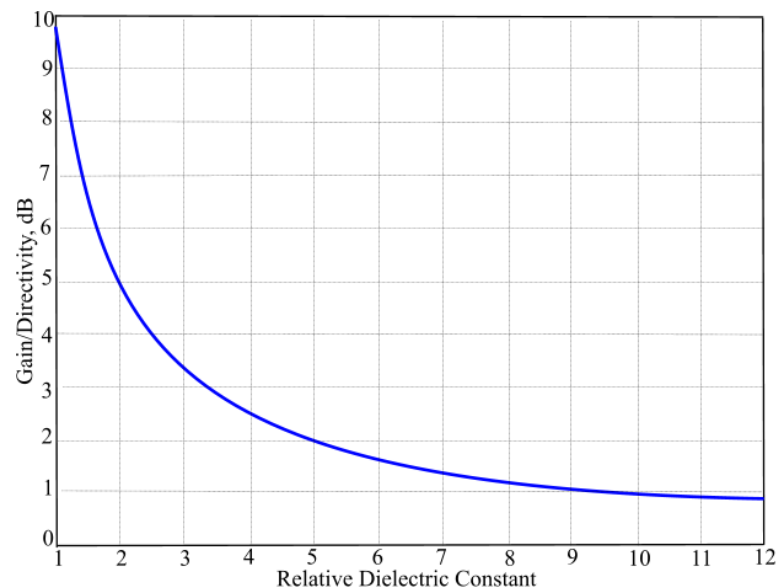
Figure 4.1 Directivity vs dielectric constant.

The authors in [73] proposed to use BCB or Bisbenzocyclobutene as a new low k antenna dielectric for antenna design.. BCB is a polymeric material available commercially as Cyclotene™ in two series, a dry etchable the 3000 series and a photosensitive the 4000 series [74] [75]. BCB exhibits a relative dielectric constant of $\varepsilon_r = 2.65$ and a loss tangent ($\tan\delta$) = 0.002 to 0.008 between 10 GHz to 1.5 THz with a few percent variations. Since being a polymeric material

BCB can be spin coated on a substrate [76] into a thick layer of 26μm for 3000 series while 20.2μm for the 4000 series.
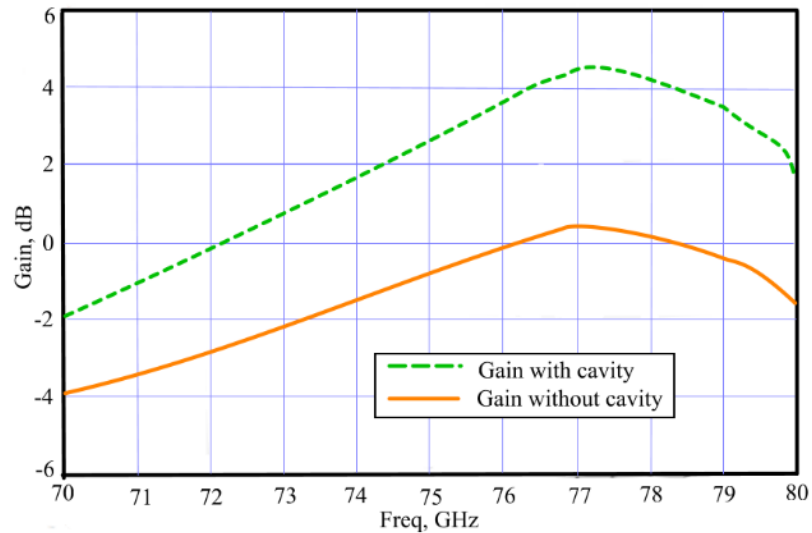
Figure 4.2 Gain achieved by an antenna with and without a dielectric cavity.

Even, though it exhibits a low dielectric constant the gain and the bandwidth achieved with its natural parameters is not enough to meet the auto industry requirements. Hence an innovative idea of synthesizing a new dielectric constant to yield a higher directivity and gain is being proposed in this thesis. Dielectric properties can be synthesized by adding a low k dielectric material on the surface of a material with a higher dielectric constant and altering the height of each of the dielectric layers to obtain a lower overall dielectric constant. The author in [23] has developed a dielectric cavity in silicon and introducing an air cavity using a deep reactive ion etching (DRIE) of silicon technique to lower the dielectric constant of silicon from 11.6 to 1.85. The authors in [39] followed a similar method to etch a cavity in silicon and lower the value of the dielectric constant to a value near that of air. These interesting techniques provided a way for this

thesis to adopt in developing a cavity in a layer of BCB using a deep reactive ion etching (DRIE) technique. Figure 4.2 shows a comparison of gain achieved for a single microstrip antenna patch in the 70-80 GHz range with and without a dielectric cavity in a 17 μm layer of BCB as a substrate.

4.2   Synthesized Dielectric Constant

Extensive research in the domain of micro and nanostructures have yielded to rapid progress in the field of fabrication for high performing millimeter wave systems. Innovative methods like surface and bulk micromachining have contributed to developing microfabricated cavities to provide required electrical properties in order to obtain necessary results. The design discussed in this thesis shows substantial improvement in the bandwidth and size of the system by 50% and 30% respectively. The table 4.1 [63] shows a comparison between a high index antenna and a micromachined antenna on a GaAs substrate. The improvement in the antenna performance can be observed from the Table 4.1.

Table 4.1 Comparison of Normal and Micromachined Substrates [63]

Parameters	Normal GaAs substrate	Micromachined GaAs substrate	Improvement
S11 BW	887 MHz	1426 MHz	539 MHz
Directivity	9.2 dB	12.6 dB	3.4 dB
Efficiency	63%	80%	17%
Gain	7.2 dB	11.6 dB	4.4 dB

Micromachined substrates work on the principle forming a cavity directly underneath the patch by removing of the material of a higher dielectric constant. The cavity formed is generally filled with air and the conjunction of the substrate with the air of unequal thickness lowers the dielectric constant of the region by a

great extent. The following expression can be utilized in order to obtain the dielectric constant of the region [23]:

$$\varepsilon_{synthesized} = \left(\frac{h_{material}}{\varepsilon_{material}} + \frac{h_{air}}{\varepsilon_{air}} \right)^{-1} \times \left(h_{eq} \right) \tag{4.1}$$

Where, $h_{eq} = h_{material} + h_{air}$ (4.2)

Figure 4.3 shows that the introduction of a cavity under the patch also reduces the number and intensity of backlobes [77]. Thereby development of a cavity underneath the patch becomes extremely necessary by reducing the number of back lobes and intensity of backlobes with and without a cavity.
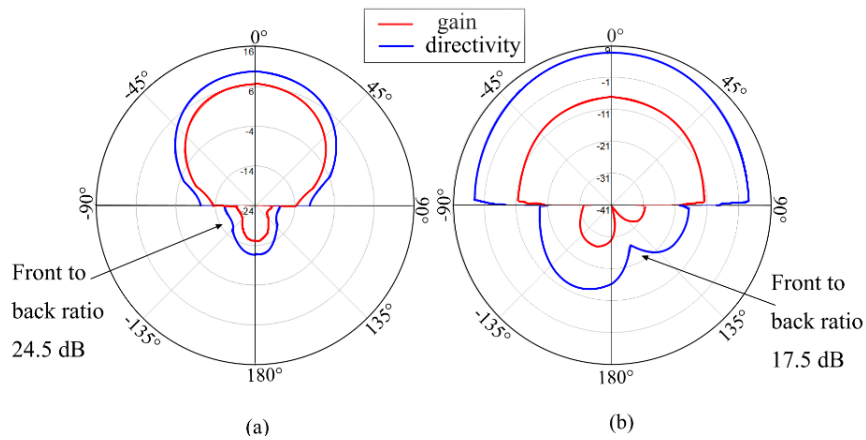
Figure 4.3 Radiation pattern (a) with a cavity (b) without a cavity.

Figure 4.4 shows the final single element patch design after the cavity was developed underneath the microstrip patch.
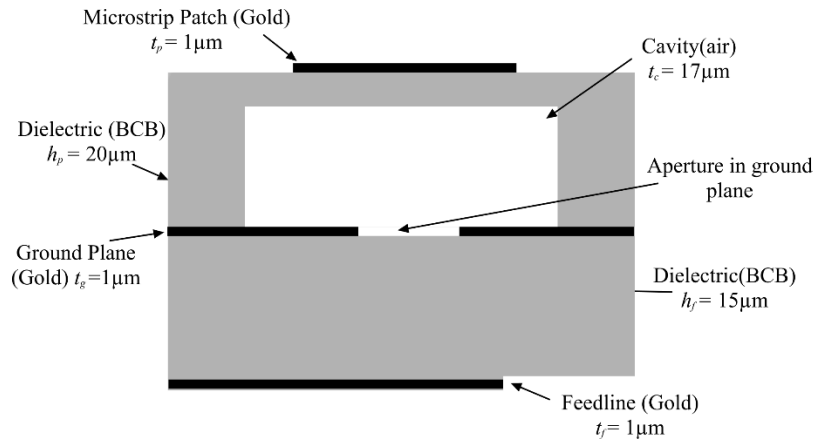
Figure 4.4 A single antenna element after the cavity was etched.

4.3 Design Specifications

The target microstrip antenna array has been designed as a planar array of rectangular microstrip patches that can be fed sequentially or simultaneously by a Butler matrix in a corporate feed (parallel feed) arrangement. The phase and amplitude alterations at each of the array ports of the Butler matrix will feed the antenna elements arranged in linear arrays (columns) at different time delays to steer the main beam of the antenna array in a desired direction. The number of patches in each column determines the gain of the antenna and thereby controls the range covered by the array. The antenna array has been designed to offer more than 4 GHz of bandwidth to function optimally in all modes of automotive radar and meet requirements set by the auto industry. To obtain a high bandwidth and gain from a lower number of patches, a cavity has been introduced in the BCB dielectric layer under each of the microstrip radiating patches. This lowered the dielectric constant of BCB (Cyclotene™ 3022-63) from 2.65 to 1.46 while utilizing its characteristics of providing a low $\tan\delta$ =0.002 to 0.008 between 10 GHz to 1.5 THz. The height of the Cyclotene™ layer has

been chosen as 20 µm for the patch substrate and 17 µm for the feed substrate. A Lower thickness of the dielectric material decreases fabrication complexities to increase the yield in a batch fabrication process. The authors in [23] presented the idea to lower the value of dielectric constant of the specific area of the substrate which will house the microstrip radiating patches. This is achieved by utilizing the DRIE technique to etch a cavity and remove the amount of material on its surface up to a specific depth [27].

Experimental techniques of DRIE based cavity formation in Cyclotene™ has been reported in [31] and [76] to realize capacitive micromachined ultrasonic transducers (CMUT) for ultrasound generation and reception.. However, using the DRIE technique to etch a cavity to realize high frequency antenna arrays has been a revelation made in this thesis. The Deep Reactive Ion etching has opened new fields of application in MEMS and device integration. Compared to the wet anisotropic etching, the DRIE process well known as Bosch process ensures uniform etching as required and eliminates lateral etching of the material resulting in high anisotropic etch profiles at high etch rates [23]. Figure 4.5 shows a conceptual cross-section of a BCB based microstrip antenna with a buried cavity. In the diagram, a thin wafer of Pyrex glass has been used at the bottom to hold the entire layer stack up.

An essential designing point that needs to be addressed for designing the microstrip antennas are the varying needs on the substrate for the radiating patch and the feed lines. The feed lines are microstrip transmission lines which need to produce guided waves in the substrate while the patch needs to produce

space waves hence the feed lines should be fabricated on a substrate of higher permittivity, in this case, a layer of Cyclotene™ has opted which has a higher permittivity of 2.65.

Using substrates with a higher dielectric constant for the feed lines also ensures the lower amount of back radiation thereby preventing loss of energy. Hence, a low permittivity substrate has to be chosen for the antenna patches while a higher dielectric constant substrate has to be chosen for the feed lines.

TOP WAFER

(a)

DRIE etched part of BCB layer in the region below
the microstrip patch

BOTTOM WAFER

(b)

Deposit 1μm thick Gold Layer on the top of a Pyrex wafer for
feedlines and spin coat 20 μm thick layer of BCB on it

(c)

Deposit 1μm thick Gold Layer on the top of BCB layer and pattern it
for the Aperture in the microstrip aperture coupled antenna

(d)

Themocompressively bond the finished top and bottom wafers

Figure 4.5 DRIE process, (a) top wafer DRIE etching of BCB (b) Deposition of a layer of gold for feedlines and a layer of BCB as feed dielectric (c) deposition of a layer of gold for ground plane and pattern it for aperture (d) thermos compressive bonding of top and bottom wafer

4.4   Design Procedure

In designing the DRIE cavity backed aperture coupled microstrip antenna, the

following mathematical formulas were used to create a mathematical model of

the proposed structure using MATLAB. Figure 4.6 shows the design parameters of the developed aperture coupled microstrip antenna .
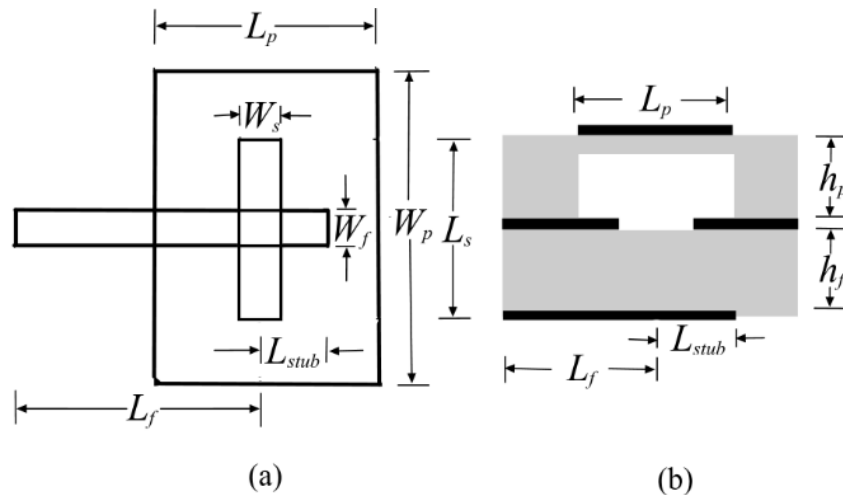
Figure 4.6 (a) top view and (b) crossectional view of the proposed antenna.

1.   Synthesized dielectric constant

As explained in the previous section the dielectric material vertically underneath the metallic patches needs to be removed in order to introduce another low index material to obtain an overall lowered dielectric constant. The synthesized effective dielectric constant as can be obtained following (4.1) and (4.2)   has been reported to produce higher performance and has been adopted by many antenna designers over the years [23] [33]. Figure 4.7 shows a comparative study of the effect of dielectric constant on the directivity when the original dielectric constant of BCB has been reduced from 2.65 to 1.46.
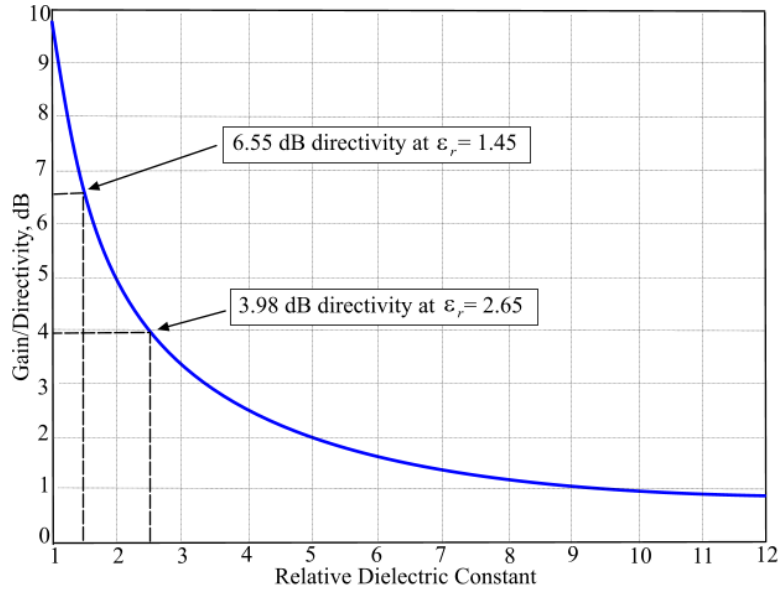
Figure 4.7 Comparative study between the directivity achieved with or without a dielectric cavity in BCB.

2.   Effective dielectric constant

An effective dielectric constant ε_{eff} of the mixed substrate comprised of BCB and the air cavity under the patch is necessary to calculate to determine the dimensions of the microstrip patch. The effective dielectric constant can be calculated following:

$$\varepsilon_{\text{eff}} = \frac{\varepsilon_{synthesized} + 1}{2} + \frac{\varepsilon_{synthesized} - 1}{2}\left[1 + 12\frac{h_p}{W_p}\right]^{-\frac{1}{2}} \text{ when, } \frac{W}{h} > 1 \qquad (4.3)$$

Where, $\varepsilon_{synthesized}$ is the synthesized dielectric constant of the mixed susbtrate, h_p is the height of the mixed substrate, and W_p is the width of the patch.

3.   The width of the Patch

The width of the rectangular patch is an important quantity as it controls the resonant impedance of the structure. The width of the antenna can be determined following [63]:

$$W_p = \frac{c}{2f_o\sqrt{\dfrac{\varepsilon_{synthesized}+1}{2}}} \tag{4.4}$$

Where f_0 is the resonance frequency, $\varepsilon_{synthesized}$ is the synthesized dielectric constant of the substrate, and c is the speed of light.

4.   Patch length

The patch length is an important aspect of a microstrip antenna as it determines the resonant frequency of the antenna. Increasing the patch length causes a decrease of the resonant frequency and vice versa.
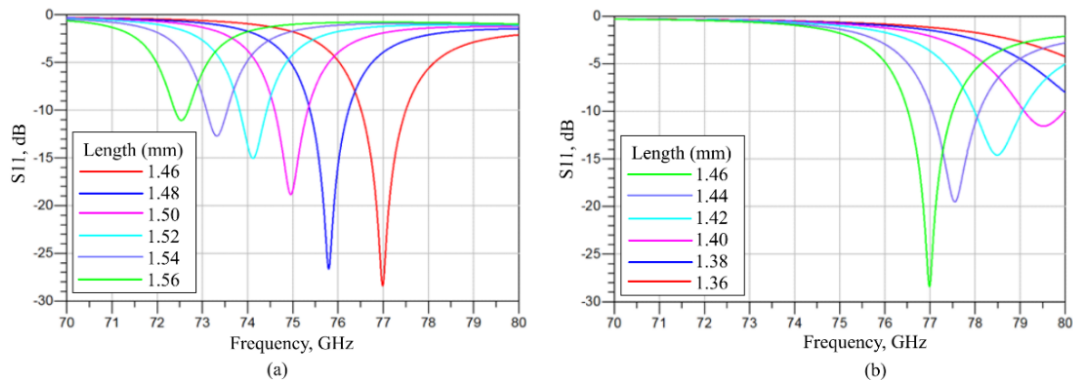

Figure 4.8 Varying lengths of the microstrip patch causes the change in resonant frequency (a) length increases and (b) decreases..

Figure 4.8 shows the effect of the patch length of the aperture coupled antenna. The microstrip antenna patch length can be calculated in three steps:

- Patch effective length

  The effective length of the patch can be calculated following:

$$L_{eff} = \frac{c}{\sqrt{\varepsilon_{eff}}} \left(\frac{1}{2f_0} \right)$$ (4.5)

  Where, f_0 is the operating frequency, ε_{eff} is the effective dielectric constant and c is the speed of light.

- Extension of patch Length due to fringing fields

  The patch length extends due to the effect of fringing fields and can be expressed as [63]:

$$\frac{\Delta L}{h_p} = 0.412 \frac{(\varepsilon_{eff} + 0.3)\left(\frac{W_p}{h_p} + 0.264 \right)}{(\varepsilon_{eff} - 0.258)\left(\frac{W_p}{h_p} + 0.8 \right)}$$ (4.6)

- True patch length

  The true patch length can be obtained when the patch length extension on either side of the radiating patch is subtracted from the effective path length. It can be expressed as following [63] as:

$$L = L_{eff} - 2\Delta L$$ (4.7)

5. Slot Dimensions

For an aperture feed microstrip antenna, an aperture or slot is necessary to be fabricated in the ground plane of the structure. The microstrip aperture acts as a medium of coupling between the microstrip feed line and the radiating antenna patch. A lot of research work has been done to investigate the perfect slot geometry [78]. Figure 4.9 shows a few different slot geometries often used for

antenna aperture designs. Traditionally microstrip aperture coupled antenna designers have favored the rectangular slot compared to other versions of it. H slot has also been widely preferred as it is said to provide a superior coupling level compared to the traditional rectangular slot [78].

| (a) H shaped slot | (b) Rectangular slot | (c) Circular slot |
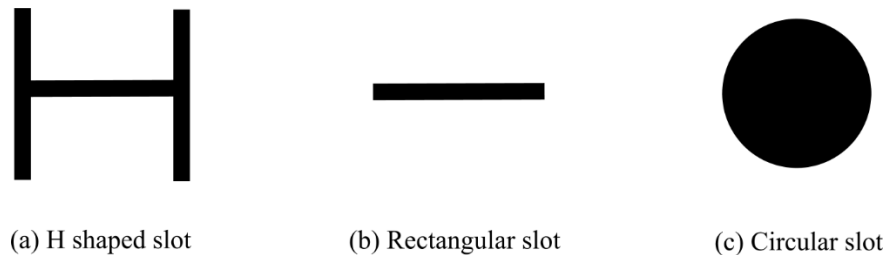
Figure 4.9 Commonly used slot geometries.

However, for this thesis, a rectangular slot is chosen for simplicity of design and anticipated ease of microfabrication.

The rectangular slot designed in this thesis also provides a lower back radiation compared to the other versions of the slot as shown in figure 4.9 (b). The slot length controls the rate of coupling while the slot width controls the polarization purity [68]. Therefore, a longer slot with a narrow width is preferred as it provides better coupling between the feed line and the top patch while ensuring better polarization purity of the structure [68]. However, it has to be kept in mind that increasing the slot length to $0.5\lambda_g$ can produce a dipole antenna which will radiate equally in both directions. There is no perfectly devised mathematical formula known to design the aperture dimensions. However, most of the aperture dimensions are based on the amount of coupling obtained through the result of a return loss plot. Figure 4.10 shows the varying level of coupling between the feed line and the patch due to change of aperture dimensions.
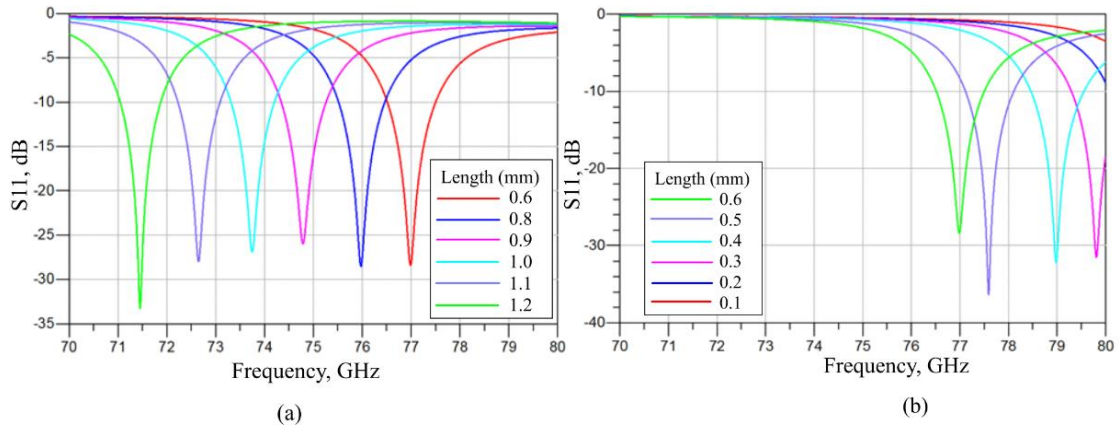
Figure 4.10 Level of coupling changes when the length of the slot was altered (a) slot length was increased and (b) decreased.

A slot length of $0.4\lambda_g$ is chosen for this research work to optimize to slot dimensions while considering all the design and fabrication constraints.

6.   Feed Line Dimensions

The feed line is another important aspect of a microstrip aperture coupled antenna and the width of the feed line corresponds to the characteristic impedance of the structure. Change in the feed line width can alter the impedance match between the port and the feed structure; thereby causing more power to get reflected and decreases the reflection coefficient. Figure 4.11 shows the effect of change of feed line width to the amount of power transferred to the feeding structure.
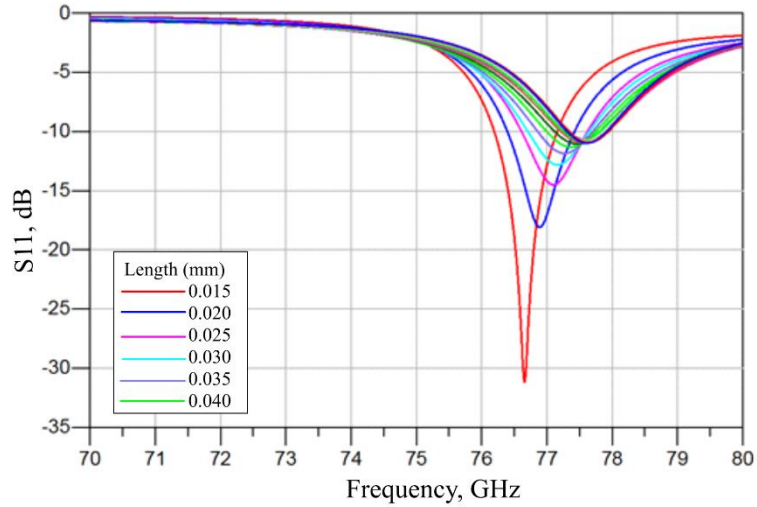
Figure 4.9 Change in the level of coupling due to increasing feed width.

The feed line width can be expressed following [68]

$$Z_c = \frac{1}{2\pi}\sqrt{\frac{\mu_0}{\varepsilon_0 \varepsilon_{\text{eff}}}} \ln\left(F\frac{h_f}{W_f} + \sqrt{1+\left(\frac{2h_f}{W_f}\right)^2} \right) \tag{4.8}$$

Where, $F = 6+(2\pi-6)\exp\left[-\left(30.666\frac{h_f}{W_f}\right)^{0.7528}\right]$ $\qquad$ (4.9)

The feed line length can be expressed as

$$L_f = \frac{\lambda_0}{\sqrt{\varepsilon_{\text{eff}}}} \tag{4.10}$$

Where, λ_0 is the resonant wavelength.

The feed line has another important portion which is beyond the slot which acts as a tuner for the resonant frequency and antenna performance. The portion of the feed line beyond the center of the microstrip aperture is called a stub. A length equivalent to $0.4\,\lambda_g$ has been chosen as the stub length for this design.

4.5 Single Patch Design Calculations

The specifications of the designed single patch microstrip antenna along with the feed line following the mathematical models provided above are listed in Table 4.2 and Table 4.3.

Table 4.2 Specifications of a single element

Parameter Description	Value
Dielectric constant of BCB(ε_r)	2.65
Synthesized dielectric constant	1.46
Loss tangent ($\tan\delta$)	0.002-0.008
Height of the BCB substrate (h_p)	20 µm
Air cavity length (L_c)	1.46 mm
Air cavity width (W_c)	1.75 mm
Air cavity thickness	17 µm
The thickness of gold patch (t_p)	0.5 µm
The thickness of ground plane (t_g)	1 µm
The thickness of feed line (t_f)	0.5 µm

As mentioned before, MATLAB™ has been used to calculate the initial dimensions of the antenna and the feed lines as listed in table 4.3 using the equations (4.1) - (4.10) listed in the previous section. Afterwards, an ADS™ based 3D finite element field solver that uses the method of moments (MoM) has been used to optimize the geometrical dimensions. ADS™ simulation results show a gain of 4.15 dBi with a directivity of 8.3 dBi. Figure 4.12 shows the S11 response of a single antenna element with and without cavity which denotes a bandwidth of 1.8 GHz. The ADS™ optimized geometrical dimensions are also included in Table 4.3.

Table 4.3 Dimensions of a single antenna element

Parameters	Dimensions in MATLAB™	ADS™ Optimized Dimensions
Length of the Patch (L_p)	1.42 mm	1.46 mm
Width of the Patch (W_p)	1.66 mm	1.75 mm
Height of Patch dielectric (h_p)	0.02 mm	0.02 mm
Length of Slot (L_s)	0.6 mm	0.6 mm
Width of Slot (W_s)	0.015 mm	0.015 mm
Height of feed dielectric (h_f)	0.015 mm	0.015 mm
Length of feed line (L_f)	2.5 mm	2.7 mm
Width of Feed line (W_f)	0.018 mm	0.015 mm
Length of Stub (L_{stub})	0.5 mm	0.5 mm
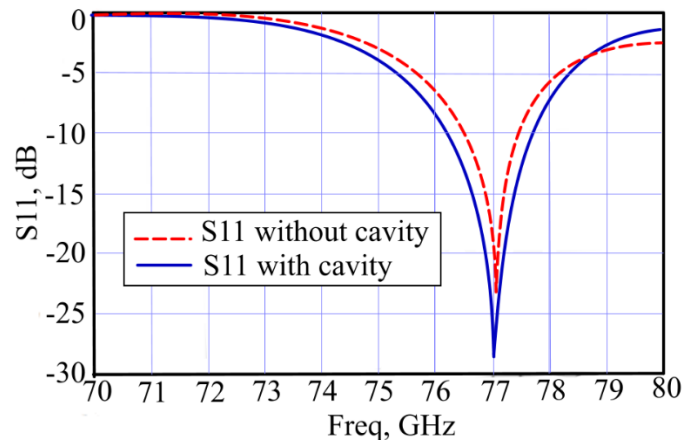
Figure 4.10 S11 of a single antenna element with and without a cavity.

Figure 4.12 shows the ADS™ simulated S11 parameter as a function of frequency. Corresponding 3D azimuth and elevation radiation patterns are provided in Figure 4.13.
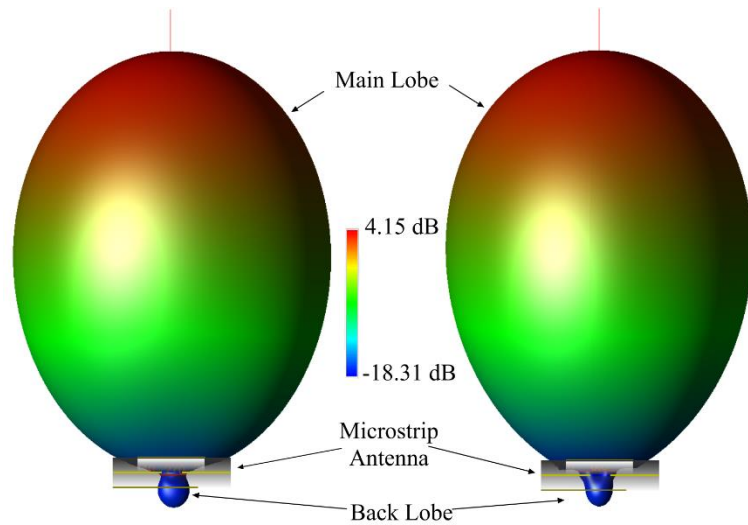
Figure 4.11 Radiation pattern of a single antenna element in (a) azimuth and (b) elevation planes.

4.6   Summary

The design procedure of a single microstrip antenna patch along with necessary theoretical mathematical modeling has been presented. A rectangular slot type aperture coupling has been determined to be optimum to feed the designed microstrip antenna patch using a microstrip feed line. The initial dimensions obtained from analytical equations are optimized using ADS™. 3D FEA simulation results done using ADS™ exhibited -28dB for S11 parameter at 77 GHz. Detailed design specifications are provided.

This chapter presents the design of a planar array of the microstrip antenna patch that was presented in the previous chapter. The array implementation generates an antenna beam with necessary beamwidth that can be steered in both azimuthal and elevation plane. Such a beamforming capability of the designed antenna would enable the target automotive radar to detect the velocity and range of other vehicles, pedestrians, and obstacles. The target antenna array needs to provide the necessary gain and directivity as required for the target multimodal automotive radars used for long, mid, and short range applications. .

5.1   Design Procedure

The microstrip antenna array has to provide a broadside radiation pattern. An important design aspect of an antenna array is the array factor. The array factor of a planar antenna array can be expressed as [63]

$$AF_{planar} = (AF_x)(AF_y) \tag{5.1}$$

$$AF_n(\theta,\varphi) = \left\{ \frac{1}{M} \frac{\sin\left(\frac{M}{2}\psi_x\right)}{\sin\left(\frac{\psi_x}{2}\right)} \right\} \left\{ \frac{1}{N} \frac{\sin\left(\frac{N}{2}\psi_y\right)}{\sin\left(\frac{\psi_y}{2}\right)} \right\} \tag{5.2}$$

$$\text{Where,} \quad \left. \begin{array}{l} \psi_x = kd_x \sin\theta\cos\varphi + \beta_x \\ \psi_y = kd_y \sin\theta\cos\varphi + \beta_y \end{array} \right\} \tag{5.3}$$

Where M and N are the antenna elements in the x and y directions, respectively.

The directivity of an antenna array factor [63] can be expressed as

$$D = \frac{4\pi \left[AF(\theta,\varphi) \right]\left[AF(\theta,\phi) \right]*\Big|_{\max}}{\int_{0}^{2\pi}\int_{0}^{\pi}\left[AF(\theta,\varphi) \right]\left[AF(\theta,\varphi) \right]*\sin\theta d\theta d\varphi} \qquad (5.4)$$

An increased directivity makes the antenna main beam more directional while decreasing the half power beamwidth of the antenna array. Figure 5.1 shows an effect of the beam width when the number of elements was altered in the antenna array.
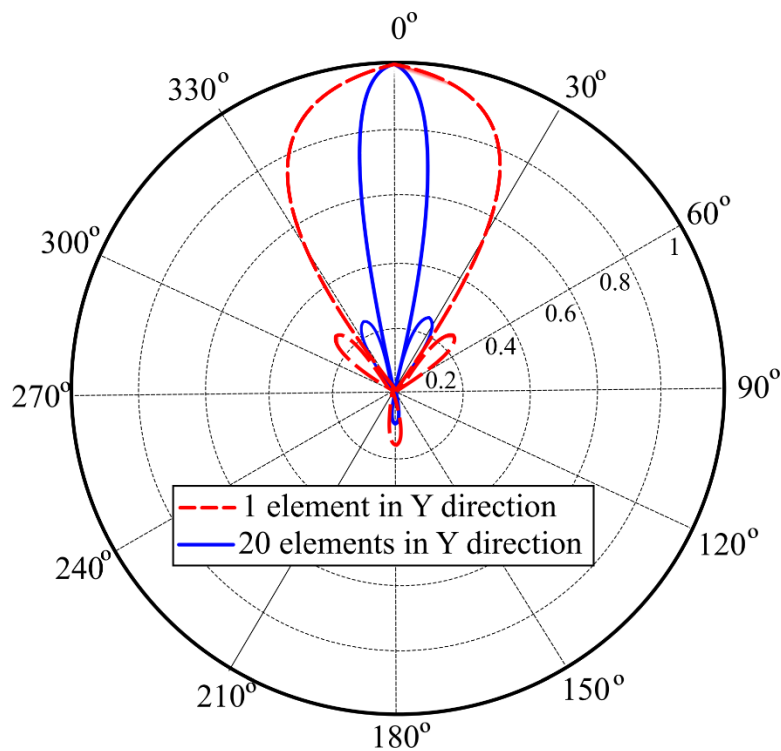

Figure 5.1 Polar Plot shows the effect of the number of patches on antenna directivity.

The automotive industry requires an antenna array with a highly directional beam that can be steered in an angular range of ±7.5⁰ for Long range applications. The long range application also requires to cover a range between 150-250 m with a opening beamwidth of 10⁰. Hence to meet the automotive radar requirements of a long-range and narrow beam width, the number of radiating patches were increased in the x and y directions. The total number of equidistant patches in the array in y direction was considered as seven while eight patches were placed in x direction. The performance factors like gain and directivity can be improved through the increase of a number of patches however due to dimension constraint set by the automotive industry the size of the array was kept to a minimum required for desired results. Figure 5.2 shows the effect on the gain when the number of rows of elements was altered in the y axis.
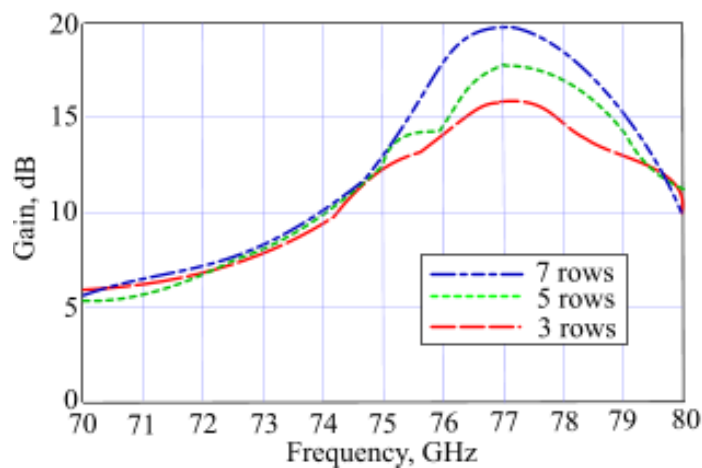

Figure 5.2 Different gains achieved by changing the number of rows of patches.

Figure 5.3 shows the top and cross-sectional view of the antenna array designed using Cyclotene™ as the dielectric material. The array element spacing

d_x and d_y has been determined to be 2.41 mm $(< \lambda_g)$ from simulation studies to minimize the sidelobes and maximize the main lobe power.
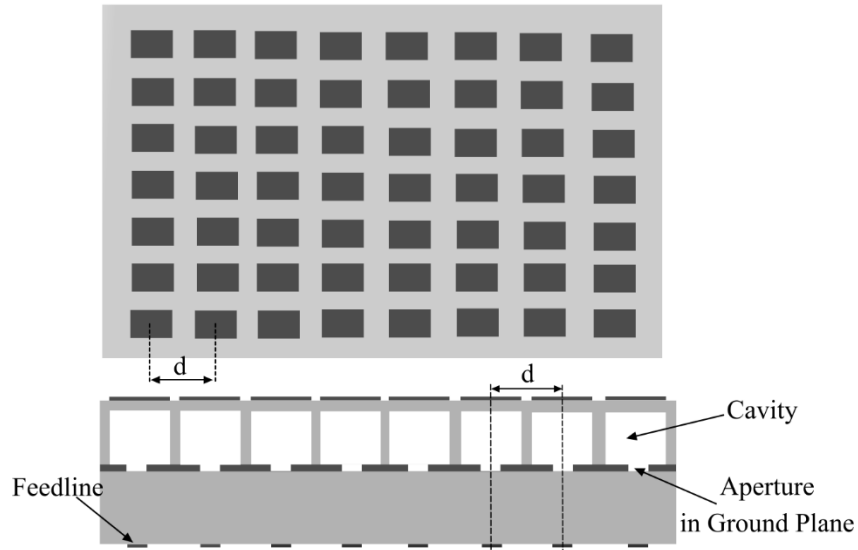
Figure 5.3 Antenna array designed for the application in tri-mode radar.

5.2   Simulation results

The simulation was carried out for three different microstrip antenna arrays of different dimensions in order to find the optimum number of elements of a planar antenna array to satisfy the automotive radar requirements. The simulations were carried out for 3, 5 and 7 rows of eight equidistant elements for the optimum gain required for functioning in the mid and long ranges. In [23], it has been mentioned that a gain of 20.5 dBi is enough to cover a range of 200-250m with necessary beamwidth. Hence, following [23] it appears that a gain of ~20 dBi is sufficient for a radar antenna to function in the mid and long ranges.

Along with the Gain and directivity of the radar antenna, a key aspect of the designed performance is the return loss of the array which determines the

amount of power reflected while being transferred from the port to the feed lines. A higher return loss signifies a better level of coupling between the feed lines and the corresponding ports [63]. Figure 5.4 shows the return loss for the antenna array designed in this thesis. The impedance bandwidth was calculated as 4.2 GHz while the return loss was at -36.5 dB. The VSWR (Voltage Standing Wave Ratio) of the antenna array was obtained through calculation as the 1.04.
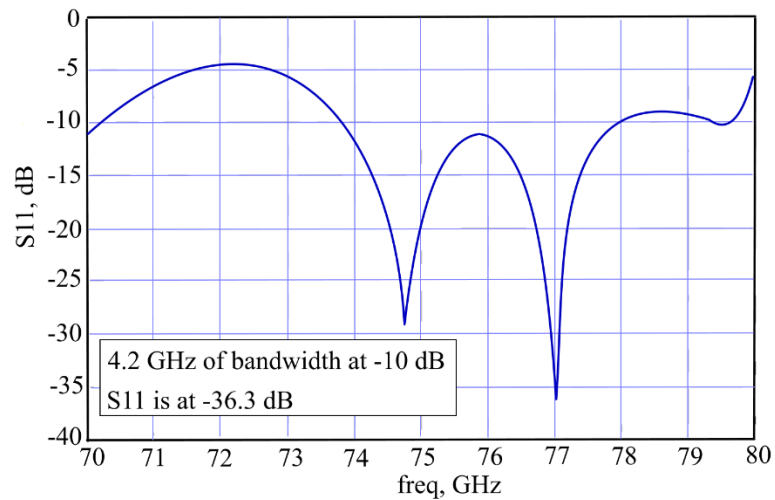
Figure 5.4 S11 of the designed microstrip aperture coupled antenna array.
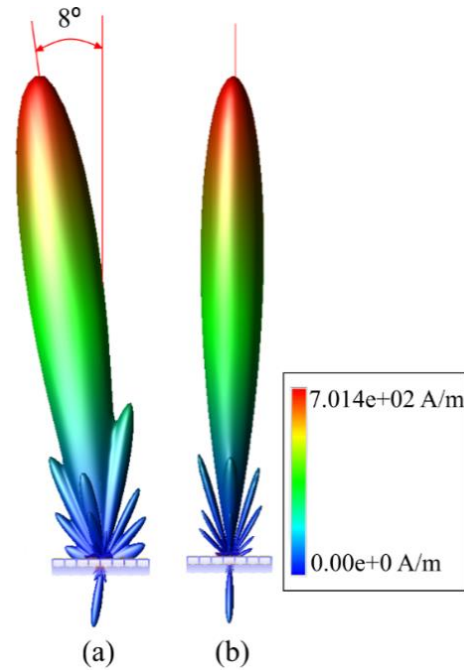
Figure 5.5 Radiation pattern of the antenna array (a) Elevation plane (b) Azimuthal plane.

The gain and directivity for the simulated antenna array were obtained as 19.78 dBi and 22.3 dBi respectively indicating a 45% radiation efficient structure. Figure 5.5 shows the azimuth and elevation plane radiation patterns of the proposed design. Figure 5.5 (a) shows a tilt in the main beam of the antenna by 8 degrees in the elevation plane. Since the beam steering would be performed in the azimuth plane of the designed antenna the main beam tilt will have little effect on the functionality of the system. However, a corrective measure of altering the angle of mounting of the antenna structure by an angle of 8 degrees can rectify any difficulties which may arise in radar beam steering and detection of the proximity of obstacles around the vehicle.

Table 5.1 presents a summary of results of the planar antenna array designed in this thesis.

Table 5.1 Antenna Array Design Specifications

Parameter	Value
Gain	19.78 dBi
Directivity	22.5 dBi
Bandwidth	4.2 GHz
Azimuth Angle tilt	0^0
Elevation Angle tilt	8^0
HPBW (Opening Angle)	$\pm5.5^0$
Return Loss	-36 dB
Radiation Efficiency (η)	45 %
VSWR	1.04
X dimension length	21.2 mm
Y dimension length	20.2 mm
No. of elements in the x direction	8
No. of elements in the y direction	7
Element spacing in the x direction	2.41 mm
Element spacing in the y direction	2.41 mm

5.3   Comparison with published results

The results of the microstrip antenna array designed in this thesis have been compared to 5 other published works on antenna arrays working in the same frequency range. The comparison results are provided in Table 5.2.

Table 5.2 Comparison against published results

Parameters	Ref [22]	Ref [23]	Ref [25]	Ref [58]	This work
Gain (dBi)	11.4	20.5	20.8	24.7	19.8
Radiation Efficiency	N/A	90 %	N/A	N/A	45 %
Bandwidth	3 GHz	1.2 GHz	5 GHz	700 MHz	4.2 GHz
Dimension (mm)	20.5 x 2 x 0.161	32 x 10x 0.5	50 x 20 x 0.127	42 x 75 x 0.2032	20 x 21 x 0.035

The antenna array in this thesis outperforms the rest in either in dimension or in terms of bandwidth. Table 5.2 shows a detailed comparison of the antenna array against four other published results. The designed antenna array is less efficient as compared to the silicon-based antenna in [23]; however, this antenna produces the same level of performance even with the lesser number of patches due to the superior individual performance of a single antenna element of the other antenna arrays. The antenna array presented in [25], [58] has a superior gain than the one designed in this thesis, but that has a larger dimension and extremely low bandwidth as compared to the current design. While the antenna array designed in [22] has smaller overall dimensions to the one designed in this research work; however, the design presented in [22] does not provide necessary gain to operate in mid and long ranges. Hence the antenna designed in this thesis optimizes most of the performance parameters to achieve the main design specifications set by the automotive radar industry.

5.5   Summary

This chapter presents the theory, design, and the simulation results of a microstrip antenna array operating in the 77 GHz center frequency for use in an automotive radar with short, mid, and long range coverage capability. Detailed antenna array design specifications are provided in Table 5.1. The designed array has been compared with other 5 recent antenna array designed published elsewhere. The comparison shows that the new antenna array offers optimized performance in terms of size, gain, bandwidth and directivity as compared to the published results elsewhere.

Micromachined antenna arrays provide several advantages compared to conventional microstrip antenna arrays. DRIE cavities in the antenna substrate reduce the dielectric constant of the region and thereby improves antenna performance in gain and bandwidth. Selective removal of material underneath the patch using a DRIE technique reduces mutual coupling of the microstrip patches due to surface waves which exist on high dielectric constant substrates.

The authors in [32] and [80] have developed a process table for BCB fabrication on silicon substrates and techniques to develop a cavity in the BCB layers. The technique has been adopted to develop and simulate a scheme to fabricate the antenna array designed in this thesis. The developed fabrication process is divided into five steps with the concept of preparation of two different wafers i.e. the top and bottom wafer. Same process techniques were utilized on each of the wafers to build the stacked layers. The last step in fabrication is to flip and use a thermosonic bonding [81] for gold to gold layer.

6.1   Top Wafer

Step 1: The die size was selected as 1.6 mm x 1.8 mm. Preparation of the top wafer starts with the RCA cleaning of a 380 μm thick <100> oriented silicon wafer. A 0.05 μm thick layer of chromium (Cr) was sputtered on the top surface of the silicon wafer. A layer of 0.5 μm of gold (Au) was then deposited using the Lift-off technique using an E-beam evaporation method using mask #1 as shown

in Appendix B on the top of the Cr layer. Another thin layer of 0.05 µm thick Cr was then sputtered on the top of the Gold layer to facilitate BCB adhesion to Au. The deposition parameters of the Au layer are listed in Table 6.1. The process parameters for etching of Au layer are listed in Table 6.2.

Table 6.1 Process Parameters for deposition of Au

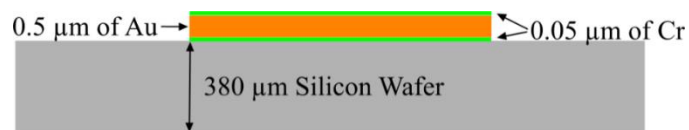| Process Parameters	Value
Rf power	100 W
Rf frequency	13.56 MHz
Temperature of deposition	100ºC
Pressure of vacuum	10 mTorr
Time of deposition	10 min

Figure 6.1 Formation of top patches using Lift of Resist technique theoretically simulated in Intellifab™

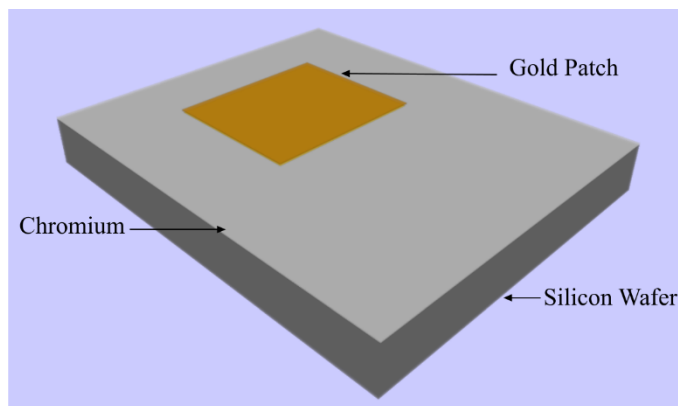

Figure 6.2 Formation of top patches using Lift of Resist technique simulated in Intellifab™

Table 6.2 Etching parameters for Au

Process Parameters	Values
Etch Temperature	80ºC
Etch Time	2 min
Etch depth	500 nm

Step 2: A dry etchable 3022-63 Cyclotene™ was spin coated on the top of the Cr layer at a speed of 1500 rpm for 10 seconds and dry baked to form a solid layer of 20 µm. The process started with the coating of AP3000 an adhesion promoter to 10 Å. The deposition process table of BCB is listed in Table 6.3.

Table 6.3 BCB deposition parameters

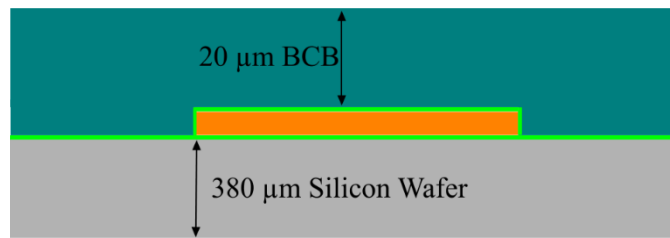| Process Parameters	Values
Spin speed	1250
Time of spin	30 sec
Temperature	90ºC
Time	90 sec
Thickness	20 µm

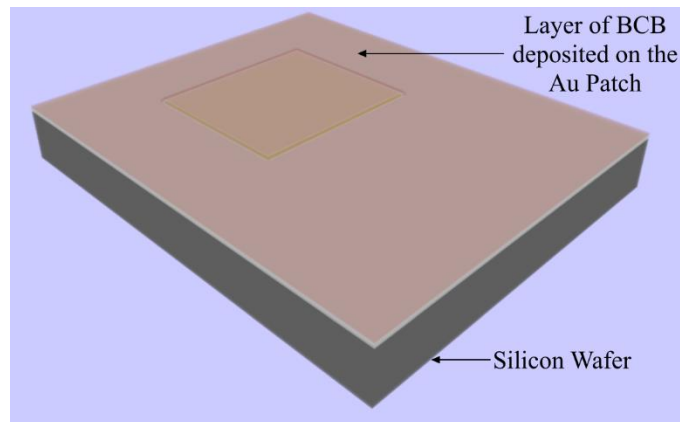Figure 6.3 BCB deposited on the top of Au patch.

Figure 6.4 BCB deposited on top of Au patch simulated in Intellifab™

Step 3: Lithographically pattern back cavities with mask #2 (Appendix B). Deposit Cr and Au on the back.
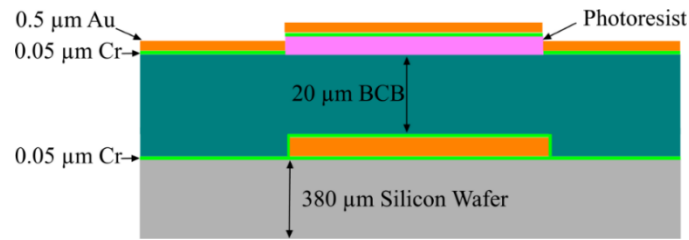
Figure 6.5 Alteration and Lithography of back cavities for DRIE etch theoretical representation
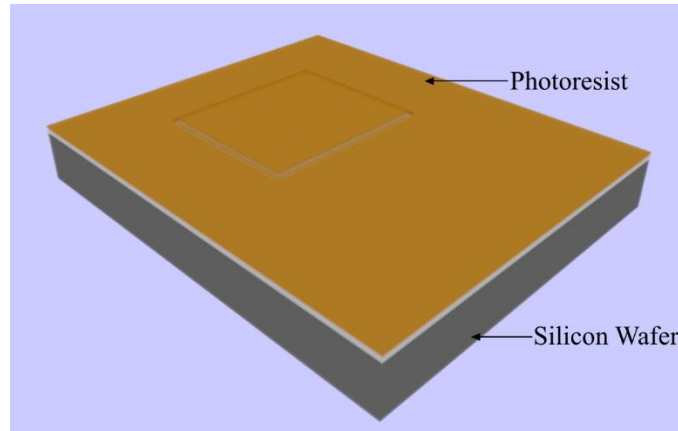
Figure 6.6 Alteration and Lithography of back cavities for DRIE etch simulation executed in

Intellifab™

Step 4: Strip Photoresist. Cover the top with photoresist and re-pattern cavities in the layer of Cyclotene™ with mask #3 (Appendix B) using the DRIE technique. BCB etching parameters are listed in Table 6.4.

Table 6.4 Etching of cavity in a layer of BCB [77] [79]

Process Parameters	Values
RF Power	200 W
Composition	22.5 sscm CF_4 ,90 sccm of O_2
Pressure	50 mTorr
Time of etch	4 min
Thickness of etch	17 μm
Sidewall angle	90º
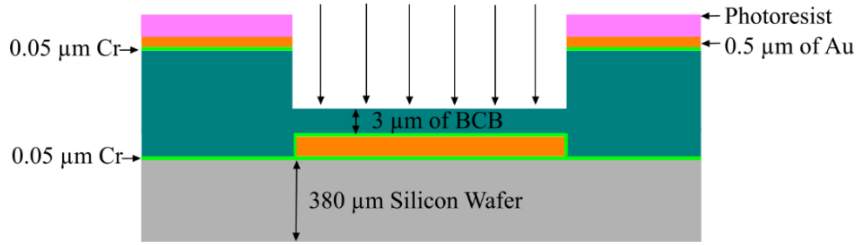
Figure 6.7 DRIE cavity formation in BCB.
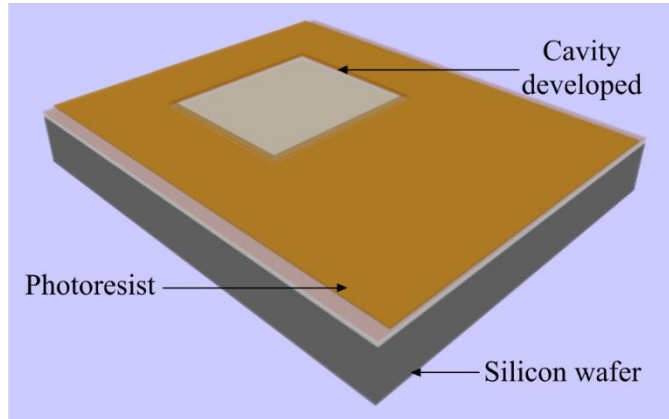
Figure 6.8 DRIE cavity formation in BCB simulated in Intellifab™

Step 5: Strip Photoresist
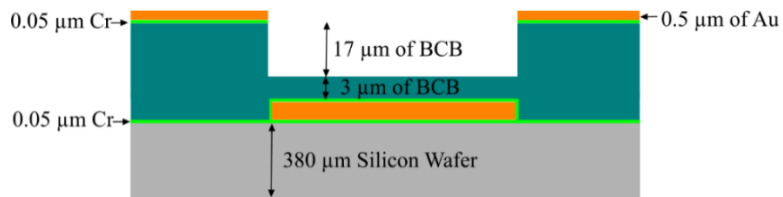
Figure 6.9 Strip photoresist
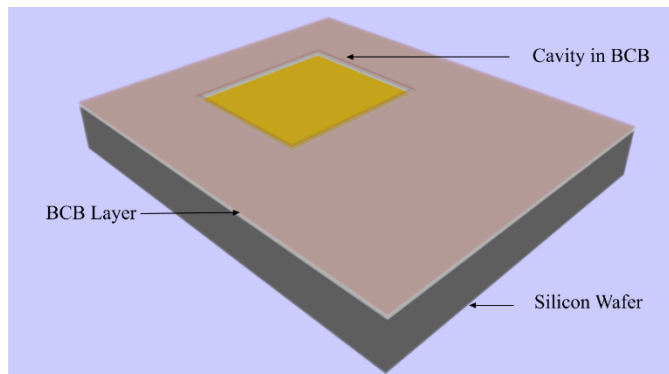
Figure 6.10 Strip Photoresist simulated in Intellifab™

6.2   Bottom Wafer

Step 6: Preparation of a commercially available 500 µm Pyrex wafer to act as a support substrate for the design.
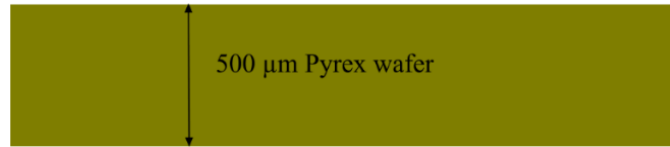
Figure 6.11 Preparation of Pyrex wafer
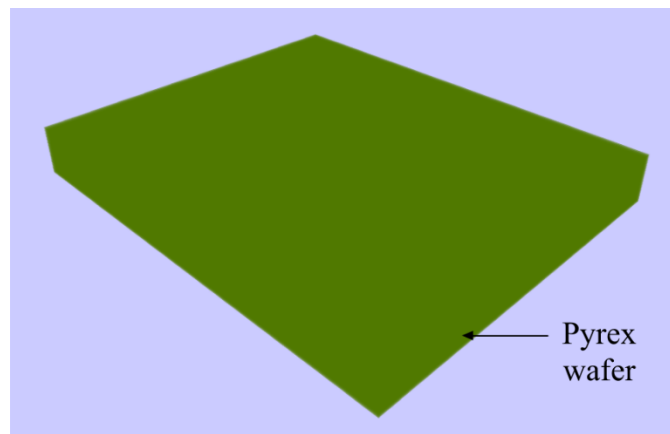
Figure 6.12 Preparation of Pyrex wafer simulated in Intellifab™

Step 7: A layer of 0.05 µm of Cr is first sputtered on the surface of Pyrex wafer and Au layer of 0.5 µm is deposited using an E-beam evaporation process using the Lift Off technique followed by another layer of Cr of 0.05 µm. Table 6.1 and 6.2 process parameters were used for deposition and patterning of gold feed lines.
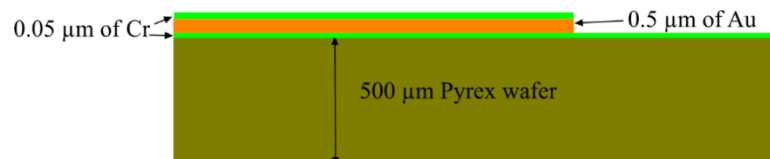
Figure 6.13 Deposition of Cr and Au for feed lines
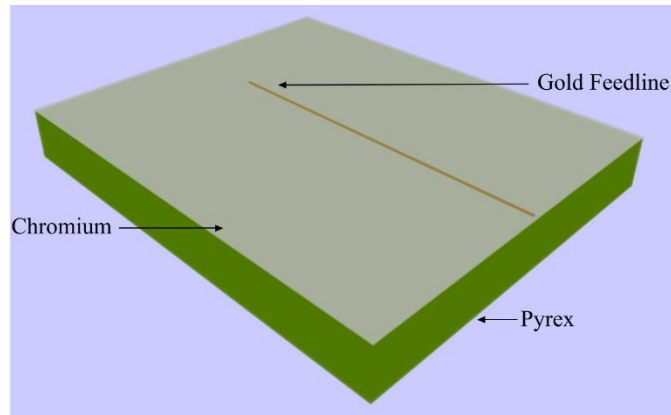
Figure 6.14 Deposition of Cr and Au for feed lines simulated in Intellifab™

The Cr layers on top of Au and Pyrex are sputtered to enhance the adhesion of Gold to both Pyrex and BCB.

Step 8: Spin coating of Dry Etchable 3022-63 Cyclotene™ on the top of metal layers and dry baking it to get a solid layer of 15 μm. Table 6.3 can be reutilized for parameters required for the development of a layer of BCB on the feed lines.
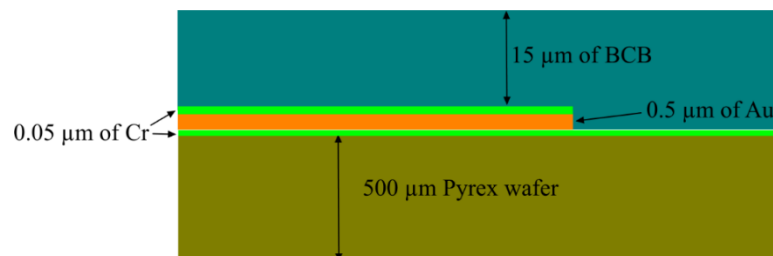
Figure 6.15 BCB was spin coated on the Au feed lines
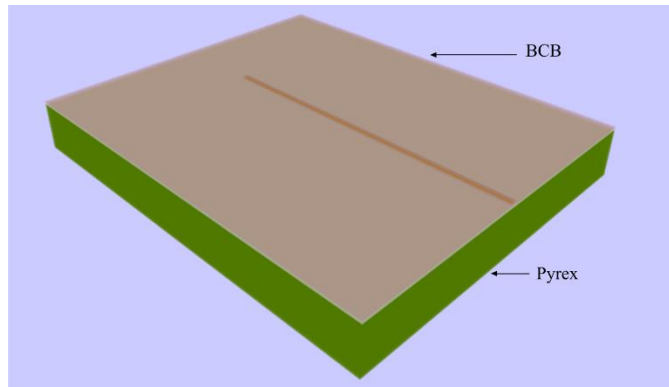
Figure 6.16 BCB spin coating simulated in Intellifab™

Step 9: A layer of 0.05 µm of Cr and 0.5µm of Au is deposited on the top of the layer of Cr using the Lift of resist technique using mask# 5. Table 6.1 and 6.2 can be used for development of the Gold layer on BCB with proper utilization of masks for aperture development.
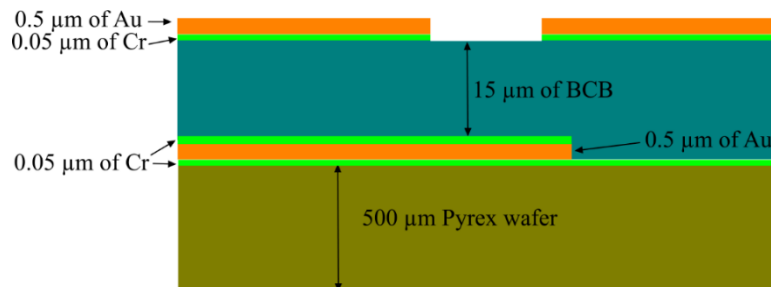
Figure 6.17 Preparation of Au ground plane with an aperture in it.
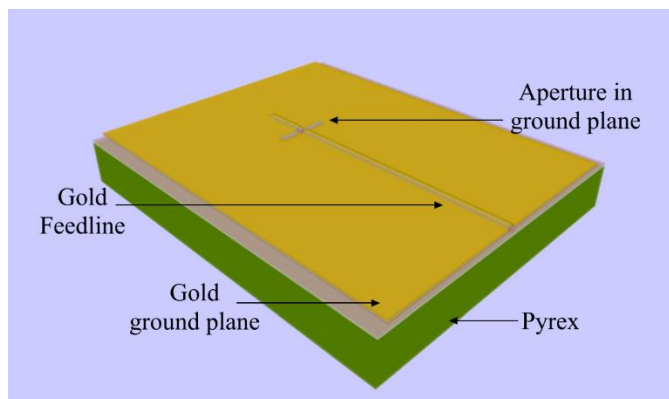
Figure 6.18 Preparation of Au ground plane and aperture modeled in Intellifab™.

6.3 Wafer Bonding

Step 10: The final step of the fabrication process is to flip the top wafer on the bottom wafer and use the thermosonic compression gold to the gold bonding of the two wafers with each other. And finally, use KOH solution to dissolve off the layer of Silicon on the top of the radiating patch. Wet Chemical etching can be used to remove the layer of Cr from the top of the structure.
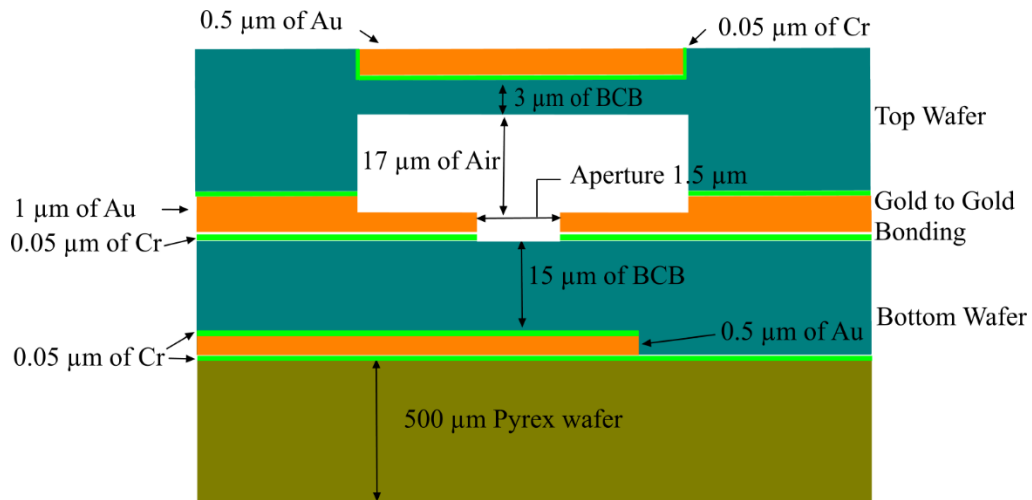
Figure 6.19 Wafer bonding a theoretical representation.
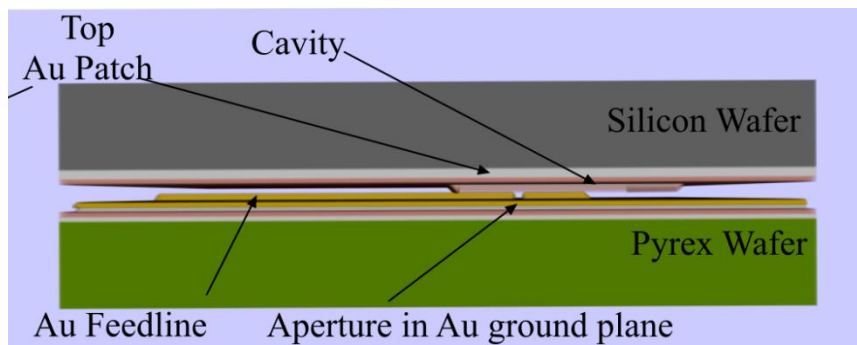
Figure 6.20 Cross-sectional view of wafer bonding.
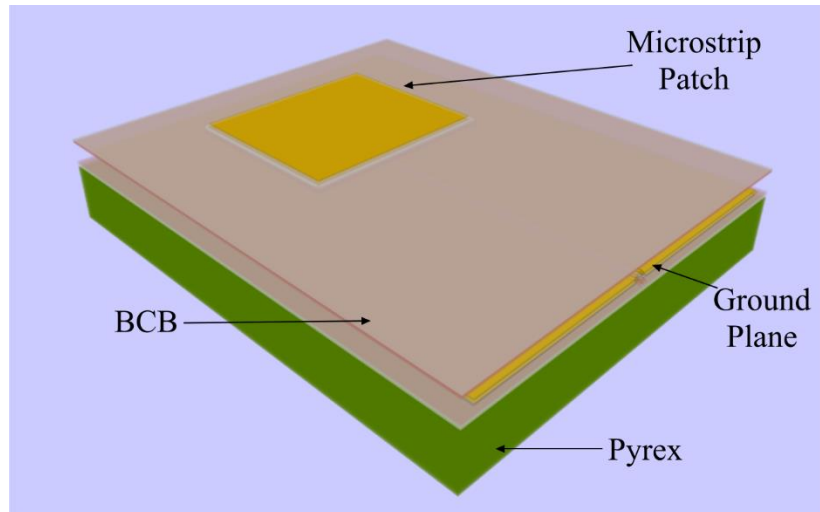
Figure 6.21 (a)Top view of the model after wafer bonding simulated in Intellifab™

6.4   Summary

A fabrication process table has been described in this chapter which indicates that the following antenna design can be easily fabricated using standard microfabrication techniques.

Chapter 7 :
CONCLUSIONS

The thesis presents the design of a wide bandwidth microstrip planar antenna array that can be used in a 77 GHz automotive radar. The wide bandwidth of ~4 GHz will enable the radar to provide superior resolutions in the long range [79], short range and midrange applications.

7.1   Conclusions

A 77 GHz DRIE etched cavity microstrip antenna array has been designed to work in conjunction with a Butler matrix for mid and long-range operations like pre-crash detection, cruise control, and collision avoidance.

This thesis provides a deep insight into the techniques to design a superior performance microstrip antenna array that can be fabricated using conventional microfabrication techniques. The thesis opens with an introduction and explains the necessity to design efficient radar systems for automotive applications to minimize numbers of road accidents. The pursuit to build efficient radar system channels the designers in building high performing antenna arrays to work in conjunction with the radar units. This section highlights some of the unique properties of the design presented in this thesis.

This work provides a detailed literature review in the field of antenna arrays for automotive radars along with design methodology for a single and multiple antennas working together to produce an effective performance. The improvement in performance in terms of bandwidth and smaller dimensions has

been achieved mainly due to the DRIE etched cavity in the dielectric material underneath the radiating patches which reduces the dielectric constant of the area by a considerable amount. Along with high levels of gains and directivity in a smaller footprint, the antenna array has an added advantage of a robust integrability with its signal processing modules unlike most antenna arrays available in the market. A rectangular antenna patch acting as a radiating element in a single stack up ensures a simple design and fabrication process.

Simulation results provided in Chapter 5 was carried out in a software by Keysight technologies commercial software ADS™. The simulation results show a direct fulfillment of requirements set forth by the automotive industry for Long Mid and short-range radars for automotive applications. The wide bandwidth achieved through the simulations indicate the number of samples generated per second would be high enough to make the radar function in shorter ranges as the resolution of this radar can achieve is approximated to be 0.1 m.

Apart from a wide bandwidth of 4.2 GHz, the antenna array achieves a gain of 19.78 dBi with a directivity of 22.5 dBi which satisfies the long-range requirements set by the auto industry. The author in [23] reports a gain of similar margin is enough to cover a distance of 200-250 m. The S11 parameters for the antenna array are at a lower magnitude than -10 dB at 77 GHz, which predicts that the antenna doesn't suffer from the increased amount of losses while transmitting signals. The voltage standing wave ratio VSWR is 1.04 against an idea of unity which in this case is extremely desirable as an outcome. The overall results with reduced dimensions predict a suitable outcome for this research

work and hope to improve on the current state of the art for antenna arrays used in automotive radars.

7.2 Future Work

The main aspects of the work to be done for completion of the designing process are limited. Although a thorough design is presented in this thesis the key aspects of the design remaining are listed below.

- Fabrication of the proposed design using a BCB substrate.

- Performance analysis and verification of the simulation results by measurement of the fabricated antenna

- Study of the radiation pattern and guarantee acceptable frequency bandwidth for the automotive radar functioning.

- Combine Butler matrix and the proposed antenna array and perform analysis while working in unison with the beam forming a network.

- Integration of the signal processing modules which would generate the FMCW signal.

APPENDIX

Appendix A

MATLAB Code for Antenna Patch Design

```
%Antenna_Patch_Design_ by Sreejit Chatterjee
clc
clear all
format long
%disp('Design of an Aperture coupled Microstrip Antenna');
%h_material = input('Enter the height of the material used in mm: ');
%e_material = input('Enter the dielectric constant of the material: ');
%h_air = input('Enter the dielectric 2 height in mm: ');
%e_air = input('Enter the dielectric constant: ');
%k = (h_material/e_material);
%k1 = (h_air/e_air);
%heq = h_material+h_air;
%e_r = ((k+k1)^-1)*heq
e_r = input('Enter the dielectric constant of the substrate used:');
h = input('Enter the thickness of the patch substrate (in mm):');
f = input('Enter the desired resonant frequency (in GHz)');
z = input('Enter the input desired impedance (in ohm):');
W = input('Enter the desired width of feedline (in mm)');
f = f*1e9;
c = 3e8;
la = (3e8/f)*1000%in mm
%guided wavelength in the substrate
la_guided = la/sqrt(e_r)
%free space impedance
eta = 119.9169832*pi; %in ohms
%calculate the width
w = (c/(sqrt((e_r+1)/2)*2*f))*1000; %in mm
%calculate the effective dielectric constant
%W = w*39.37%width in mils
e_eff = ((e_r+1)/2)+(((e_r-1)/2)*(1+((12*h)/w))^-0.5);
%e_eff = ((e_r+1)/2)+(((e_r-1)/2)*(1+((12*h)/W))^-0.5);
%calculations for the extensions of the length
del_l = (((e_eff+0.3)*((w/h)+0.264))/((e_eff-
0.258)*((w/h)+0.8)))*(0.412*h); %in mm
%calculate the effective length
m_n = sqrt(e_eff);
l_eff =(c/(2*f*m_n))*1000;
%calculate the actual length
L = l_eff-(2*del_l);
%calculation for guided wavelength
lambda_g = c/(f*sqrt(e_eff));
k = (2*pi)/la;%wave number
x = k*w;
i_1 = -2+cos(x)+(x*sinint(x))+(sin(x)/x);
g_1 = i_1/(120*pi*pi);%in siemens
a =
@(th)(((sin((x./2).*cos(th))./cos(th)).^2).*(besselj(0,(k.*L.*sin(th)))
).*(sin(th)).^3);
a1 = integral(a,0,pi);
```

```matlab
g12 = a1/(120*pi*pi);%in siemens
r_in = 1/(2*(g_1+g12));%in ohms
inset = (L/pi)*(acos(sqrt(z/r_in)));
Lg_min = 6*h+L; %Punit S. Nakar (2004 book)
Wg_min = 6*h+w;
B = 60*pi*pi/(z*sqrt(e_r));
m1 = 2*B-1;
m = log(m1);
n1 = B-1;
n = log(n1);
p_m = ((2*pi*h)/la)^2;%from Michael Civerolo Thesis
G = ((pi*w)/(eta*la))*(1-(p_m)/24);%from Michael Civerolo Thesis
B_1 = 0.01668*(del_l/h)*(w/la)*e_eff;%from Civerolo Thesis
%Radiation Resistance
R_rad = 1/G;% from A Kuchar Thesis
%Fringe Capacitance
C_fringe = B_1/(2*pi*f);% from A Kuchar Thesis
%inset feed length y0
k1 = sqrt(z/r_in);
y0 = (L/pi)*(acos(k1));%in mm
z_1 = 120*pi/(sqrt(e_eff));
z_2 = 0.667*log((w/h)+1.444);
%microstrip line impedance
Zc = z_1/((w/h)+1.393+z_2);
k = (8*h/W);
p = (W/4*h);
Zo = (60/(e_eff))*(log(k+p));
%feedline width
M = (2*h/pi)*(B-1-m+(((e_r-1)/(2*e_r))*(n+(0.39*0.61)/e_r)));%Liang
J.book (2004)
%inset feedline gap calculation
g = (c*4.65e-9)/(sqrt(2*e_eff)*f*10^-9);% journal by M A Martin (2010)
%Input impedance
Zin = (90*(e_r^2)/(e_r-1))/((L^2)/(w^2));%from paper 1 comparison
disp(['Rectangular patch aperture coupled:'])
disp(['The resonant frequency of the patch is: ',num2str(f),'GHz'])
disp(['The free space impedance is: ',num2str(eta),'ohm'])
disp(['The resonant wavelength of the patch is: ',num2str(la),'mm'])
disp(['The epsilon effective of the patch is: ',num2str(e_eff)])
disp(['The guided wavelength of the patch is: ',num2str(lambda_g)])
disp(['The width of the patch (Wp) is: ',num2str(w),'mm'])
disp(['The length of the patch is (Lp) is: ',num2str(L),'mm'])
disp(['The resonant input resistance is (Rin) is:
',num2str(r_in),'ohms'])
disp(['The inset feed length (Fi) is:',num2str(inset),'mm'])
disp(['The width of the feed line: ',num2str(W),'mm'])
disp(['The gap of the feedline Gpf: ',num2str(g),'mm'])
disp(['The minimum length of the ground plane is
',num2str(Lg_min),'mm'])
disp(['The minimum width of ground plane is ',num2str(Wg_min),'mm'])
disp(['The radiation resistance is ',num2str(R_rad),'ohm'])
disp(['The fringe Capacitance is ',num2str(C_fringe),'F'])
disp(['The microstrip line characteristic impedance is
',num2str(Zo),'ohm'])
```

MATLAB Code for Array factor and Radiation Pattern

```matlab
%function[]=radiationplot
%M=1800;
%Array_Factor_ by Sreejit Chatterjee
%8/22/2017
%Values to be considered for planar array are 1. Y- 14(49 mm)* X-
8(23.84 mm)
%Values for beta_x and beta_y taken as 0
%Values for spacing of elements in x and y direction are 1.96 mm
clc
clear all
c = 2.99e11;
f = 77e9;
lambda_o = c/f;
F = 200000;
k = 2*pi/lambda_o;%wavenumber
phi = linspace(-pi/2,pi/2,F+1);%(-pi/2):(pi/1000):(pi/2);
theta =  linspace(0.01,pi,F+1);%(0.01):(pi/1000):pi;
theta_1 = linspace(0,2*pi,F+1);
%theta=linspace(0,2*pi,M+1);
%phi = linspace(0,2*pi,N+1);
N = input('number of elements in the Y direction:');
M = input('number of elements in the X direction:');
beta_x = input('phase difference between elements in x direction:');%in
either degrees or radians
beta_y = input('phase difference bewteen elements in y direction:');%in
degrees or radians
d_x = input('spacing between elements in x direction(mm):');% distance
between two elements in x direction
d_y = input('spacing between elements in y direction(mm):');% distance
between two elements in y direction was generally 1/4 before
Y_x = k.*d_x.*sin(theta).*cos(phi) + beta_x;
Y_y = k.*d_y.*sin(theta).*sin(phi) + beta_y;
E = cos(theta_1);
AF_x = (1/M).*(sin((M./2).*Y_x)./(sin(Y_x./2)));
AF_y = (1/N).*(sin((N.*Y_y)./2)./(sin(Y_y./2)));
AF_planar = (AF_x).*(AF_y);
Pat = abs(E.*AF_planar);
%AFdb=20*log10(Pat/max(Pat));
AFdb=20.*log10(Pat);
U=(abs(AF_planar)./max(abs(AF_planar))).^2;
figure;
polar(theta_1, abs(E.*AF_planar));%polar(theta_1, abs(E.*AF_n));
%[x y z] = theta_1,phi,Pat;
%surf(x,y,z,'EdgeColor','none')
%plot3();
%figure;
%polar(theta, abs(E.*AF_n));
figure;
plot(theta_1.*180./pi,abs(E.*AF_planar),'k');%theta_1./180
hold on
plot(-theta_1.*180./pi,abs(E.*AF_planar),'k');
axis([-50 50 0 1])
xlabel('Theta(deg)');
ylabel('Relative Amplitude (dB)');
```

```
grid on;
figure;
plot(-theta_1.*180./pi,AFdb,'b');%theta_1./180
hold on
plot(theta_1.*180./pi,AFdb,'b');
axis([-80 80 -50 0])
xlabel('Scan angle(deg)');
ylabel('Gain of the radiation pattern in dB');
grid on;
%[X,Y] = meshgrid(1:0.5:10,1:20);
%Z = abs(E.*AF_n);
%C = X.*Y;
%surf(X,Y,Z,C)
%colorbar
```

MATLAB Code for Directivity and Gain

```
%Gain_And_Directivity_ by Sreejit Chatterjee
W = 1.75;
Leff = 1.56;
h = 0.02;
r = 1;
phiMin = -90;
phiMax = 90;
thetaMin = 0.1;
thetaMax = 180;
c = 2.99e11;
f = 77e9;
lambda_o = c/f;
%j = sqrt(-1);
%function [direct, directdB, prad]=directivity(phiMin, phiMax,
thetaMin, thetaMax, h);
Umax = 0;
d_theta = pi/180;
d_phi = pi/180;
prad = 0;
phiMin1 = phiMin+1;
%double Integration
for phi = phiMin1:phiMax
    phi_rad = phi*pi/180;
    thetaMin1 = thetaMin+1;
    for theta = thetaMin:thetaMax
        theta_rad = theta*pi/180; %code for theta
        %radiation = radiation_intensity(f, theta_rad, phi_rad, W,
Leff, h);
        j = sqrt(-1);
%function radiation = radiation_intensity(f, theta, phi, W, Leff, h)
        phi = (-pi/2):(pi/1000):(pi/2);
        theta = (0.01):(pi/1000):pi;
        ko = (2*pi)/lambda_o;
        const = ((j)*ko*h*W*(exp((-j)*ko*r)))/(2*pi*r);
        X = (ko*h/2).*(cos(phi(1:997)).*(sin(theta(1:997)))));
        Y = (ko*W/2)*cos(theta);
```

```matlab
            radiation =
((abs(const.*(sin(X)./X).*(sin(Y)./Y).*sin(theta)))).^2)./(2.*120.*(pi.^
2)));
        %if radiation > Umax
            Umax = radiation;
        %end
        UA = d_theta*d_phi*radiation*sin(theta_rad);
        prad = prad+UA;
    end
end
direct = 4*pi*Umax/prad;
directdB = 10*log10(direct);
r = 1;
phi = (-pi/2):(pi/1000):(pi/2);
c = 2.998e11;
lambda_o = c/f;
ko = (2*pi)/lambda_o;
const = ((j)*W*ko*(exp((-j)*ko*r)))/(pi*r);
B = sin(((ko*h)/2)*cos(phi));
C = (((ko*h)/2)*cos(phi));
D = B/C;
E = cos(((ko*Leff)/2)*sin(phi));
plane1 = abs(const*D*E);
plane_max = max(plane1);
E_plane = (20*log10(plane1/plane_max))+directdB;
polar(phi,E_plane)
%,'rlim',[-30,10],'rtick',[-30 -20 -10 0 10],'tstep',60,'color','b'),
title('Eplane E(\phi)');
plotedit on;
B1 = ((sin(((ko*W)/2)*cos(theta)))/(((ko*W)/2)*cos(theta)));
C1 = (sin(((ko*h)/2)*sin(theta)))/(((ko*h)/2)*sin(theta));
D1 = sin(theta);
plane2 = (abs(const*(B1*C1*D1)));
plane_max = max(plane2);
h_plane = (20*log10(plane2/plane_max))+directdB;
polar(theta,h_plane)
%,'rlim',[min(h_plane) 10],'rtick',[-30 -20 -10 0
10],'tstep',30,'color','r')
```

MATLAB Code to find Feedline Width

```matlab
%%Feed_Width_ by Sreejit Chatterjee
%Calculation for feedline characteristic impedance
%Width Calculated as 0.062 mm to get 49.9435 Ohms
%Length of feed line is lambda_eff = 2.4198 mm
clc
clear all
W = input('Enter the width of the feed line in mm: ');
H = input('Enter the height of the feed substrate in mm: ');
e0 = 8.85e-15; %permittivity in free space
e_eff = 1; %effective permittivity in BCB of 26 microns is 2.57 and for
5 microns is given 2.6334
u0 = 1.257e-9; %permeability in free space
F = 6+ ((2*pi)-6)*exp(-(30.66*H/W)^(0.7528));
a = sqrt(u0/(e0*e_eff));
```

```
Z_a = 1/(2*pi)*(a);
b = sqrt(1+(2*H/W)^2);
Z_b = log((F*H/W)+b);
Z_c = Z_a*Z_b
```

MATLAB Code to find the synthesized permittivity

```
%Synthesized_Permittivity_ by Sreejit Chatterjee
clc
h_material = input('Enter the height of the material used in mm: ');
e_material = input('Enter the dielectric constant of the material: ');
h_air = input('Enter the dielectric 2 height in mm: ');
e_air = input('Enter the dielectric constant: ');
k = (h_material/e_material);
k1 = (h_air/e_air);
heq = h_material+h_air;
e_r = ((k+k1)^-1)*heq
```

Appendix B

Masks for Fabrication Processes

Mask 1:

Mask 2
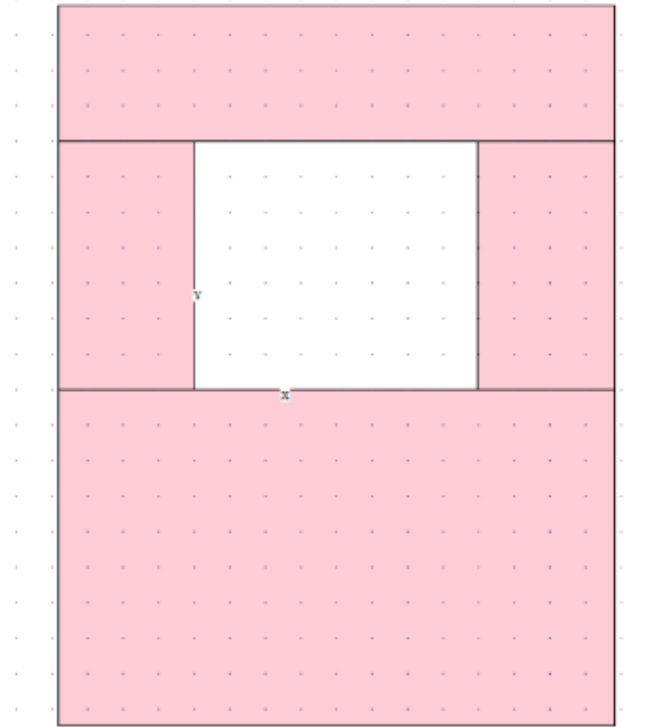
Mask 3:
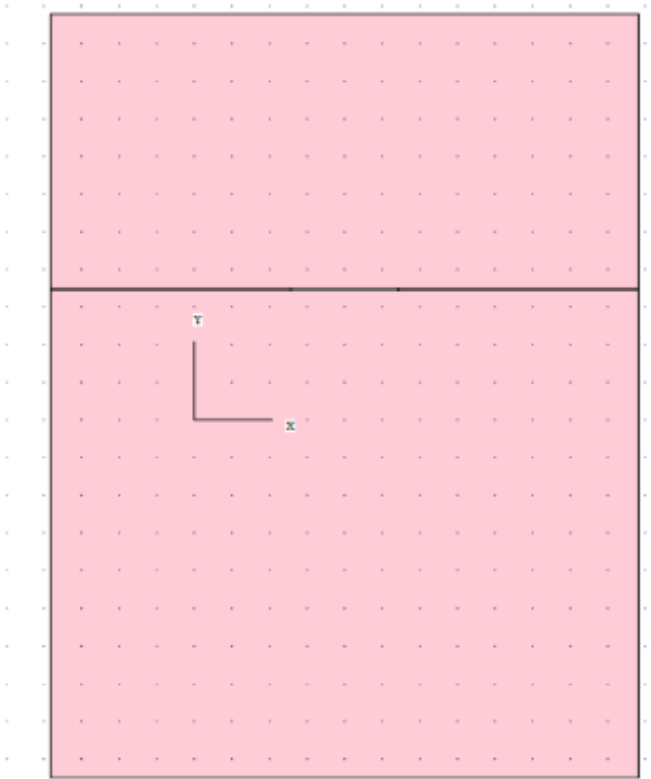
Mask 4:

Appendix C
- Process Table for Fabrication of Top Wafer

Type	Material	Process	Process ID	Process Option
Definition	Si	Czochralski	Generic	N/A
Deposition	Cr	Sputter	Ar-Ambient	Conformal
Deposition	Au	Evaporate	E-beam	Conformal
Deposition	PR-S1800	Spin	Generic	Conformal
Exposure	UV	Contact	Suss	N/A
Etch	Au	Wet	Iodide-Etch	Partial Etch
Deposition	Cr	Sputter	Ar-Ambient	Conformal
Deposition	BCB	Spin	Generic	Conformal
Depostion	PR-S1800	Spin	Generic	Conformal
Exposure	UV	Contact	Suss	N/A
Etch	BCB	DRIE	Bosch	Partial Etch
Etch	PR-S1800	Wet	Lift-off	Partial Etch
Bonding	Au	Thermosonic	7747	N/A
Etch	Si	Wet	KOH-Etch	Sacrifice

- Process Table for Fabrication of Bottom Wafer

Type	Material	Process	Process ID	Process Option
Definition	Glass	Pyrex	7740	N/A
Deposition	Cr	Sputter	Ar-Ambient	Conformal
Deposition	Au	Evaporate	E-beam	Conformal
Deposition	PR-S1800	Spin	Generic	Conformal
Exposure	UV	Contact	Suss	N/A
Etch	Au	Wet	Iodied Etch	Partial Etch
Deposition	BCB	Spin	Generic	Conformal
Deposition	Cr	Sputter	Ar-Ambient	Conformal
Deposition	Au	Evaporate	E-beam	Conformal
Deposition	PR-S1800	Spin	Generic	Conformal
Exposure	UV	Contact	Suss	N/A
Etch	Au	Wet	Iodide	Partial Etch
Etch	Cr	Sputter	Ar-Ambient	Partial Etch
Etch	PR-SU1800	Wet	Lift-off	Partial Etch

REFERENCES

1. US Traffic Deaths Jump to Make 2016 Deadliest year on Roads since 2007 [Online]. Available (fortune.com/2017/02/15/traffic-deadliest-year/).

2. Sivak M, "Is the US on the path to lowest motor vehicle fatalities in decades?" Report No. UMTRI-2008-39. Ann Arbor: The Universiy of Michigan Transportation Research Institute, 2008.

3. Koptis E, Cropper M. Traffic fatalities and economic growth, Washington DC, World Bank, (Policy Research Working) Paper No. 3035, 2003.

4. Research and Markets "Automotive Radar Market- Expected to Reach $12.1 billion by 2025" [Online]. Available :(www.prnewswire.com) Dec, 2017.

5. Toyota, Dynamic Cruise Control "What are the benefits of Dynamic Radar Cruise Control?" [Online]. Available: (www.totyota.ca) March 2017.

6. Miovision Trafficlink, Pedestrian Detection System "Introducing Miovision Trafficlink detection" [Online]. Available : (www.miovision.com)

7. Nissan Motor Corporation, Blind spot warning system [Online]. Available: (www.nissam-global.com)

8. Toyota, Pre-Collision System "What it is and how it helps you drive" [Online]. Available :(www.totota.ca) March 2017.

9. K. Sakiyama, T.Shimizu, K.Sako "Fujitsu-Ten, Parking Assist System".

10. S. Das, "Autonomous driving: How good is LiDar under heavy rain or fog?" [Online]. Available:(www.quora.com) Jan 2018

11. A. Malinka, E. Zege, G. Heygster and L. Istomina "Reflective properties of white sea ice and snow" *Copernicus Publications on behalf of European geosciences union, The Cryosphere*, No. 10, pp 2541-2557, 2016.

12. S. Lal "An FPGA based 77GHz Radar Signal Processing System for Automotive Collision Avoidance" Faculty of Graduate Studies University of Windsor, 2010.

13. Radar Chipset to bring safety to mid-range cars [Online]. Available: www.eetimes.com, Nov 2007.

14. D. Hoetzer, D. Freundt, "Driver Assist & Crash Avoidance Technologies: Radar and Video Systems", Robert Bosch GmbH, presented at Telematics Detroit, Detroit, MI, 2008.

15. Van Loon B.: "Radar 101" Celebrating 101 years of development", *In Proceedings of IEEE*, 93, (4), pp. 844-84, April 2005.

16. M. Schneider, "Automotive Radar-Status and Trends", Robert Bosch GmbH, Corporate Research, 2005.

17. T. Wu, T. S. Rappaport, C. M Collins "The Human Body and Millimeter Wave Wireless Communication Systems: Interactions and Implications" *In Proc of IEEE International Conference on Communications (ICC),* No. 1, Vol. 1, pp 1-7, June 2015.

18. Skin Anatomy [Online]. Available: (www.emedicine.medscape.com), Nov 2017.

19. D. Platt, L. Petterson, D. Jakonis, M. Salter and J. Haglund, "Integrated 79 GHz UWB automotive radar front-end based on Hi Mission MCM-D silicon

platform" *International Journal of Microwave and Wireless Technologies,* Cambridge University Press and the European Microwave Association, Vol 2, no. 3-4, pp 325-332, August 2010.

20. BOSCH, "Chassis Systems Control, Fourth generation long-range radar sensor (LRR4)" [Online]. Available :(www.cds.bosch.us)

21. Channel Bandwidth, Sample Rate, FFT (Size), Number of Resource Blocks [Online] Available : (www.lteuniversity.com)

22. D. Wu "76-81 GHz Planar Antenna Development and Utilization for Automotive Radar Applications" Department of Microtechnology and Nanoscience, Chalmers University of Technology, 2004, pp 58-61, Beijing China.

23. I. Hamieh, "A 77 GHz Reconfigurable Micromachined Microstrip Antenna Array", Electronic Theses and Dissertations. University of Windsor, Windsor, ON, 2012.

24. D. Shin, K. Kim, J. Kim, S. Park "Design of a Low Side Lobe Level Millimeter-Wave Microstrip Array Antenna for Automotive Radar" 2013 *Proceedings of the International Symposium on Antennas & Propagation (ISAP), 2013,* Nanjing, China, pp. 677-680.

25. J. Xu, W. Hong, H. Zhang, Y. Yu and Z. H. Jiang, "An Array Antenna for Both Long- and Medium Range 77 GHz Automotive Radar Applications" *IN Proc. Of IEEE Transactions on Antennas and Propagation,* Vol. 65, No. 12, Dec 2017.

26. B.R. Norvell, R. J. Hancock, J. K. Smith, M. L. Pugh, S.W. Theis and J. Kwiatkowski, "Micro Electro Mechanical Switch (MEMS) Technology Applied to Electronically Scanned Arrays for Space-based Radar", *IEEE Aerospace Conference Proceeding,* Vol. 3, pp. 239-247, 1999.

27. N. Ghafar, "Design of a Compact Microstrip Antenna at 2.4 GHz", M.S. Thesis, Department of Electrical Engineering, Universiti Teknologi Malaysia, Nov 2005.

28. Continental Automotive "Short Range Radar SRR510" [Online]. Available: (www.continental-automotive.com)

29. M. Kishida, K. Oguchi, and M. Shono "79 GHz-Band-High-Resolution Millimeter-Wave Radar " *Fujitsu Sci-Tech. Journal,* Vol. 51, No. 4, pp. 55-59, Oct 2015.

30. W.Wei, X.Wang, "A 77GHz Series fed Weighted Antenna Arrays with Suppressed Side-Lobes in E- and H- Planes" *Progress In Electromagnetics Research Letters,* Vol. 72, pp-23-28, 2018.

31. R. Manwar, "A BCB Diaphragm Based Adhesive Wafer Bonded CMUT Probe for Biomedical Application" Ph.D. Dissertation, University of Windsor 2017.

32. A. Lopez, J. Papapolymerou, A. Akiba, K. Ikeda, S. Mltarai, G. Ponchak "60 GHz Micromachined Patch Antenna for Wireless Applications" *In Proc. Of IEEE,* Vol. 1, No.1 pp 515-517, 2011.

33. R. Manwar, T. Simpson, A. Bakhtazad, and S. Chowdhury, "Fabrication and characterization of a high frequency and high coupling coefficient CMUT

array", Microsystems technologies, Springer-Verlag Berlin Heidelberg, DOI: 10.1007/s00542-016-3225-4, pp. 1-13, December 2016. [Online]. Available http://link.springer.com/article/10.1007/s00542-016- 3225-4.

34. Registered Motor Vehicles in India as of March 2015 [Online]. Available (www.community.data.gov.in)

35. 253 million cars and trucks on US roads; the average age is 11.4 years [Online] Available: (www.latimes.com)

36. World Health Organization "Road Traffic Injuries" [Online]. Available: (www.who.int)

37. S. Y Abbas "A Non-Planar CMUT Array for Automotive Blind Spot Detection", Master's Thesis, University of Windsor, 2009.

38. Future of Automotive Radar Testing, Microwave Journal [Online]. Available (www.microwavejournal.com)

39. (2007) The KOKON website [Online]. Available: (www.kokonproject.com)

40. R. A. Mucci, "A Comparison of Efficient Beamforming Algorithms" *IEEE Trans. Acoustics, Speech and Signal Processing,* Vol. ASSP-32, No. 3, pp. 548-558, June 1984.

41. A. Kawakubo, S. Tokoro et al., "Electronically Scanning Millimeter Wave Radar for Forwarding Objects detection", *SAE Congress 2004,* pp. 127-134, Detroit, 2004.

42. H. Nord, "Implementation of an 8x8-Butler Matrix in Microstrip", Diploma Thesis, Technische Universitat Wien, 1998.

43. A. Attaran, S. Chowdhury, "Fabrication of a 77GHz Rotman Lens on a High Resistivity Silicon Wafer Using Lift-Off Process" *International Journal of Antennas and Propagation,* Vol 2014, Article ID 471935, pp 1-9, 2014.

44. Antennas Patterns and their meaning, CISCO [Online]. Available: (www.cisco.com)

45. S. Sharma, S. Sharma "Design of High Gain Wang Shape Microstrip Patch Antenna for Wireless System" *In Proc. Of IEEE ICCCNT'12,* Vol 1, No. 20180, pp 1-3

46. BOSCH mid-range radar sensor [Online]. Available: (www.bosch-mobility-solutions.com)

47. J. Hasch, E. Toprak, R. Schnabel, T. Zwick, R. Weigel, C. Waldschmidt "Millimeter Wave Technology for Automotive Radar Sensors in 77 GHz Frequency Band" *IEEE Trans. On Microwave Theory and Techniques,* Vol 60, No. 3, March 2012.

48. Autonomous Cruise Control System Wikipedia [Online]. Available: (www.en.wikipedia.org)

49. TRW AC20 User Manual "AC20 Vehicle Mounted field disturbance sensor User Manual PRO_SPC_276_B0013393723, AUTOCRUISE S.A."[Online]. Available: (www.fccid.io)

50. Delphi ESR [Online]. Available (www.autonomousstuff.com)

51. Denso [Online]. Available (www.globaldenso.com)

52. 76 GHz Millimeter Wave Automobile Radar using single chip MMIC [online]. Available: (www.denso-ten.com).

53. S. Honma, N. Uehara, "Millimeter Wave Radar Technology for Automotive Application" *Technical Reports Automotive Electronics Development Center*, Mitsubishi Electric, June 2001.

54. Yi-An Li, Meng-Hsiung Hung, and Shih-Jou Huang, "A Fully-Integrated 77-GHz FMCW Radar Transceiver in 65-nm CMOS Technology", *IEEE JOURNAL OF SOLID-STATE CIRCUITS*, Vol. 45, No. 12, December 2010.

55. Dong-hun Shin, Ki-beam Kim, Jong-Duk Kim, Seong-ook Park, "Design of Low Side Lobe Level Millimeter wave array antenna for Automotive Radar"

56. Bo-Hyun Ku, Paul Schmalenberg, Ozgu Inac, Ozan Dogan Gurbuz, Jae Seung Lee, Koji Shiozaki, Gabriel M. Rebeiz,"A 77–81-GHz 16-Element Phased-Array Receiver With ±50° Beam Scanning for Advanced Automotive Radars*", IEEE TRANSACTIONS ON MICROWAVE THEORY AND TECHNIQUES*, Vol. 62, No. 11, November 2014.

57. Siew-Bee Yeap, Xianming Quing, Zhi Ning Chen"77-GHz Dual-Layer Transmit-Array for Automotive Radar Applications", *IEEE TRANSACTIONS ON ANTENNAS AND PROPAGATION*, Vol. 63, No. 6, June 2015.

58. S. Yasini, Karim M. Aghdam,"Design and Simulation of a Comb-line fed Microstrip Antenna Array with low side lobe level at 770Hz for Automotive Collision Avoidance Radar",*2016 4th International Conference on Millimeter Wave Terahertz Technologies(MMWaTT)*, pp 87-90, Dec 2016.

59. C. A. Winterhalter, J.Teverovsky, P. Wilson, J. Slade, W. Horowitz, E. Tierney and V. Sharma, "Development of electronic textiles to support networks, communications and medical applications in future U.S. Military

protective clothing systems" *IEEE Trans. Information Technology in Biomedicine,* Vol. 9, pp 402-406, 2005.

60. R. Ibrahim, M. Yagoub, R. Habash, "Microstrip Antenna for RFID applications", *In Proc of Canadian Conference on Electrical and Computer Engineering*, No. 0840-7789, pp. 1-4, May 2009.

61. Sherif Sedky, Post-processing Techniques for Integrated MEMS, Artech House, Massachusetts, 2006.

62. P. Lopato, M. Herbko "A Circular Microstrip Antenna Sensor for Direction Sensitive Strain Evaluation" *In Proc of Sensors MDPI,* Vol 2018, No. 18 pp 1-11.

63. C. Balanis (n.d.), Antenna Theory, Wiley & Sons, NJ; 3rd edition, 2005.

64. Lo, Y.T. Solomon D and Richards, "Theory and Experiment on Microstrip Antennas", *IEEE Trans on Antennas and Propagation,* AP-27, 1979, pp.137-149.

65. D. M. Pozar and D. H. Schaubert, Microstrip antennas, the analysis and design of Microstrip antennas and arrays, New York: IEEE press 1995.

66. Bandwidth [Online]. Available: (www.memscap.com/aboutmems.html)

67. M. Mathur, A. Vats, A. Agarwal, "A New Design Formulae for FeedLine Dimensions of the Rectangular Microstrip patch Antenna by using Equivalent Design Concept" *In Proc. Of IEEE,* Vol 1, No. 1, pp 105-110, 2015.

68. A. Kuchar "Aperture-Coupled Microstrip patch Antenna Array", Master's Thesis, Technische Universitat Wien, Austria, 1996.

69. W.F. Richards, "Microstrip Antennas", Chapter 10 in Antenna Handbook: Theory and Applications and Design (Y.T Lo and S.W. Leeds), Van Norstrand Reinhold Co., New York, 1988.

70. A. Jaiswal, S. Dey, M.P. Abegaonkar, S.K. Koul "77 GHz Polarization Reconfigurable Micromachined Antenna for Automotive Radar Applications" *IEEE MTT S-Latin America Microwave Conference (LAMC 2016)* Vol 1, No. 1, pp 1-3.

71. M. Gouker, G. Smith "A Millimeter-Wave Integrated Circuit Antenna Based on the Fresnel Zone Plate", *IEEE Trans on Microwave Theory and Techniques,* Vol. 40, No. 5, May 1992.

72. A. Roy, J. Mom, D. Kureve "Effect of Dielectric Constant on the Design of Rectangular Microstrip Antenna" *2013 IEEE International Conference on Emerging & Sustainable Technologies for Power & ICT in a Developing Society (NIGERCON)* Vol 1. Pp 111-115, 2013.

73. S. Constanzo, I. Venneri, G.D. Massa, A. Borgia, "60 GHz Microstrip Reflectarray on Benzocyclobutene Dielectric Substrate" *IET Science Measurement and Technology,* 2011, vol. 5, no. 4, pp 134-139.

74. CYCLOTENE™ 3000 Series Advanced Electronic Resins (Dry Etched BCB) Dow Chemical [Online]. Available: (www.dow.com).

75. CYCLOTENE™ 4000 Series Advanced Electronic Resins (Dry Etched BCB) Dow Chemical [Online]. Available: (www.dow.com).

76. V. Yashvanth, S. Chowdhury "A new Scheme for High-Frequency Ultrasound Generation", *2017 IEEE 30th Canadian Conference on Electrical and Computer Engineering (CCECE),* Vol.1, No. 1 pp 1-4, May 2017.

77. S. Chatterjee and S. Chowdhury, "A Low-Cost BCB Based 77 GHz Microstrip Aperture Coupled Antenna Array for Automotive Radars" *In Proc of Mid West Symposium of Circuits and Systems,* Vol 1, No. 1, pp 1-5, 2018

78. Z. Aijaz, S. Shrivastava "Effect of Different Shapes: Aperture Coupled Microstrip Slot Antenna", *International Journal of Electronics Engineering,* Vol 2(I), pp103-105, 2010.

79. Radar Tutorial "Bandwidth and Range Resolution" [Online]. Available: (www.radartutotial.eu)

80. R. Manwar and S. Chowdhury, "Experimental Analysis of Bisbenzocyclobutene Bonded Capacitive Micro machined Ultrasonic Transducers," MDPI Sensors: Integrated Sensor Arrays and Array Signal Processing, vol. 16(7), no. 959, June 2016.

81. C.F. Luk, Y. C. Chan, K. C. Hung "Development of gold to gold interconnection flip chip bonding for the chip on suspension assemblies" *Microelectronics Reliability,* Vol. 42, pp 381-339, 2002.

VITA AUCTORIS

Sreejit Chatterjee was born in the year of 1993 in Kolkata, West Bengal India. He had completed his Bachelor of Technology (B. Tech) degree in the year of 2016 from the West Bengal University of Technology in the field of Electronics and Communication Engineering with a CGPA of 8.8. He has published a patent (regd. under Indian govt. titled "High DOF Interpreted Knowledge-Based Prosthetic Arm" application no. 201631017724 A, dated: 09/30/2016.) while working with his undergraduate mentor Dr. Sudipta Ghosh. After his B. Tech he was working briefly with Tech Mahindra as an Associate Software Engineer trainee when he decided to join the University of Windsor, Electrical and Computer Engineering Department as a master's student.

At the time of writing this thesis, Sreejit is a member of the MEMS Lab at the University of Windsor working under the supervision of Dr. Sazzadur Chowdhury. He has an aggregate score of 90.25% in his M.A.Sc and has also received the prestigious University of Windsor Graduate Entrance Scholarship for International Students on the year of joining. His received a Scholarship for Research Assistantship from his supervisor which was funded through NSERC, CFI, CMC Microsystems, Intellisense Inc., and Angstrom Engineering, Kitchener. He has published a conference paper in the oldest IEEE conference 61st MWSCAS 2018, Windsor, Ontario Canada. Sreejit has been working as Webmaster for IEEE Windsor Section since October 2016 and later got elected as Vice Chair for IEEE Young Professionals Windsor Section in November 2017.